THE FLOWING AFTERGLOW AS A CHEMICAL REACTION MASS SPECTROMETER: ACCURACY DETERMINATIONS AND REAGENT ION DEVELOPMENT

by

Thomas H. Watson

B.S., Allegheny College, 2003

Submitted to the Graduate Faculty of

Arts and Sciences in partial fulfillment

of the requirements for the degree of

Master of Science

University of Pittsburgh

2009

UNIVERSITY OF PITTSBURGH

Arts and Sciences

This thesis was presented

by

Thomas Watson

It was defended on

August 11th, 2009

and approved by

Dr. David Pratt, Professor, Chemistry

Dr. Kenneth Jordan, Professor, Chemistry

Thesis Director: Dr. Joseph Grabowski, Associate Professor, Chemistry

THE FLOWING AFTERGLOW AS A CHEMICAL REACTION MASS SPECTROMETER (CR-MS): ACCURACY DETERMINATIONS AND REAGENT ION DEVELOPMENT

Thomas Watson, M.S.

University of Pittsburgh, 2009

Henry's Law was utilized to determine the accuracy of the flowing afterglow at the University of Pittsburgh as a Chemical Reaction Mass Spectrometer (CR-MS). H_3O^+ and its first three hydrates were utilized as reagent ions in the CR-MS technique to quantify headspace concentrations over multiple series of dilute aqueous acetone, acetonitrile, and benzaldehyde/THF solutions. The temperature corrected Henry's Law constants, k_H^{θ}, of acetone, acetonitrile, benzaldehyde, and THF were calculated as 32.1±3.3, 45.2±6.5, 41.6±2.1, and 14.8±1.0 M atm^{-1}, respectively. These values for acetone, acetonitrile, benzaldehyde, and THF are in agreement within error of the literature values of 28±3, 51±3, 39±3, and 14 M atm^{-1}, respectively. These measurements suggest that our flowing afterglow can be utilized to accurately quantify multiple VOCs simultaneously via the CR-MS technique.

H_3O^+ is the most commonly utilized reagent ion for the CR-MS technique due to its many advantages. This ion possesses two main limitations; it readily clusters with water and cannot decipher between isobaric (of the same mass) molecules. Due to its size and tendency to react like a proton, the trimethylsilyl group (TMS^+) can be substituted for a proton to reduce clustering. Substitution of the nitrosyl cation for a proton creates a NO^+ donor and an ion that can decipher between isobaric molecules.

The preparation of $R((CH_3)_3Si)ONO^+$, where R is a proton, trimethylsilyl, alkyl, or NO^+ moiety, was attempted in order to make a reagent ion that can decipher between isobaric molecules, does not cluster, and, yet, maintains the advantages of H_3O^+ as a reagent ion. There were four different preparations attempted for ions of this type: NO^+ + methoxytrimethylsilane, NO^+ + hexamethyldisiloxane, $((CH_3)_3Si)_2OH^+$ + methyl nitrite, and $((CH_3)_3Si)OH_2^+$ + methyl nitrite. The clean production of $R((CH_3)_3Si)ONO^+$ remains elusive. The reactions of NO^+ and methoxytrimethylsilane and NO^+ and hexamethyldisiloxane resulted in hydride and/or methide abstraction. No reaction occurred between protonated hexamethyldisiloxane and methyl nitrite. The reaction of protonated trimethysilanol with methyl nitrite did not produce an ion of the type $R((CH_3)_3Si)ONO^+$ cleanly as it resulted in $H(TMS)ONO^+$ (*m/z* 120) and $(CH_3)(TMS)ONO^+$ (*m/z* 134).

TABLE OF CONTENTS

LIST OF TABLES

LIST OF FIGURES

LIST OF SCHEMES

PREFACE

I would first and foremost like to thank my advisor, Dr. Joseph J. Grabowski, for his guidance and instruction these past years. Joe has introduced me to the world of mass spectrometry and the unlimited possibilities that such knowledge includes. He has also assisted in molding me into a professional in the scientific community. I would like to recognize my committee members Dr. David Pratt, Dr. Kenneth Jordan and the departed Dr. Peter Siska for their time and suggestions. I would also like to thank Dr. John Williams for training me on commercial mass spectrometry instrumentation at the University of Pittsburgh. Not only has he provided great assistance to me from a technical aspect, but he has helped me develop personal interaction skills as well as the ability to handle the pressure of a high throughput setting. I would like to thank Randall Pedder and Dr. Mark Bier. They have assisted me greatly in networking amongst the mass spectrometry community. I would also like to thank current and former Grabowski group members: Mark Morris, Kevin Davies, Kathryn Tarney, Christopher Taormina, and Kyle Tilger for their valuable assistance.

I would also like to thank everyone in the machine shop. Jeff and Dennis Sicher as well as Tom Gasmire and Roy Watters have provided invaluable assistance in fixing the pumping technology of our flowing afterglow as well as making parts for the flowing afterglow in a quick and timely manner. I would like to thank everyone in the electronics shop. Dave

Emala, Chuck Fleishaker, Jim McNerney, and Bob Muha have been useful in fixing any problems with our control boxes or diagnosing electrical problems on our diffusion pumps. I would also like to thank all the secretaries and staff in the main office in Rm. 234 of Chevron for their assistance and support.

Finally, I would like to thank my family. My wife, Natalie, has been there with me through the toughest of times and I could not have done this without her. Her unbelievable amount of faith in me has kept me pushing forward, while her love and care kept me mentally, emotionally, and physically healthy enough to finish. I want to thank the rest of my family as well, including my father and mother, my brothers, Natalie's parents, siblings, and grandparents, my Clawson side of the family, and the Boulder family for all their love and support through this process.

1.0 INTRODUCTION

1.1 Volatile Organic Chemical Analysis

Volatile organic chemicals (VOCs) are of importance due to their food quality, medical, and environmental applications. Ethyl acetate, 2-methyl-1-butanol, methanol, ethanol, acetic acid, and acetaldehyde have all been shown to be indicators of the ripeness of fruit.[1,2] The presence of methane thiol and dimethyl sulfide emissions has been correlated to the degree of spoilage of meats.[3,4] Ethane and pentane in human breath have both been suggested to be biomarkers for the presence of lung inflammatory diseases.[5,6,7] The presence of various alkanes in human breath has been linked to oxidative stress, which can lead to cancer.[8,9] Some VOCs can also directly cause cancer as well as damage to the liver, kidneys, and central nervous system.[10,11] Aromatic hydrocarbons react with nitrogen oxides to form tropospheric ozone.[12] Methane is known as an extremely efficient greenhouse gas. These are just some of the reasons the detection and quantification of VOCs have garnered increased interest over the past 25 years.

There are three methods that are commonly utilized for VOC analysis. Gas Chromatography-Mass Spectrometry (GC-MS) can provide quantitative analysis at the parts per trillion by volume (pptv) level. However, obtaining results from a GC-MS can take as long as 30 minutes, which effectively prevents real-time analysis. Electronic noses are designed to detect various VOCs through the utilization of an array of chemical sensors that each respond to a

particular VOC through varying resistance proportional to analyte concentration.[13] These sensors can provide real-time analysis. They typically have detection limits at the sub part per million by volume (ppmv) level and have limited sensor lifetimes. In addition, both the GC-MS technique and utilization of electronic noses require external calibration such as the use of prepared standards. A third technique, Chemical Reaction Mass Spectrometry (CR-MS) allows online, real-time quantification of VOCs at the pptv level without the need for external calibration.

1.2 Chemical Reaction Mass Spectrometry

1.2.1 *Overview*

CR-MS is a technique that utilizes ion-molecule reactions to identify and quantify gaseous compounds. A large excess of reagent ions, with respect to the amount of the reactant gas, is formed in an ion source. These reagent ions are allowed to react with the trace gases, ppm by number density or lower, present. The resulting swarm of ions is sampled, mass filtered, and detected. Previous characterization of these ion-molecule reactions, which includes the measurement of the ratios of products formed and the rate coefficient, along with the specific experimental parameters employed, allows for quantification of the trace VOCs. The choice of an appropriate reagent ion is one of the keys to the successful utilization of the CR-MS technique.

1.2.2 *Reagent Ions*

The ideal reagent ion fulfills four requirements. The reagent ion should be able to be generated cleanly. It should also produce one product ion upon reaction with each VOC of interest. These first two requirements are designed to avoid multiple product ions corresponding to each neutral and the resulting complicated data analysis. The reagent ion should also be unreactive towards the bulk gases in the gaseous matrix of interest so that the products observed can be assumed to be only from ion-molecule reactions with the trace VOCs. Finally, the ion-molecule reaction utilized to quantify the trace VOCs should proceed with a reaction efficiency of unity; that is every ion-molecule collision results in a reaction.

1.2.2.1 H_3O^+

The most commonly utilized reagent ion for CR-MS is the hydronium ion. H_3O^+ can be generated relatively cleanly by electron ionization (e.i.) or Penning ionization (p.i.) of water vapor (Scheme 1.1). Penning ionization is the ionization of the precursor gas (B) by excited state buffer gas (M^*), eq. 1.1.

$$M^* + B \rightarrow M + B^+ \quad (1.1)$$

H_3O^+ reacts with most neutrals via proton transfer to form the VOC-H^+ ion, eq. 1.2. This

$$H_3O^+ + VOC \rightarrow VOC\text{-}H^+ + H_2O \quad (1.2)$$

reaction has been shown to proceed at an efficiency of unity when it is exothermic.[14,15] Proton transfer from the hydronium ion is exothermic if the proton affinity (PA), defined as the negative of the heat of reaction for addition of a proton to a neutral of interest, of the trace gas is sufficiently greater than the proton affinity of water; PA(H_2O)=165 kcal mol^{-1}.[16] The bulk components of air possess proton affinities below this value (Table 1.1) and are unreactive with

H_3O^+. The majority of VOCs has proton affinities much greater than that of water and reacts with the hydronium ion with unit efficiency. The hydronium ion also has the benefit of usually producing one product ion upon reaction. For ketones[17], alkenes[18], and aromatic hydrocarbons[19], this is the only product ion formed. For many alcohols[20], aldehydes[21], and carboxylic acids[22], $(M\text{-}OH)^+$ ions are produced in addition to or instead of MH^+ ions. In the case of esters, an alcohol can be lost from the MH^+ ion to form $(M\text{-}OR)^+$.[22] This reaction pathway is also common to ethers in addition to, for higher ethers, loss of RH to form $(M\text{-}R)^+$ ions.[23]

Table 1.1:
Proton affinities and ionization potentials of the four most abundant components of dry air

Compound	Air Composition (%)	Proton Affinity (kcal mol^{-1})	Ionization Potential (eV)
Nitrogen	78.084	118.0	15.581
Oxygen	20.946	101.0	12.0697
Argon	0.934	88.24	15.759
Carbon Dioxide	0.0314	129.2	13.777

[a]Air composition percentages obtained from Brimblecombe[24]
[b]Proton affinities and ionization potentials obtained from NIST Chemistry Webbook[25]

The hydronium ion possesses a few disadvantages as a CR-MS reagent ion. Clustering can occur between H_3O^+ and excess water molecules either in the ion source or in humid samples to form the hydrates of the hydronium ion (Scheme 1.1). The hydrates of H_3O^+ can react with the neutrals in the sample, which complicates all aspects of VOC detection and quantification. Another limitation is that the hydronium ion is not an effective reagent ion for detection of alkanes. Smaller alkanes ($n<5$), where n is equal to the number of carbon atoms, do not react with H_3O^+ while larger alkanes ($n\geq5$) do not react with efficiencies close to unity.[26]

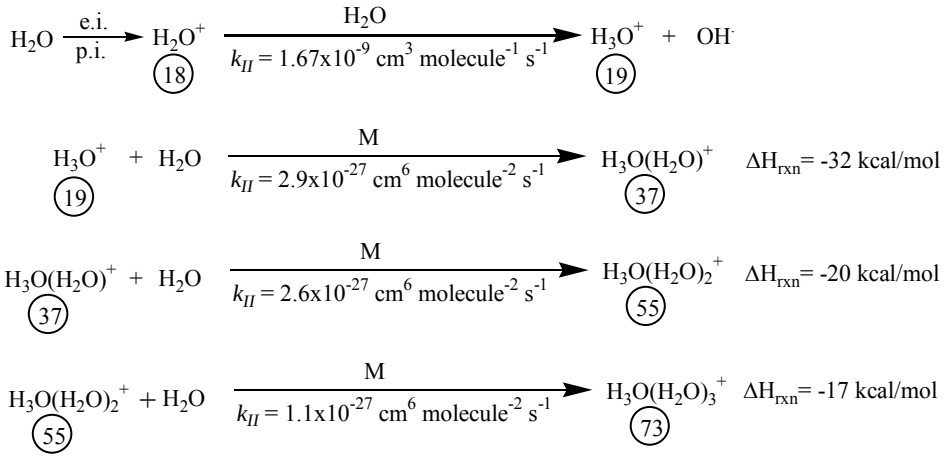

Scheme 1.1: Formation of the hydronium ion and its hydrates at 298 K in a CR-MS experiment, where M is a third body. Kinetic data obtained from Lau et. al.[27] Thermodynamic data obtained from Kebarle.[28] Circled values represent the *m/z* of the ion above it.

1.2.2.2 NO^+

Another ion utilized for CR-MS is NO^+. NO^+ is generated cleanly via electron ionization of nitric oxide. The nitrosyl cation can react with trace gases by hydride abstraction, hydroxide transfer, alkoxide transfer, adduct formation, and/or charge transfer. Fortuitously, only one or two of these pathways occur for a reaction with NO^+. Ionization energies of aromatic hydrocarbons are usually less than the ionization energy (IE) of nitric oxide (9.26 eV)[25] and react predominantly via non-dissassociative charge transfer to produce M^+ ions.[19] Many aldehydes[21], ethers[23], and primary and secondary alcohols[20] produce exclusively the hydride transfer product upon reaction with NO^+. Hydroxide transfer is the exclusive pathway for tertiary alcohols.[20] Association reactions with NO^+ are observed when $0 \leq IE_{Neutral}\text{-}IE_{NO} \leq 1$ eV, which is the case for carboxylic acids[22], ketones[17], and esters.[22] In addition to association, alkoxide and hydroxide transfer often occur for esters and carboxylic acids, respectively.[22] Including association reactions, these reactions of NO^+ all typically occur with a reaction efficiency of unity. NO^+ also possesses the advantage of being unreactive towards the bulk

components of air due the fact that the ionization potentials of these compounds are significantly greater than that of nitric oxide (Table 1.1). Unfortunately, like H_3O^+, smaller alkanes ($n<5$) do not react with NO^+ and the larger alkanes ($n\geq5$) do not react with an efficiency close to unity.[26]

One advantage of NO^+ over H_3O^+ is that it can distinguish between some isobaric (i.e. identical molecular mass) compounds. This is due to the fact that NO^+ can react via numerous pathways while H_3O^+ reacts solely via proton transfer. For example, butanone and THF react with H_3O^+ to produce solely *m/z* 73. The reaction of NO^+ with butanone produces an ion at *m/z* 102 via association while reaction with THF results in *m/z* 71 via hydride transfer (Scheme 1.2).

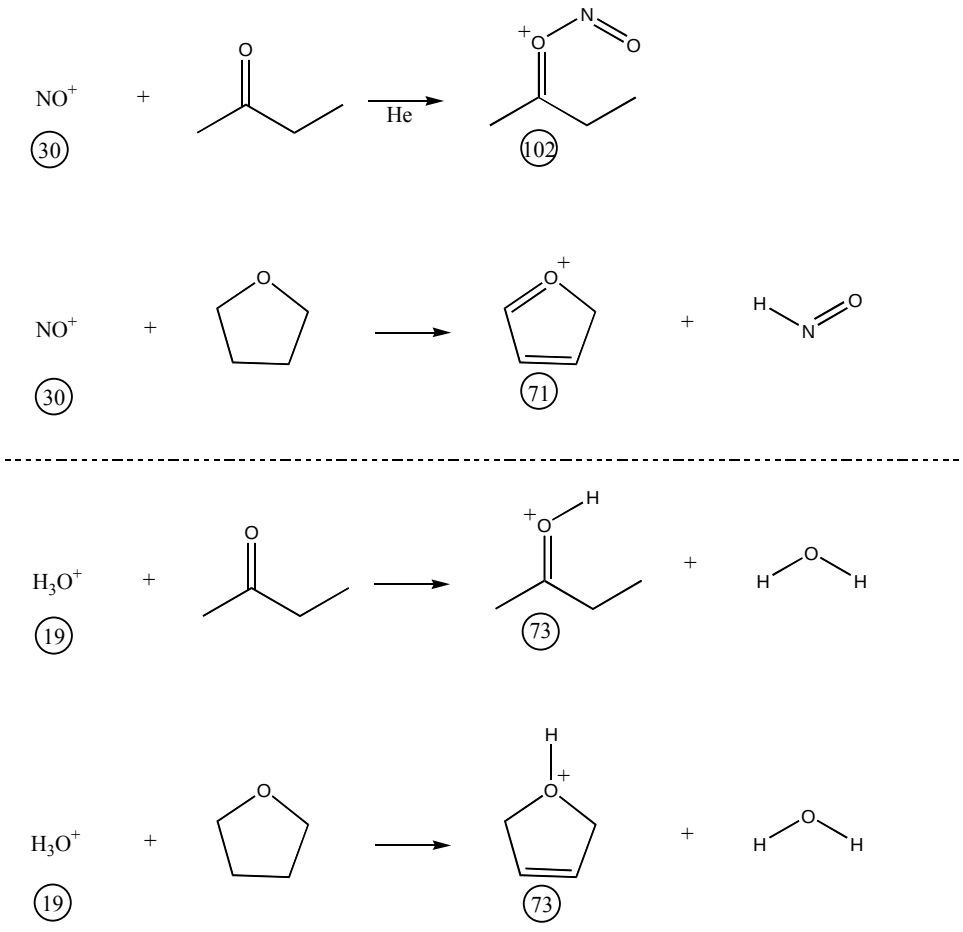

Scheme 1.2: Comparison of the NO^+ and H_3O^+ reactions with THF and butanone.

1.2.2.3 O_2^+

A third ion that has been utilized for analysis via the CR-MS technique is O_2^+. This ion can be generated cleanly by electron ionization of oxygen. The ionization energy of O_2 is sufficiently large (12.07 eV)[16] such that O_2^+ undergoes charge transfer reactions with most compounds. Fortuitously, the ionization energy of O_2 is low enough such that it does not react with the bulk components of air (Table 1.1). O_2^+ also has the advantage of typically reacting with an efficiency of unity.[17,21,22] As opposed to H_3O^+ and NO^+, O_2^+ even reacts with small molecules such as the smaller alkanes[29], NO[30], NO_2[30], and CS_2[30], via dissociative charge transfer with a reaction efficiency of unity. Unfortunately, for most compounds, numerous dissociative charge transfer reaction pathways result in multiple product ions due to the high ionization potential of O_2.

1.2.3 *Previous Endeavors*

Since its inception, Chemical Reaction Mass Spectrometry (CR-MS) has been a useful tool for the identification and quantification of VOCs for food quality, environmental, and medical applications. CR-MS studies on human breath have been performed to quantify acetonitrile and benzene in smokers, isoprene as a possible biomarker for oxidative stress, and ethanol.[31] In addition, this technique has been used to suggest a correlation between isopropanol and formaldehyde in human breath and lung cancer.[32] Dimethyl sulfide and methane thiol have been quantified and correlated to the spoilage of meat.[31] Concentrations of acetaldehyde, acetone, acetic acid, methanol, propanol and ethanol have been monitored and shown to correlate to the degree of ripeness of various types of fruit.[31] Acetaldehyde and formaldehyde have been identified and quantified as the two most abundant VOC components in diesel exhaust

emissions.[33] Other anthropogenic emissions such as benzene and toluene have been identified and quantified in urban areas.[34] Due to their effects on ozone chemistry, non-methane volatile organic chemicals (NMVOCs) emissions from plants and other biogenic sources have also been quantified.[35]

1.3 Flowing Afterglow Mass Spectrometry

One type of mass spectrometer that has been extensively utilized for the CR-MS technique is the flowing afterglow mass spectrometer. The flowing afterglow mass spectrometer was first designed and utilized by Fehsenfeld et al.[36] at the National Oceanic and Atmospheric Administration (NOAA) in the 1960's for the study of ion-molecule reactions in the earth's atmosphere. A flowing afterglow mass spectrometer is composed of three regions; an ion generation region, a reaction region, and a detection region. Reactant ions are produced by an ion source. These ions are then carried and thermalized to room temperature down a pyrex, quartz, or stainless steel flow tube (typically 1 m long by 8 cm i.d.) by a buffer gas (typically helium). Neutral sample is introduced at some point down the flow tube and allowed to react with the reagent ions. The resulting swarm of ions is carried to the end of the flow tube by the buffer gas. Here, the ions are sampled through an orifice (0.5-1.0 mm i.d.) into an analyzing chamber where they are mass analyzed and detected.

A mass analyzer that is often utilized is a quadrupole mass filter, **Figure 1.1.** A quadrupole mass filter consists of four parallel metal rods. Opposing rods are electrically connected. One pair of rods has an applied potential of $-\{U+V\cos(\omega t)\}$ while the other has a potential of $+\{U+V\cos(\omega t)\}$, where U is a fixed potential and $V\cos(\omega t)$ is an sinusoidally

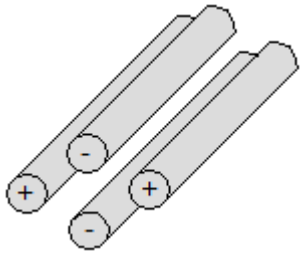

Figure 1.1: Quadrupole mass filter where (+) indicates where +{U+Vcos(ωt)} potential is applied and (–) indicates where –{U+Vcos(ωt)} potential is applied.

alternating potential with amplitude V and frequency ω. These applied potentials cause the entering ions to have trajectories dependent on their mass-to-charge ratio. Each combination of the fixed potential and alternating potential results in ions of a specific *m/z* having a stable trajectory to traverse through the quadrupole. The remaining ions possess unstable trajectories, do not pass through the quadrupole, and are not detected.

1.4 Conclusions

The analysis of volatile organic chemicals is of importance due to their food safety, medical, and environmental applications. Chemical Reaction Mass Spectrometry is an accurate and precise method that allows for online, real-time, quantification of VOCs without the need for external calibration or sample preconcentration. One type of instrumentation that is often utilized as a CR-MS instrument is a flowing afterglow mass spectrometer equipped with a quadrupole mass analyzer.

The success of the CR-MS technique, which utilizes ion-molecule reactions to quantify trace gases, relies heavily on the choice of the reagent ion. Despite its disadvantages of

clustering with excess water and inability to decipher between isobaric compounds, H_3O^+ is the most commonly utilized reagent ion due to its ease of preparation, propensity for producing a single product ion for reaction with each neutral of interest, tendency to react with an efficiency of unity, and unreactive nature towards the bulk components of air. Even though it only sometimes produces a single product ion upon reaction with a neutral, NO^+ is easily prepared, tends to react with an efficiency of unity, does not react with the bulk components of air, and can even discern between isobaric compounds. O_2^+ most often produces multiple product ions upon reactions with a specific neutral, but, is produced cleanly, reacts with an efficiency of unity, is unreactive towards the bulk components of air, and reacts with the smaller ($n<5$) alkanes; an inability of H_3O^+ and NO^+.

Herein, the validation, utilization, and development of the CR-MS technique to identify and quantify VOCs via our flowing afterglow mass spectrometer equipped with a quadrupole mass analyzer. The flowing afterglow mass spectrometer at the University of Pittsburgh as well as the theory behind how VOCs are quantified via the CR-MS technique are described in Chapter 2. The validation and accuracy of the CR-MS technique on our instrumentation via Henry's Law experiments is discussed in Chapter 3. Advances towards the development of novel trimethylsilated reagent ions are discussed in Chapter 4.

2.0 EXPERIMENTAL METHODOLOGY

2.1 The Flowing Afterglow Mass Spectrometer

2.1.1 *Overview*

The flowing afterglow at the University of Pittsburgh is schematized in **Figure 2.1** and pictured in **Figure 2.2**. Any flowing afterglow is composed of three regions; an ion generation

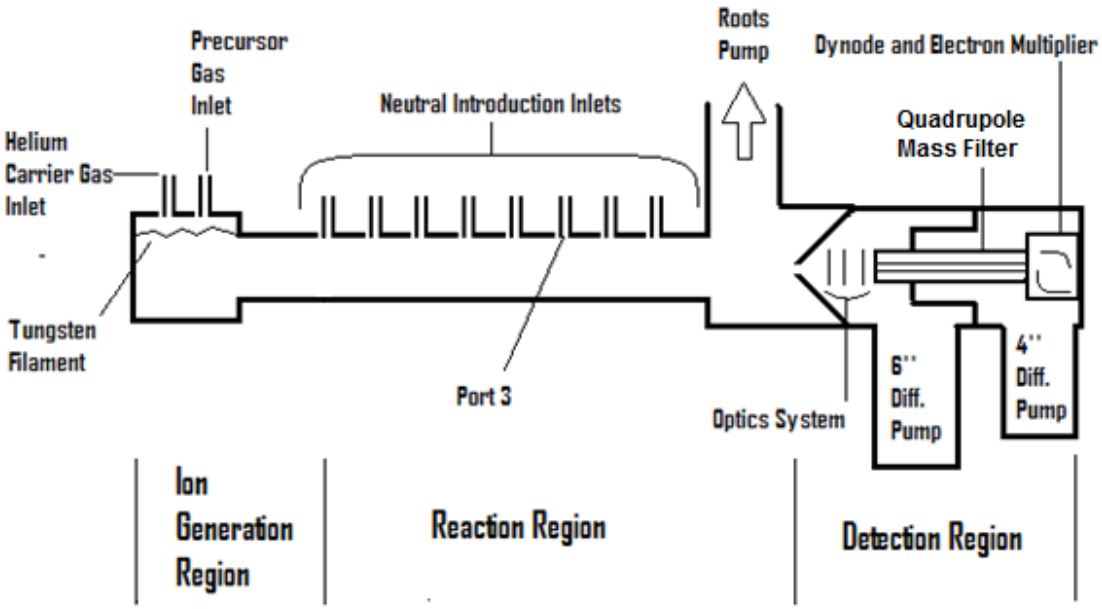

Figure 2.1: A schematic diagram of the flowing afterglow mass spectrometer at the University of Pittsburgh

region, a reaction region, and a detection region. Helium (99.9%) was further purified via passage through a liquid nitrogen trap (292 cm long by 1.6 cm i.d.) and the flow (0−12 SLPM) was regulated by a Tylan mass flow controller. Precursor gas was introduced into the ion source

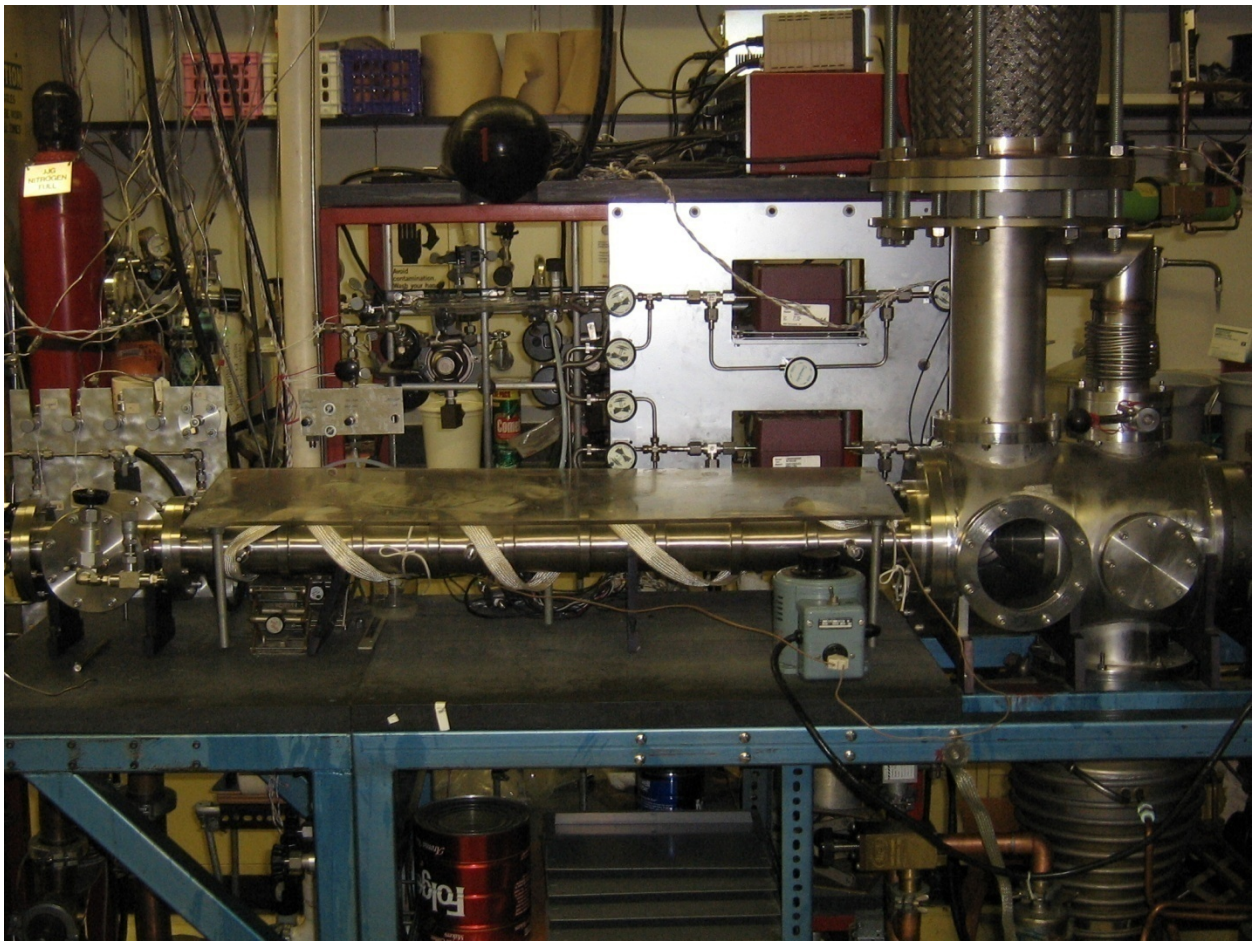

Figure 2.2: Photograph of the flowing afterglow mass spectrometer at the University of Pittsburgh

and ionized by electron ionization or via Penning ionization with excited state helium. The reagent ions were thermalized to room temperature and transported down a stainless steel flow tube (1 m long by 7.3 cm i.d.) via the helium buffer gas. Neutrals were introduced through a vacuum rack and into one of 10 equally spaced (9.1 cm) radial inlets along the flow tube, which were controlled by solenoid valves. Flow rates of the neutrals were calculated by measuring the time it took the pressure in the calibrated volume of the vacuum rack to increase, eq. 2.1, where

$$F_{Neutral} = \frac{\Delta PV}{\Delta t} \tag{2.1}$$

ΔP is the pressure change in Torr, V is the volume being filled in cm^3, and Δt is time for the pressure to change in seconds. During their use, all flasks containing sample liquids or solutions

were immersed in a 500 mL beaker of room temperature water to maintain a constant temperature. Prior to ion sampling, neutrals were removed via a roots pump (Leybold-Heraeus WA 2000). Ions were sampled at the end of the reaction region through a 1 mm orifice and focused through a series of electronic lenses. Mass analysis and detection were accomplished through the use of the MAX 1000 (Extrel CMS) system. Ions were mass analyzed by a trifilter quadrupole (19 mm, 880 kHz) and directed towards an electron multiplier for detection. The optics, quadrupole, and high voltage electronics were monitored and controlled by the Merlin (Extrel CMS) Data Automation System.

During operating mode, the detection region and flow tube were maintained at $<10^{-5}$ and 0.3-0.4 Torr, respectively. The system was kept under vacuum by 6″ (Edwards Diffstak Model 160) and 4″ (Edwards Diffstak Model 100) diffusion pumps backed by a mechanical pump (Leybold-Heraeus Model D16AC), which maintained a backing pressure of 0.05-0.1 Torr in operating mode. The pressure in the backing line was monitored by thermocouple gauges (Granville-Phillips Model 270006). Ion gauges (Kurt J. Lesker Co. G100N) were utilized to monitor the pressures in the detection region. Pressures in the neutral introduction system and flow tube were monitored by 0-1000 Torr and 0-10 Torr Baratrons (MKS), respectively.

2.1.2 *Methods of Data Collection*

Two methods of spectra collection were utilized; Full Scan Mode and Selected Ion Monitoring (SIM). Full Scan Mode and SIM involve collecting one, large *m/z* range (e.g., 10−100 amu) or a series of specified *m/z* windows, respectively. Full Scan Mode allows the observation of an entire spectrum, but often results in duty cycles of less than 2%. The duty cycle is the percent of data collected that is utilized for analysis. SIM results in much higher

duty cycles at the expense of not being able to observe the entire spectrum. For qualitative data collection, where the reaction products were not known, the Full Scan method was used whereas SIM was utilized for most quantitative analyses.

2.1.3 *Carrier Gas Flow*

In order to accurately study the ion-molecule reactions, the gas flow in the flow tube must be viscous and laminar. During viscous flow, the average distance particles travel between collisions is much less than the dimensions of the vacuum system. This results in intermolecular interactions and not interactions of particles with the walls of the flow tube defining the flow of the gas. Laminar flow is uniform, streamlined gas flow.

In order to determine if the helium flow within the flow tube is viscous or molecular, the Knudsen number for the carrier gas is calculated. The Knudsen number gives insight into the nature of the flow and is defined in eq. 2.2, where d is the diameter of the flow tube and λ

$$K_n = \frac{\lambda}{d} \tag{2.2}$$

is the mean free path of the helium carrier gas. The mean free path is the average distance particles travel between collisions and is determined using eq. 2.3, where k_B is the Boltzmann

$$\lambda = \frac{k_B T}{P_{He}\,\sigma\sqrt{2}} \tag{2.3}$$

constant, P_{He} is the pressure in the flow tube, T is the temperature, and σ is the collisional cross section for the helium carrier gas. If K_n>1, then the carrier gas experiences molecular flow. Molecular flow is characterized by high mean free paths and low pressures. During molecular flow, the mean free path of the gas is greater than the dimensions of the vacuum system. If K_n< 0.01, then the carrier gas experiences viscous flow, which is characterized by high pressures and

low mean free paths. If $1 \geq K_n \geq 0.01$, then the gas flow is in the transition range. The typical flow tube pressure and temperature for the purposes of the studies in this paper are 0.3-0.4 Torr and 298 K, respectively. A collisional cross section of 0.21 nm^2 has been determined for helium.[37] Substituting these values into eq. 2.3, a mean free path of 0.03-0.05 cm is calculated. Recognizing that the diameter of the flow tube is 7.3 cm, the Knudsen number for the flow in our flowing afterglow is 0.004-0.007, which places the flow for all our experiments in the viscous regime, as desired.

The gas flow can further be characterized as either turbulent or laminar. The Reynolds number, calculated from eq. 2.4, gives insight into whether the gas flow is laminar or turbulent,

$$R_e = \frac{v_{He} d \rho}{\eta} \tag{2.4}$$

where v_{He} is the average velocity of the carrier gas, ρ is the gas density, and η is the viscosity of the gas. When $R_e > 2200$, the carrier gas experiences turbulent flow while $R_e < 1200$ indicates laminar flow. Laminar flow is uniform, streamlined gas flow whereas turbulent flow is chaotic and non-uniform. The viscosity of helium and the gas density are 1.86×10^{-4} g cm^{-1} s^{-1} and 4.03×10^{-9} g cm^{-3}, respectively.[37] Recognizing this and the fact that the helium flow velocity was typically 7,000−8,000 cm s^{-1}, the Reynolds number for the carrier gas in the flow tube was 1.11−1.27, which places the gas in the flow tube in the laminar regime, as desired.

Laminar flow is also achieved before the gas reaches the reaction region. After helium introduction, the gas travels a finite distance, the entry length, l_{entry}, before laminar flow was reached. The equation for the entry length is displayed in eq. 2.5. For a flow tube diameter of

$$l_{entry} = \frac{R_e d}{30} \tag{2.5}$$

7.3 cm and Reynolds numbers in the range of 1.11−1.27, the entry length of the carrier gas is 0.27−0.31 cm , which is much less than the 10 cm between the helium carrier gas inlet and the reaction region.

The radial dependence of the velocity of a gas in a cylindrical tube under laminar conditions is described by the Poiseuille equation, eq. 2.6, where a is the radius of the tube,

$$v(r) = \left(\frac{\Delta P}{4L\eta}\right)(a^2\text{-}r^2) \tag{2.6}$$

r is the distance of the gas particle from the center of the tube, L is the length of the tube, and ΔP is the pressure differential between the beginning and end of the tube. The Poiseuille velocity profile is conically shaped with its maximum at the center of the tube and non-zero velocity at the walls. Because ions are sampled at an orifice at the center of the flow tube, the velocity of the sampled ions, v_{ion}, is the same as the maximum velocity of helium. This velocity has been previously characterized to be a factor, α or 1.6, multiplied times the average velocity of the helium carrier gas, eq. 2.7.[38]

$$v_{ion} = \alpha v_{He} \tag{2.7}$$

2.2 Quantitative Analysis via CR-MS

2.2.1 *Rate Coefficients*

2.2.1.1 *Introduction*

Before gases can be quantified using the CR-MS technique, the reaction under study must be characterized. Characterization involves collection of qualitative, full scan spectra, which indicates the ions to be monitored and utilized for analysis, as well as knowledge of the rate of

the reaction. The rate of the reaction can either be ideally measured as the observed rate coefficient, k_{obs}, calculated as the collisional rate coefficient, k_c.

2.2.1.2 *Measurement of the bimolecular rate coefficient, k_{II}*

For an ion-molecule reaction like the one displayed in eq. 2.8, the rate of change of the

$$AH^+ + B \rightarrow A + BH^+ \tag{2.8}$$

concentration of the reactant ion, $[AH^+]$, can be described by eq. 2.9, where t is the reaction time

$$\frac{d[AH^+]}{dt} = -k_{II}[AH^+][B] \tag{2.9}$$

in seconds, and k_{II} is the bimolecular rate coefficient. Recognizing that dt is related to the ion velocity, v_{ion} (cm/s), and the reaction distance, z (cm), by eq. 2.10, then eq. 2.11 can be written.

$$dt = \frac{dz}{v_{ion}} \tag{2.10}$$

$$\frac{d[AH^+]}{dz} = -\frac{k_{II}[AH^+][B]}{v_{ion}} \tag{2.11}$$

Substituting eq. 2.7 for the ion velocity into eq. 2.11 yields eq. 2.12. Rearranging eq. 2.12 to

$$\frac{d[AH+]}{dz} = -\frac{k_{II}[AH^+][B]}{\alpha v_{He}} \tag{2.12}$$

$$k_{II} = -\frac{d[AH^+]}{dz}\frac{\alpha v_{He}}{[AH^+][B]} \tag{2.13}$$

solve for k_{II}, eq. 2.13 is derived. The reagent ion concentration is proportional to its measured ion count rate, $\{AH^+\}$, times a constant, C, that is dependent on the specific parameters and settings of the instrument. A ratio of ion concentrations cancels out this constant and is equivalent to a ratio of ion count rates. Recognizing that $d\{AH^+\}/\{AH^+\}=d\ln\{AH^+\}$ results in

$$k_{II} = -\frac{d\{AH^+\}}{dz}\frac{\alpha v_{He}}{\{AH^+\}[B]} \tag{2.14}$$

eq. 2.15. The only variables in eq. 2.15 that are not known or that cannot be directly measured

$$k_{II} = -\frac{d\ln\{AH^+\}}{dz}\ \frac{\alpha v_{He}}{[B]} \tag{2.15}$$

in a flowing afterglow experiment are v_{He} and [B].

Because the helium carrier gas can be described as an ideal gas, v_{He} is derived from the ideal gas equation. Starting with eq. 2.16, where V is the reaction volume in cm^3, T is the

$$V = \frac{nRT}{P_{He}} \tag{2.16}$$

reaction temperature in Kelvin, P_{He} is the flow tube pressure in Torr, n is the number of moles of helium in the defined reaction volume, and R is the universal gas constant. Substituting $z\pi a^2$ for the reaction volume yields eq. 2.17. Differentiating with respect to time and recognizing that

$$z\pi a^2 = \frac{nRT}{P_{He}} \tag{2.17}$$

v_{He}=dz/dt and that F_{He}, the flow of helium in mol/s, is equivalent to dn/dt allows eq. 2.18 to be

$$\pi a^2 v_{He} = \frac{F_{He}RT}{P_{He}} \tag{2.18}$$

written. Substituting for π, 3.65 cm for a, 62,365.6 cm^3 Torr mol^{-1} K for R, and converting F_{He} (mol/s) to F_{He} (cm^3/s) at STP (273 K and 1 Torr), eq. 2.19 is derived for the average velocity

$$v_{He} = \frac{F_{He}T}{P_{He}} 6.684 \text{ x } 10^{-2} \tag{2.19}$$

of helium.

The concentration of the neutral in the flow tube, [B], is described via eq. 2.20, where F_B

$$[B] = \frac{F_B}{\pi a^2 v_{He}} \tag{2.20}$$

is the flow of the neutral in $cm^3\ s^{-1}$. Eq. 2.20 is then normalized to STP conditions. Recognizing that at STP the number density of an ideal gas is $3.535 \text{ x } 10^{16}$ particles cm^{-3} and substituting for πa^2, eq. 2.21 is reached. Substituting eq. 2.21 and eq. 2.19 into eq. 2.15 results in eq. 2.22 for

$$[B] = \frac{F_B}{v_{He}} 6.415 \text{ x } 10^{17} \tag{2.21}$$

$$k_{II} = -\frac{d\ln\{AH^+\}}{dz}\ \frac{\alpha T^2 F_{He}^2}{F_B P_{He}^2}\ 6.965 \times 10^{-21} \quad (2.22)$$

the bimolecular rate coefficient. Recalling that α is equivalent to 1.6 (Sec. 2.1.3) results in eq. 2.23, which includes only variables that can be directly measured within the laboratory.

$$k_{II} = -\frac{d\ln\{AH^+\}}{dz}\ \frac{T^2 F_{He}^2}{F_B P_{He}^2}\ 1.114 \times 10^{-20} \quad (2.23)$$

Therefore, in order to determine the rate constant in cm^3 $molecules^{-1}$ s^{-1} for a bimolecular rate coefficient, k_{II}, $\ln\{AH^+)$ is plotted vs. varying reaction distances with the slope of the line being directly related to the rate coefficient for the reaction. This was done by introducing a known, constant flow rate of neutral into the flow tube sequentially at ports 2 through 8 and recording the resultant reagent ion intensities.

A commonly reported parameter within the literature that is related to k_{obs} is the reaction efficiency, k_{eff}. The reaction efficiency is defined as the fraction of the time that an ion-molecule collision results in a reaction. This is calculated by the fraction k_{obs}/k_c, where k_c is the collisional rate coefficient.

2.2.1.3 *Calculation of the reaction rate at the collisional limit, k_c*

The collisional rate coefficient is the calculated rate if every collision results in a reaction. Therefore, k_c serves as the upper limit for the rate of a reaction. Various theories have been developed in order to calculate k_c.

The collisional rate constant is derived from an expression for the interaction potential, V(r), between an ion and neutral of interest. Gioumousis and Stevenson[39] developed Langevin theory, which assumes that the ion and neutral are point particles and that their long-range interaction can be described by eq. 2.24, where α is the polarizability of the neutral, q is the

$$V_L(r) = \frac{-\alpha q^2}{2r^4} \quad (2.24)$$

charge of the ion, and r is the distance between the ion and the center of mass of the neutral. Eq. 2.25 is then derived for k_L, the Langevin rate coefficient, where μ is the reduced mass of the

$$k_L = 2\pi q(\alpha/\mu)^{1/2} \quad (2.25)$$

ion-neutral pair. This theory is accurate for ion-molecule collisions where the neutral is a non-polar molecule. However, this theory does not account for the dipole moment of the neutral. As a result, for molecules with large dipole moments such as CH_3CN, k_{obs} is up to 400% larger than k_L.[40]

Moran and Hamill[41] modified Langevin theory into Locked-Dipole theory, which accounts for the effect of the permanent dipole of the neutral on k_c. The effective potential between the ion-molecule colliding pair is described by eq. 2.26, where μ_D is the permanent

$$V_{LD}(r) = V_L + (-q\mu_D/r^2)\cos\theta \quad (2.26)$$

dipole moment of the neutral and θ is the angle the dipole makes with r. A simplifying assumption is made that the dipole "locks in" at a certain θ, θ=0, and eq. 2.27 for the

$$k_{LD} = \pi[(4q^2\alpha/\mu)^{1/2}+(2q\mu_D/\mu v)] \quad (2.27)$$

Locked-Dipole rate constant, k_{LD}, is derived, where v is the relative velocity at infinite ion-molecule separation. At thermally averaged velocities, eq. 2.27 becomes eq. 2.28. k_{LD} typically

$$k_{LD} = (2\pi q/\mu^{1/2})[\alpha^{1/2}+\mu_D(2/\pi k_B T)^{1/2}] \quad (2.28)$$

is larger than k_{II}, especially when it comes to charge transfer reactions, where it can result in rate coefficients up to 250% larger than k_{obs}. In addition, Dugan et al.[42] have solved the equation of motion for a collision of an ion with a rotating molecule with the results indicating that "locking in" is not likely to occur.

Su and Bowers[43] modified Locked-Dipole theory into Average Dipole Orientation (ADO) theory to account for the fact that the orientation of the dipole in relation to the ion is better

described as random rather than "locked in". This has been achieved by calculating an average orientation, Ö, of the neutral in the ion-molecule collision. Ö is calculated by determining θ as a function of r from infinite distance, where θ=90°, to 5 Å, where θ=0° and approaches the Locked-Dipole approximation. The effective potential, $V_{ADO}(r)$, between an ion and neutral molecule under ADO theory is displayed by eq. 2.29, where L is the translational

$$V_{ADO}(r) = \frac{L^2}{2\mu r^2} - \frac{\alpha q^2}{2r^4} - \frac{q\mu_D}{r^2}\cos\ddot{\Theta}(r) \quad (2.29)$$

angular momentum. The translational angular momentum is further described by eq. 2.30, where

$$L = \mu b v \quad (2.30)$$

b is the impact parameter. The ADO rate constant, k_{ADO}, then is described by eq. 2.31, where c

$$k_{ADO} = (2\pi q/\mu^{1/2})[\alpha^{1/2} + c\mu_D(2/k_B\pi T)^{1/2}] \quad (2.31)$$

is a parameter that can be adjusted between 0 and 1 to compensate for the effectiveness of the charge "locking in". A c value of 1 results in the upper limit to k_c, equivalent to that predicted by Locked-Dipole theory, and a value of 0 is equivalent to the lower limit for k_c as predicted by Langevin theory. At constant temperature, c is a function of $\mu_D/\alpha^{1/2}$ only. The c values as a function of $\mu_D/\alpha^{1/2}$ have been previously determined by Su and Bowers[44] at varying temperature. ADO theory has been shown to accurately predict the dependence of the rate constant on the dipole moment of the neutral molecule.[45] However, as increasing measurements of k_{II} were compared to ADO theory, it was noticed that the measurements were consistently a factor of 1.6 larger than those predicted.[40] One of the possible explanations for this is the fact that ADO theory assumes there is no net transfer of angular momentum upon collision.

AADO theory is a modified form of ADO theory that accounts for the conservation of angular momentum within the ion-molecule system.[46] For simplicity of calculation, this theory assumes that the collision between the ion and dipole occurs in a plane. It also assumes that the

angular momenta are decoupled from the orbital motion and ion-induced rotation of the molecule. The translational angular momentum is then modified from ADO theory and eq. 2.30 to eq. 2.32, where C_L is the increase in angular momentum as r decreases. C_L can be

$$L = \mu b v\text{-}C_L \tag{2.32}$$

characterized using eq. 2.33, where I is the moment of inertia of the polar rigid rotor molecule

$$C_L = (2I E_R)^{1/2} - (I k_B T)^{1/2} \tag{2.33}$$

and E_R is the average rotational energy of the molecule in the plane of collision. Substituting into eq. 2.28, the effective AADO potential is described by eq. 2.34. For sake of simplicity, a

$$V_{AADO}(r) = \frac{(\mu b v\text{-}C_L)^2}{2\mu r^2} - \frac{\alpha q^2}{2r^4} - \frac{q\mu_D}{r^2}\cos\ddot{\Theta}(r) \tag{2.34}$$

parametrized AADO rate constant, eq. 2.35, was derived from V_{AADO}, which was shown to

$$k_{AADO} = (2\pi q/\mu^{1/2})[\alpha^{1/2} + c\mu_D(2/k_B\pi T)^{1/2} + Z\mu_D I^{1/2}/\mu^{1/4}] \tag{2.35}$$

reproduce the exact calculation to $\pm$3%. The first two terms of eq. 2.35 are k_{ADO} while the third term accounts for the angular momentum conservation. Z is the angular momentum parameter, which is dependent on temperature and has been calculated in the range of 200−600 K. AADO theory has been shown to predict the rate constant to <8% of the measured rate.[46]

The theory that is utilized within this paper as well as the most commonly utilized to calculate the collisional rate coefficient is Parametrized Trajectory Theory.[47] This theory assumes that all particles are point particles and that the potential energy between the ion and neutral is only influenced by ion-dipole and ion-induced dipole forces. Su and Chesnavich demonstrated that k_L is related to k_{cap}, the trajectory calculated rate, by eq. 2.36, where I^* and T_R

$$k_{cap} = K_{cap}(T_R, I^*)k_L \tag{2.36}$$

are described by eq. 2.37 and eq. 2.38, respectively. For small values of I^*, which is defined by

$$I^* = \mu_D I/\alpha q\mu \tag{2.37}$$

$$T_R = 2\alpha k_B T/\mu_D^2 \tag{2.38}$$

eq. 2.39 and is the case for most physically realistic systems, K_{cap} is equivalent to eq. 2.40, where

$$I^* \leq \frac{0.7+x^2}{2+0.6x} \tag{2.39}$$

$$K_{cap} = \begin{cases} 0.4767x+0.6200; & x\geq 2 \\ \frac{(x+0.5090)^2}{10.526} + 09754; & x\leq 2 \end{cases} \tag{2.40}$$

$x=T_R^{-1/2}$. Parameterized Trajectory theory has been suggested to be accurate to within 3% of k_{obs}.[47]

2.2.2 *Quantification of Trace Gases*

2.2.2.1 *Derivation*

The expression for the quantification of trace gases can be derived by starting with a chemical equation such as eq. 2.8 and an expression for the change with respect to time for the concentration of the trace neutral, eq. 2.41. Rearranging eq. 2.41 then yields eq. 2.42. Assuming

$$\frac{d[B]}{dt} = -k_{II}[AH^+][B] \tag{2.41}$$

$$\frac{d[B]}{[B]} = -k_{II}[AH^+]dt \tag{2.42}$$

that $[AH^+]$ is constant and integrating with respect to time from t=0 to t=t results in eq. 2.43 and eq. 2.44. Recognizing that $[B]_t$ is equivalent to $[B]_0$-$[BH^+]_t$ and substituting this expression in

$$\ln([B]_t/[B]_0) = -k_{II}[AH^+]t \tag{2.43}$$

$$[B]_t/[B]_0 = e^{-k_{II}[AH^+]t} \tag{2.44}$$

eq. 2.44 results in eq. 2.45. Assuming that $k_{II}[AH^+]t<<1$ and recognizing that $\lim_{x\to 0}(1-e^{-x})=x$,

$$[B]_0 = \frac{[BH^+]}{1-e^{-k_{II}[AH^+]t}} \tag{2.45}$$

eq. 2.45 becomes eq. 2.46. Recalling that the ratio of two ion concentrations is simply a ratio of

$$[B]_0 = \frac{[BH^+]}{k_1[AH^+]t} \tag{2.46}$$

their raw ion count intensities (**Sec. 2.2.1.2**), leads to eq. 2.47 for the number density of the neutral.

$$[B]_0 = \frac{\{BH^+\}}{k_1\{AH^+\}t} \tag{2.47}$$

$$t = \frac{zP_{He}\pi a^2}{\alpha F_{He}RT} \tag{2.48}$$

When the neutral reacts with multiple ions and the effect of radial diffusion of the ions is neglected, the number density of the neutral has been suggested to be equivalent to eq. 2.49,

$$[B]_0 = \frac{1}{t}\frac{I_{p1}+I_{p2}+I_{p3}\ldots}{I_{i1}k_1+I_{i2}(k_1+k_2)/2+I_{i3}(k_1+k_3)/2\ldots} \tag{2.49}$$

where I_{p1}, I_{p2}, and I_{p3} represent the intensities of the ionic products, I_{i1}, I_{i2}, and I_{i3} represent the intensities of the reactant ions, and k_1, k_2, and k_3 are the rate constants for the reaction of each of the individual reactant ions with neutral.[48] The error associated with the CR-MS technique for quantification of trace gases is $\pm$ 20%. This is due to the fact that the error typically associated with the measurement of the rate coefficient is $\pm$ 20% and that this is the only major source of error associated with CR-MS analysis.[48]

With knowledge of the number density of the neutral, the concentration of the VOC in the sample headspace and flow tube can be determined. The concentrations of the analyte in the sample and flow tube are determined through the utilization of number density mixing ratios, eq. 2.50 and eq. 2.51. It should be recognized that the concentration of the neutral in the sample

$$[B]_{ppm} = \frac{[B]_0}{[Sample]}10^6 \tag{2.50}$$

$$[B]_{ppb} = \frac{[B]_0}{[Helium]}10^9 \tag{2.51}$$

headspace is on the order of parts per million while that in the flow tube is on the order of parts per billion. This is because the sample is diluted by the helium carrier gas upon its introduction into the flow tube.

2.2.2.2 *Underlying Assumptions*

Using eq. 2.7 as an example, the first assumption in the utilization of the CR-MS technique to quantify trace VOCs is that $\{AH^+\}$ is constant throughout the experiment. This is accomplished by ensuring that the intensity of the reagent ion is much greater than its corresponding product ion intensity. $\{AH^+\}$ was typically on the order of 3×10^6 cps (counts per second) while $\{BH^+\}$ for reactions with k_{eff}=1 was never greater than 100,000 cps and often no greater than 50,000 cps. The intensity of the product ions is, therefore, $\leq 3\%$ and often $\leq 1\%$ of the reagent ion intensity, resulting in a constant $\{AH^+\}$.

The second assumption is that $k_{II}\{AH^+\}t << 1$. If eq. 2.48 is evaluated with F_{He} as 7,000 cm s^{-1}, a as 3.65 cm, z as 36.3 cm, P_{He} as 0.3 Torr, T as 298 K, α as 1.6 (**Sec 2.1.3**), and R as 62,365.6 cm^3 Torr mol^{-1} K^{-1} as common experimental conditions then a reaction time of 2.19×10^{-9} s is calculated. If k_{II} and $\{AH^+\}$ are taken as 2.5×10^{-9} cm^3 s^{-1}, which is the rate of a very fast ion-molecule reaction, and 3×10^6 cps, respectively, then $k_{II}\{AH^+\}t$ is equivalent to 1.64×10^{-11}, which is much less than 1.

A third assumption is that diffusive losses of ions are negligible and that ions are only lost via reaction. Diffusive losses result in erroneously high count rates for the heavier, often product, ions as the lighter ones diffuse faster to the walls. This effect has been previously quantified using the diffusion enhancement factor, D_e, as is displayed in eq. 2.52, where $D(AH^+)$

$$D_e = \frac{\exp\left(t\frac{D(AH^+)-D(BH^+)}{\Lambda^2}\right)-1}{t\frac{D(AH^+)-D(BH^+)}{\Lambda^2}} \qquad (2.52)$$

and $D(BH^+)$ are the diffusion coefficients in the carrier gas for the reactant ion and product ion, respectively, and Λ is the characteristic diffusion length for the vessel.[49] For large, cylindrical flow tubes, as is the case here, Λ has been shown to be equivalent to eq. 2.53, where A is the

$$\Lambda = \sqrt{A/18.17} \tag{2.53}$$

cross sectional area of the flow tube. When diffusion is accounted for, the rate of reaction can be described by eq. 2.54.[50] This is especially useful in narrow flow tubes where diffusion is

$$[B]_0 = \frac{1}{t}\frac{I_{p1}/D_{ep1}+I_{p2}/D_{ep2}+I_{p3}/D_{ep3}\ldots}{I_{i1}k_1/D_{ei1}+I_{i2}(k_1+k_2)/(2D_{ei2})+I_{i3}(k_1+k_3)/(2D_{ei3})\ldots} \tag{2.54}$$

significant. Comparing the mean free path for particles in the flow tube, ≈0.04 cm (**Sec 2.1.3),** to the radius of the flow tube, 3.65 cm, and recalling that the gases in the flow tube experience laminar flow, it is apparent that diffusive losses of ions to the walls is negligible in our flow tube. This is a safe assumption for larger flow tubes.

The last assumption is that the effect of mass discrimination is negligible. Mass discrimination is a tendency for ions of different *m/z* values to be transmitted with different efficiencies through the orifice plate and mass analyzer. This leads to diminished intensities at higher masses. It has been shown previously that this effect is dependent primarily on the resolution setting of the quadrupole and, to a lesser extent, the energy of the ions in the analyzing field.[49] Mass discrimination is an instrumental side effect, however, and a large, high quality analytical quadrupole, like the one in our flowing afterglow, is expected to have a small degree of mass discrimination, especially under 150 amu. In addition, the minimal diminishing effect of mass discrimination at higher masses is for all intensive purposes negated by the minimal diffusion enhancement.

3.0 DETERMINATION OF THE ACCURACY OF THE CR-MS TECHNIQUE VIA HENRY'S LAW

3.1 Background

The two most commonly utilized methods of VOC detection are Gas Chromatography Mass Spectrometry (GC-MS) and electronic noses. One of the main disadvantages to the utilization of these techniques, however, is the need for external calibration such as the use of prepared standards. While the theory of CR-MS towards VOC quantitation demonstrates that external calibration is not necessary, it is still appropriate to demonstrate the accuracy of the CR-MS technique.

Under the assumption that a solution is dilute, Henry's Law relates the concentration of an analyte dissolved in that solution to the concentration in the headspace above it. Henry's Law, eq. 3.1, where C_{HS} is the headspace concentration of the analyte by number density, C_{soln} is

$$C_{HS} = \frac{1}{k_H} C_{soln} \tag{3.1}$$

the concentration of the analyte in solution in molarity, and k_H is the Henry's Law constant in M/atm.[51] Henry's Law constants for many analytes have been measured and exist in compilations.[25,51] Utilization of the CR-MS technique to determine analyte concentrations above aqueous solutions of known concentrations has been one method to determine Henry's Law constants.[52,53,54]

Herein, the accuracy with which our flowing afterglow mass spectrometer quantifies trace VOCs through the CR-MS technique is determined via comparison of measured Henry's Law constants for acetonitrile, acetone, benzaldehyde, and THF in water with those from the literature. In the first part of this study, the headspaces above a series of acetone or acetonitrile solutions in water were quantified to determine the Henry's Law constants. To determine the accuracy of our flowing afterglow as a CR-MS instrument for quantification of multiple analytes, Henry's Law constants for benzaldehyde and THF were measured from quantifying the headspaces above a series of aqueous solutions containing both benzaldehyde and THF.

3.2 Experimental

3.2.1 *Reagents and Chemicals*

The following chemicals were used without any further purification: acetone (99%, Fisher Scientific), acetonitrile (99%, Fisher Scientific), benzaldehyde (>98%, Sigma-Aldrich), tetrahydrofuran (>99.5%, EMD Chemicals), and distilled water, utilized for solution preparation.

3.2.2 *Sample Preparation*

Distilled water, utilized to make the reagent ions, was placed in a 250 mL round-bottom flask and degassed via the freeze-pump-thaw technique.

Acetone and acetonitrile solutions of 5, 50, 500, and 5000 ppm (v/v) were prepared in the following manner. All glassware with the exception of volumetric flasks and pipettes were

baked overnight at 150°C prior to their use. A 500 µL aliquot of either acetone or acetonitrile was transferred via micropipette into a 100 mL volumetric flask and diluted to the mark to make a 5,000 ppm stock solution. A 500 ppm solution was made by transferring 10 mL of the 5,000 ppm solution via pipette (TD) into a 100 mL flask and diluting to the mark. Solutions of 50 and two 5 ppm solutions were made by similar serial dilutions using a 100 mL volumetric flask. A 25 mL portion of each solution was transferred into its own 250 mL single-neck round-bottom flask and capped with a septum prior to analysis. This entire procedure was repeated to create three sets of acetonitrile solutions and two sets of acetone solutions.

Acetone solutions of 5, 60, 260, and 500 ppm (v/v) for the third acetone run were constructed in the following manner. All glassware, with the exception of volumetric flasks and pipettes, were baked overnight at 150°C prior to their use. A 5 µL aliquot of acetone was transferred via micropipette into a 1 L flask and diluted to the mark with distilled water. The 60, 260, and 500 ppm (v/v) solutions were prepared in a similar manner. A 25 mL portion of each solution was transferred into its own 250 mL single-neck round-bottom flask and capped with a septum prior to analysis.

Benzaldehyde/THF solutions of 0:10, 10:20, 20:30, 30:40, 40:50, and 50:0 µM were made in the following fashion. All glassware, with the exception of volumetric flasks and pipettes, were baked overnight at 150°C prior to their use. Aliquots of 50 µL of benzaldehyde and 40 µL of THF were transferred via micropipette into separate 1 L volumetric flasks and diluted to the mark with water to make 500 µM stock solutions. Via pipettes (TD), 2 and 4 mL of the benzaldehyde and THF stock solutions, respectively, were transferred to a 100 mL volumetric flask and diluted to the mark to make the 10:20 µM benzaldehyde/THF solution. The 0:10, 20:30, 30:40, 40:50, and 50:0 µM benzaldehyde/THF solutions were made in similar

manners. A 25 mL portion of each solution was transferred into its own 250 mL single-neck round-bottom flask and capped with a septum prior to analysis. This entire procedure was repeated to create two sets of solutions, corresponding to the first two benzaldehyde/THF runs.

Benzaldehyde/THF solutions of 98:123, 196:247, 294:370, 393:493, and 491:617 μM were prepared as follows. All glassware with the exception of volumetric flasks and pipettes were baked overnight at 150°C prior to their use. Aliquots of 10 μL of benzaldehyde and 10 μL of THF were transferred via micropipette into a 1 L volumetric flask and diluted to the mark with water to make the 98:123 μM benzaldehyde/THF solution. The 196:247, 294:370, 393:493, and 491:617 μM benzaldehyde/THF solutions were prepared in a similar manner. A 25 mL portion of each solution was transferred into its own 250 mL three-neck round-bottom flask, capped with septa, which included one septum pierced by a cannula in order to keep the sample at atmosphere. This set of solutions corresponds to the third benzaldehyde/THF run.

3.2.3 *Data Collection*

The general procedure for data collection is explained in **Sec. 2.1**. Only details particular to these experiments are mentioned here. During data collection, a solenoid valve (port) and on/off valve to the lower arm of the vacuum rack were open, the metering valve on the lower arm of the vacuum rack was attached to a cut syringe and hypodermic needle via Cajon connection and set to a specific flow, and the on/off valve to the vacuum pump and on/off valve to the calibration bulb in the vacuum rack were closed, **Figure 3.1**. Port 3, corresponding to a

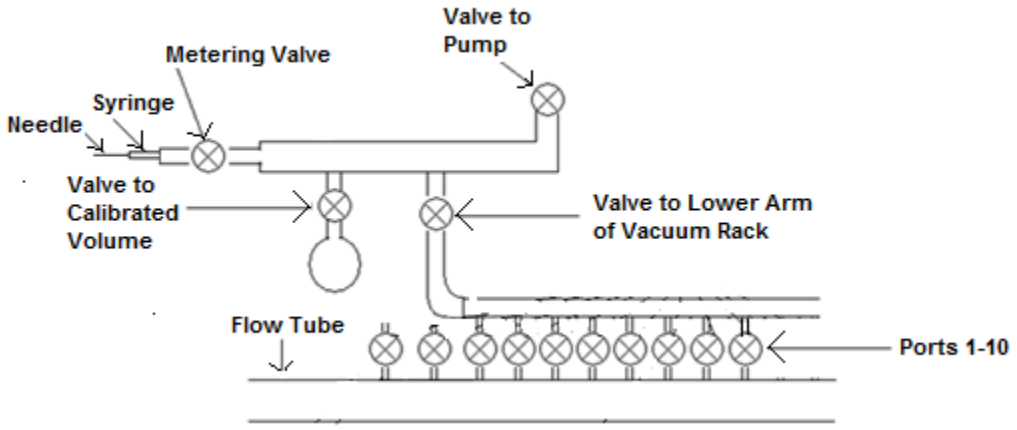

Figure 3.1: Diagram of the neutral introduction apparatus for the Henry's Law experiments.

reaction distance of 36.3 cm, was utilized for all of the acetone experiments, all of the acetonitrile experiments, and the third run of the benzaldehyde/THF experiments. Port 4, corresponding to a reaction distance of 45.4 cm, was utilized for the first two runs of the benzaldehyde/THF experiments. Water vapor was introduced, in the standard fashion, into the ion source to produce the hydronium ion. Background spectra, where lab air was added to the flow tube via the needle to port as shown in **Figure 3.1**, were collected for 2-3 minutes. The septum of one of the sample flasks was then pierced via the needle (**Figure 3.1**) and the sample's headspace was introduced into the flow tube, **Figure 3.2** and **Figure 3.3**. The sample's headspace was then allowed to react with the reagent ions for 2-5 minutes. minutes. The sample flask was then removed and background spectra were again collected for 2-3 minutes. This procedure was repeated for each sample solution. Before and after all the experiments for that day, the flow of the sample was measured via the $\Delta P/\Delta t$ method **(Sec. 2.1.1)**.

Spectra for the acetonitrile and acetone experiments were collected in full scan mode (10-100 amu, 8 points/amu, 1 s/scan). Spectra for the benzaldehyde/THF experiments

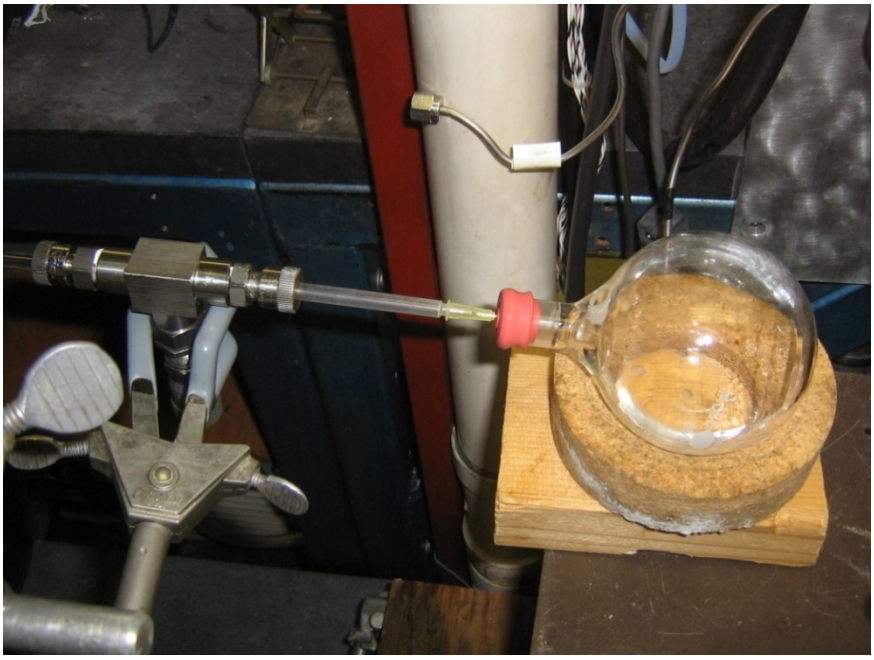

Figure 3.2: Method of introduction into the flow tube for the headspaces of all the acetonitrile and acetonitrile solutions as well as those for runs one and two of the benzaldehyde/THF solutions.

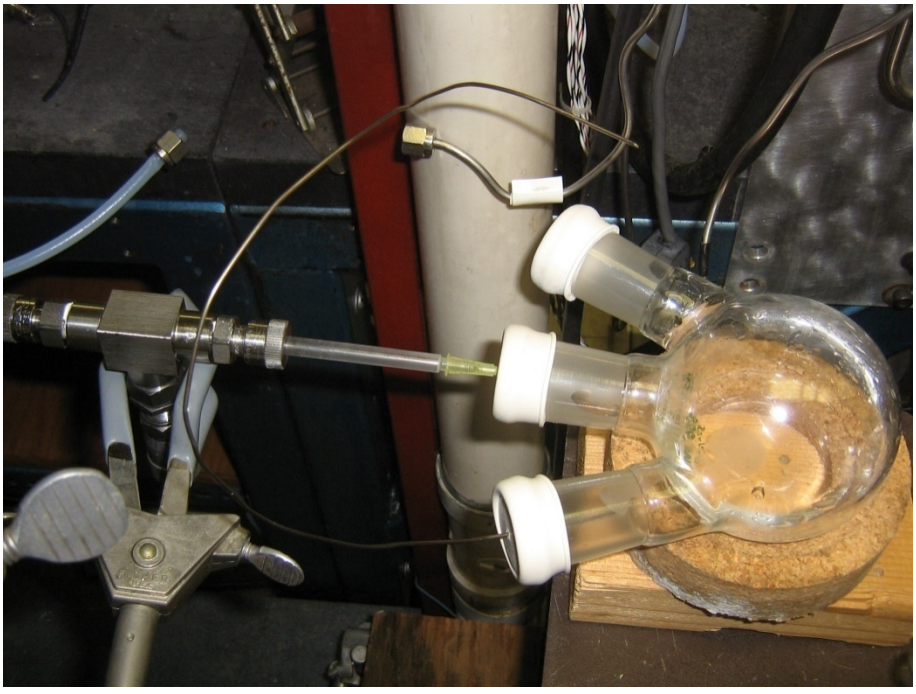

Figure 3.3: Method of introduction into the the flow tube for the headspaces of the third run of the benzaldehyde/THF solutions.

were collected in SIM mode; runs 1 and 2 (10 points/amu, 2 s/scan) and run 3 (10 points/amu, 5 s/scan). SIM windows were 2 amu wide and centered on *m/z* 15, *m/z* 19, *m/z* 37, *m/z* 55, *m/z* 73, *m/z* 91, *m/z* 107, and *m/z* 125. *m/z* 15 was collected in all cases to be utilized as a noise ion; an ion in an experiment that can only be attributable to instrumental noise. *m/z* 19, *m/z* 37, *m/z* 55, and *m/z* 73 were collected to measure the signal intensities of the hydronium ion and its first, second, and third hydrates. The *m/z* range in the acetone experiments was chosen to include the noise ion, hydronium and hydrates, protonated acetone (*m/z* 59), the first hydrate of acetone (*m/z* 77), and the second hydrate of acetone (*m/z* 95). The *m/z* range in the acetonitrile experiments was chosen to include the noise ion, hydronium and hydrates, protonated acetonitrile (*m/z* 42), first hydrate of acetonitrile (*m/z* 60), and second hydrate of acetonitrile (*m/z* 78). For the benzaldehyde/THF experiments, the *m/z* windows were selected to account for the noise ion, hydronium ion and its hydrates, protonated THF (*m/z* 73), the first hydrate of protonated THF (*m/z* 91), protonated benzaldehyde, (*m/z* 107), and the first hydrate of protonated benzaldehyde (*m/z* 125).

3.2.4 *Data Analysis*

The following was performed within the Merlin software. Background spectra were averaged and utilized to determine the *m/z* values for each reagent ion of interest. Spectra during sample introduction were averaged and used to determine the *m/z* values of interest for each of the acetone, acetonitrile, and benzaldehyde/THF experiments. For each experiment, chromatogram lists, intensity (cps) vs. time (s), were created for each of the relevant average *m/z* values at maximum intensities via a macro that computes the intensities as the area under five

points about the *m/z*. These lists were exported from the Merlin software and imported into Excel (Microsoft Office 2007).

The concentration of the analytes of interest in the headspaces of each flask was calculated in Excel using the method described in **Sec 2.2.2**. The exported chromatogram lists were used to determine the ion intensities utilized in eq. 2.49. For all experiments, the reactant ion intensities for the *m/z* values about 19, 37, 55, and 73 were calculated by averaging the intensities during the background regime. The product ion intensities for the *m/z* values about 59, 77, and 95 for the acetone experiments, 42, 60, and 78 for the acetonitrile experiments, and 107 and 125 for the benzaldehyde/THF experiments were calculated by averaging the intensities over the time period corresponding to the first two minutes of sample introduction. Because protonated THF and its first hydrate are isobaric with $H_3O(H_2O)_3^+$ and $H_3O(H_2O)_4^+$ respectively, the utilized intensities of *m/z* 73 and *m/z* 91 for the benzaldehyde/THF studies were determined by averaging the intensities over the time period corresponding to the two minutes of sample detection followed by subtraction of the average *m/z* 73 and *m/z* 91 background intensities, respectively. The rate constants utilized for the reactions of H_3O^+, $H_3O(H_2O)^+$, $H_3O(H_2O)_2^+$, and $H_3O(H_2O)_3^+$ with acetone, acetonitrile, benzaldehyde, and THF were determined from previous measurements and/or Parametrized Trajectory Theory (**Sec. 2.2.1.3**), Table 3.1. When the measured rate constants, k_{obs}, were available, as was the case for the reactions of acetone and acetonitrile with the hydronium ion and its hydrates, they were utilized over k_{coll}. k_{coll} was calculated and utilized, as was the case for benzaldehyde and THF, when no prior measurements of the rate constant were available. A test of the assumption that the k_{coll} values are accurate predictions of the rate coefficients is in the Results and Discussion.

Table 3.1: Rate coefficients of the hydronium ion and its hydrates with acetone, acetonitrile, benzaldehyde, and THF that were utilized for headspace analysis via the CR-MS technique. All rate coefficients are reported in units of x10^{-9} cm^3 $molecule^{-1}$ s^{-1}. In parentheses are the k_{obs} literature values used to determine the rate constant for analysis.

	Acetone	Acetonitrile	Benzaldehyde	THF
H_3O^+	3.90 (3.9[b],3.9[c],3.9[d],3.8[e])	5.10 (5.1[b],4.9[e],5.1[h],4.7±0.7[d])	4.36[a]	2.67[a]
$H_3O(H_2O)^+$	3.20 (3.2[e],3.3[f],3.5±0.9[g])	4.00 (4.0[e],4.0[i])	3.34[a]	2.10[a]
$H_3O(H_2O)_2^+$	2.80 (2.8[e],2.5[f],3.0±0.8[g])	3.70 (3.6[e],3.7[i])	2.91[a]	1.85[a]
$H_3O(H_2O)_3^+$	2.40 (2.4[e],2.4[f],2.9[g])	3.50 (3.4[e],3.5[i])	2.66[a]	1.72[a]

[a]Calculated from Parametrized Trajectory Theory (**Appendix A**)
[b]Lindinger et al.[31]
[c]Adams et al.[55]
[d]Mackay et al.[56]
[e]Castleman et al.[57]
[f]Spanel and Smith[58]
[g]Bohme et al.[59]
[h]Spanel and Smith[60]
[i]Smith et al.[61]

The temperature normalized Henry's Law constants, k_H^θ, were then determined in the following fashion. For each run, headspace concentrations in ppm by number density vs. solution concentration in μM were plotted for each analyte of interest. The Henry's Law constant at that particular temperature, k_H, was determined as the inverse of the slope of the line of each plot. k_H^θ was then calculated using eq. 3.2, where T^θ is the standard temperature in

$$k_H^\theta = k_H / e^{-\Delta H_{soln}/R\left(\frac{1}{T}-\frac{1}{T^\theta}\right)} \quad (3.2)$$

Kelvin, 298.15 K, and $\Delta H_{soln}/R$ is an experimentally determined constant that is analyte and solvent dependent. From previous studies, 5100, 4100, 4800, and 5700 were substituted for $\Delta H_{soln}/R$ for acetone, acetonitile, benzaldehyde, and THF, respectively.[51]

3.3 Results and Discussion

Intensities utilized in eq. 2.49 for quantification of each analyte for each *m/z* studied were obtained from a macro that computes the area under five points about a specific *m/z*. For a typical peak resulting from the particular conditions in these Henry's Law experiments, integrating under five points about the maximum peak intensity allowed much of the peak to be analyzed without also integrating under another peak; **Figure 3.4, Figure 3.5, Figure 3.6,** and **Figure 3.7.** This is significant as all data points that compose a specific peak correspond to the same nominal *m/z*.

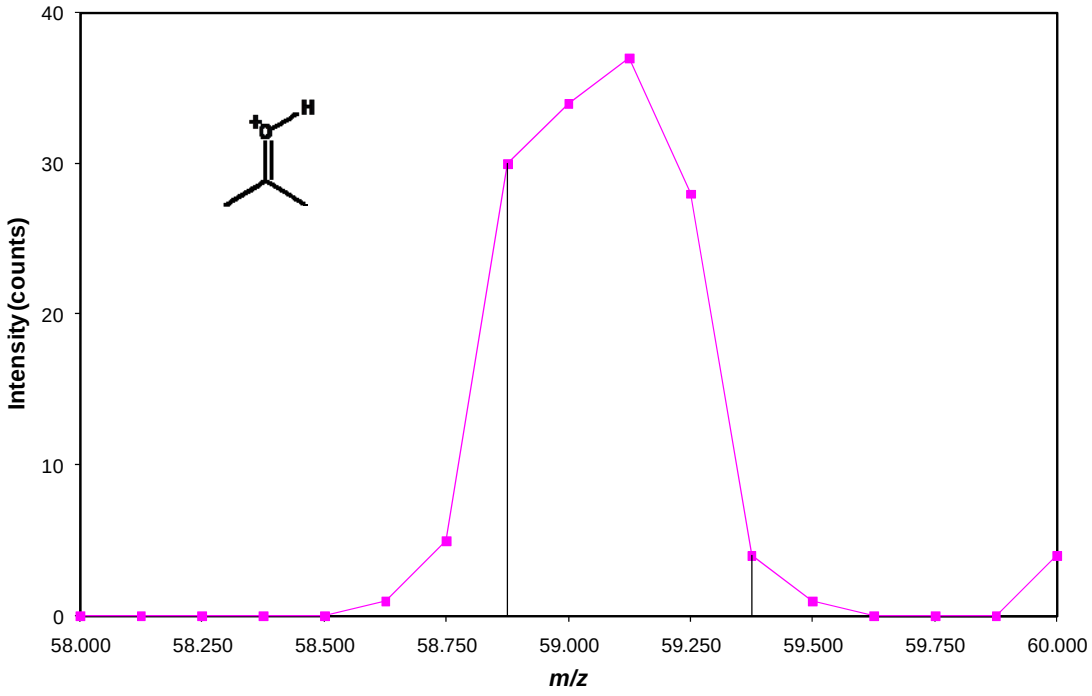

Figure 3.4: Peak profile for a peak about *m/z* 59 under the particular instrumental parameters utilized in the acetone Henry's Law experiments. Vertical lines indicate the limits of integration of the macro.

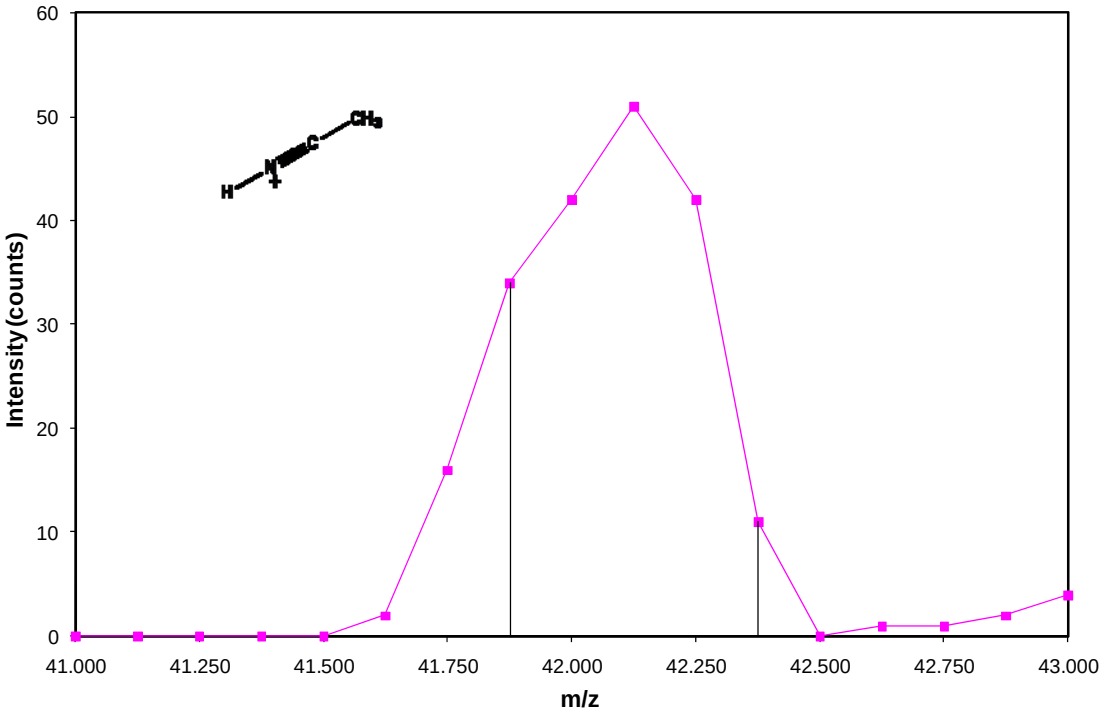

Figure 3.5: Peak profile for a peak about *m/z* 42 under the particular instrumental parameters utilized in the acetonitrile Henry's Law experiments. Vertical lines indicate the limits of integration of the macro.

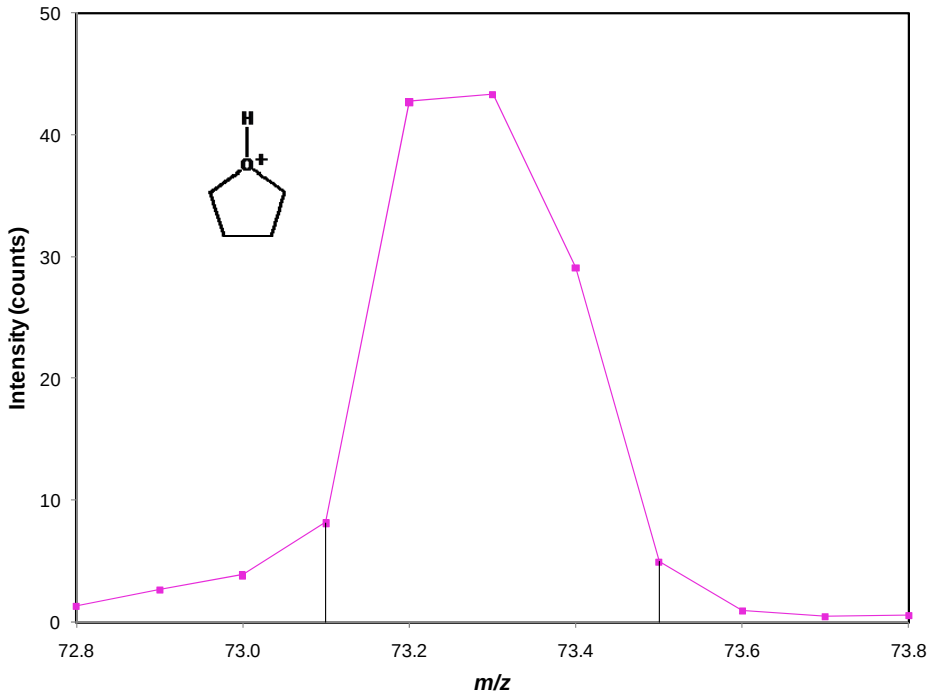

Figure 3.6: Peak profile for a peak about *m/z* 73 under the particular instrumental parameters utilized in the benzaldehyde/THF Henry's Law experiments. Vertical lines indicate the limits of integration of the macro.

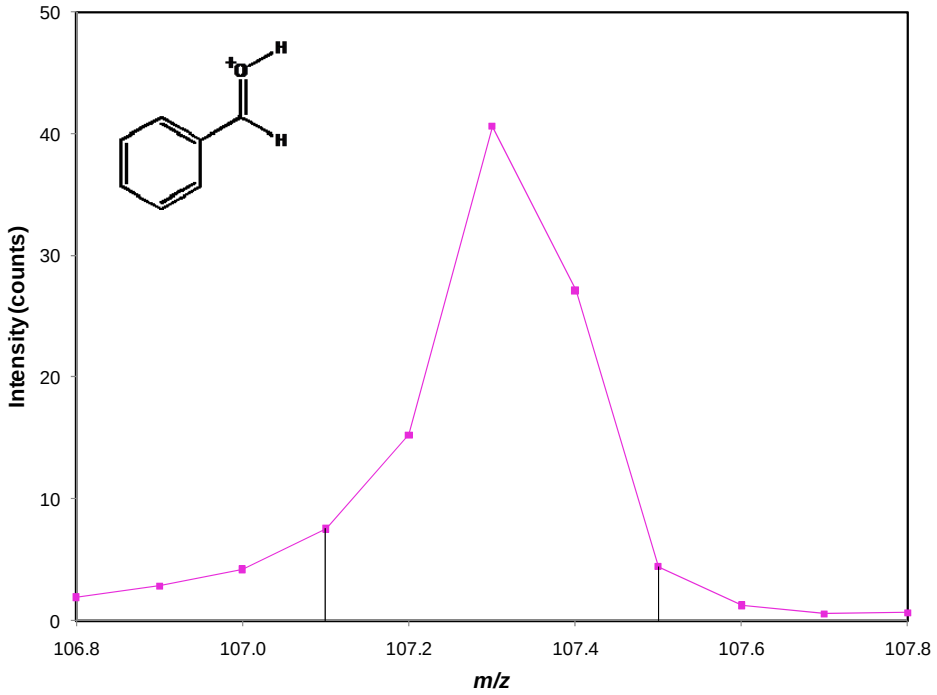

Figure 3.7: Peak profile for a peak about *m/z* 107 under the particular instrumental parameters utilized in the benzaldehyde/THF Henry's Law experiments. Vertical lines indicate the limits of integration of the macro.

The rate coefficients listed in Table 3.1 that were utilized to measure headspace concentrations of acetone, acetonitrile, benzaldehyde, and THF were obtained through previous studies or through calculation of the collisional rate coefficient, k_{coll}. Paramaterized Trajectory Theory was utilized to calculate the rate coefficients for the reactions of H_3O^+, $H_3O(H_2O)^+$, $H_3O(H_2O)_2^+$, and $H_3O(H_2O)_3^+$ with benzaldehyde and THF (**Appendix A**) because the rate coefficients of these reactions have not been measured. In order to utilize collisional rate coefficients to measure VOC concentrations, it is necessary to assume that the reactions proceed at the collisional rate. In general, exothermic proton transfer reactions from H_3O^+, which is the expected case for both benzaldehyde, ΔH_{rxn}= -34 kcal/mol, and THF, ΔH_{rxn}= -32 kcal/mol, have been demonstrated as proceeding at or near the collisional rate.[14,15] In addition to proton

transfer, the hydrates of the hydronium ion can react via ligand-switching reactions, eq. 3.3.

$$H(H_2O)_2^+ + A \rightarrow HA(H_2O)^+ + H_2O \quad (3.3)$$

Fortuitously, both proton transfer and ligand-switching reactions of neutrals with $H_3O(H_2O)^+$, $H_3O(H_2O)_2^+$, and $H_3O(H_2O)_3^+$ often proceed near or at the collisional rate, Table 3.2. Bohme et

Table 3.2: Comparison of the observed rate coefficients, k_{obs}, to the collisional rate coefficients, k_{coll}, calculated by Parameterized Trajectory Theory, for the reactions of $H_3O(H_2O)^+$, $H_3O(H_2O)_2^+$, and $H_3O(H_2O)_3^+$ with acetone, acetonitrile, methyl acetate, methanol, and ethanol. Values in parentheses are literature rate constants utilized to determine the best rate constant for comparison to k_{obs}.

	$H_3O(H_2O)^+$			$H_3O(H_2O)_2^+$			$H_3O(H_2O)_3^+$		
	k_{obs}	k_{coll}	k_{eff}	k_{obs}	k_{coll}	k_{eff}	k_{obs}	k_{coll}	k_{eff}
Acetone	3.2 (3.2[c], 3.3[d],3.5±0.9[e])	3.2	1.00	2.8 (2.8[c],2.5[d],3.0±0.8[e])	2.8	1.00	2.4 (2.4[c],2.4[d],2.9[e])	2.6	0.92
Acetonitrile	4.0 (4.0[c],4.0[e])	4.2	0.95	3.7 (3.6[c],3.7[e])	3.8	0.97	3.5 (3.4[c],3.5[e])	3.6	0.97
Methyl Acetate	2.2[c]	2.1	1.05	1.9[c]	1.9	1.00	1.7[c]	1.7	1.00
Methanol	2.2 (1.9[d],2.4±0.6 [e])	2.2	1.00	2.0 (1.9[d],2.0±0.5[e])	2.1	0.95	1.9 (1.9±0.5[e])	2.0	0.95
Ethanol	2.4 (2.3[d],2.5±0.6[e])	2.2	1.09	2.0 (2.1[d],2.0±0.5[e])	2.0	1.00	1.7 (1.7±0.4[e])	1.9	0.90

[a]All rate constants are in units of $x10^{-9}$ cm^3 s^{-1}
[b]Parameters utilized to calculate k_{coll} are in **Appendix A**
[(c)]Castleman et al.[57]
[d]Spanel and Smith[58]
[e]Bohme et al.[59]
[f]Smith et al.[61]

al.[59] have demonstrated that this is the case for all of the first three hydrates of the hydronium ion whenever the gas-phase basicity (GB) of the neutral is greater than 173 kcal/mol and the proton affinity is greater than 181 kcal/mol. Benzaldehyde and THF fulfill both of these requirements; (**Appendix B)**.

Henry's Law plots were created by plotting headspace concentration in ppm by number density vs. solution concentration in μM. The 5,000 ppm (v/v) acetone and acetonitrile

experiments were not fitted to the Henry's Law plots because it cannot be assumed that the headspaces of these solutions were accurately quantified. The intensities of *m/z* 19 and m/z 37, corresponding to H_3O^+ and $H_3O(H_2O)^+$, were not constant, **Figure 3.8** and **Figure 3.9**, and

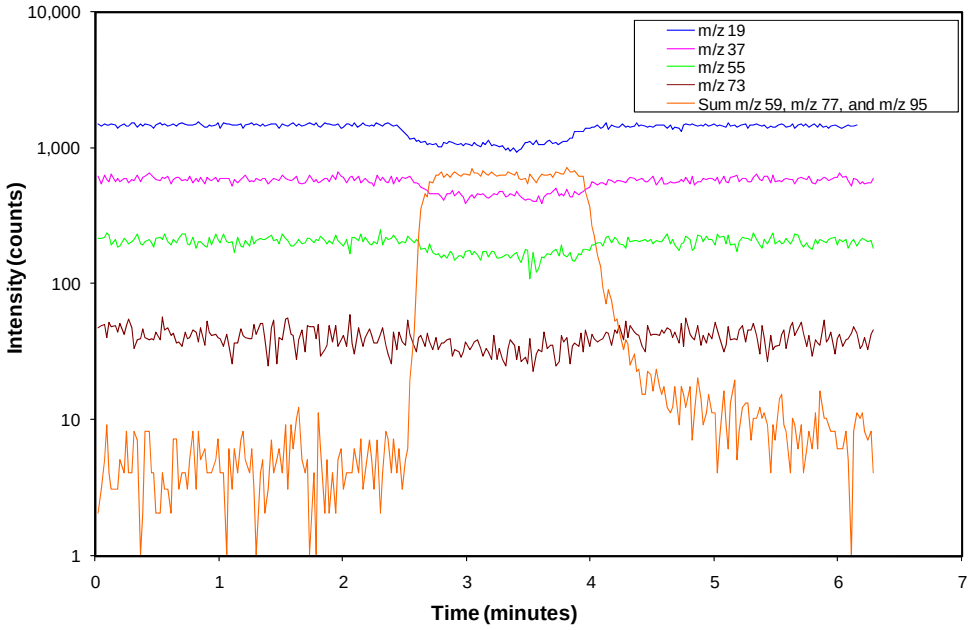

Figure 3.8: Chromatogram for the quantification of the headspace of the 5,000 ppm(v/v) acetone solution.

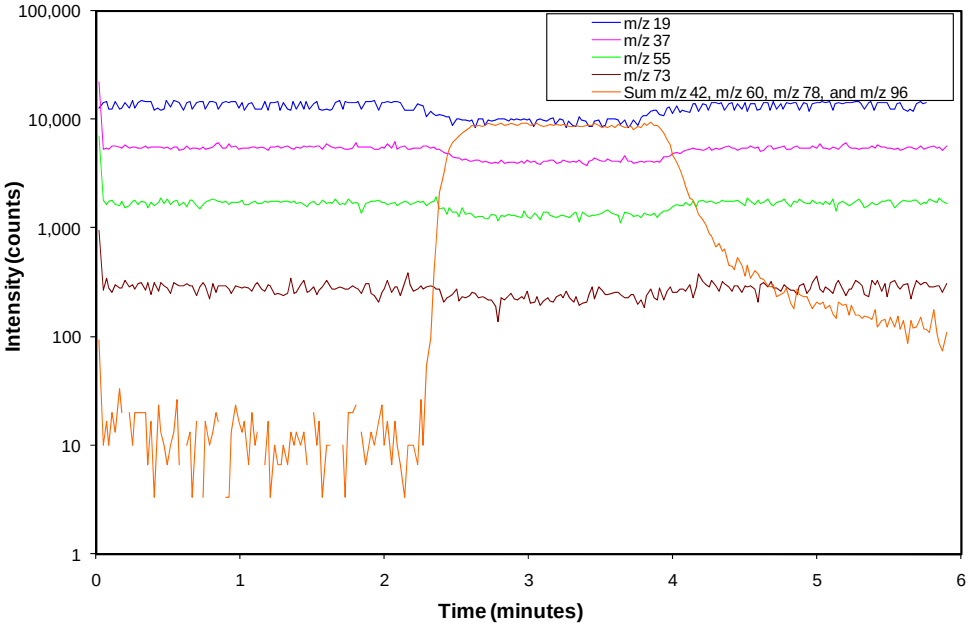

Figure 3.9: Chromatogram for the quantification of the headspace of a 5,000 ppm(v/v) acetonitrile solution.

pseudo-first order reaction conditions could not be assumed to exist. Because pseudo-first order conditions are one of the assumptions made in order to utilize the CR-MS technique (**Sec. 2.2.2.2**), the headspaces above the 5,000 ppm (v/v) acetone and acetonitrile solutions cannot be assumed to be accurately quantified. A chromatogram of acceptable quality for CR-MS analysis is displayed in **Figure 3.10**. Headspace concentrations of the

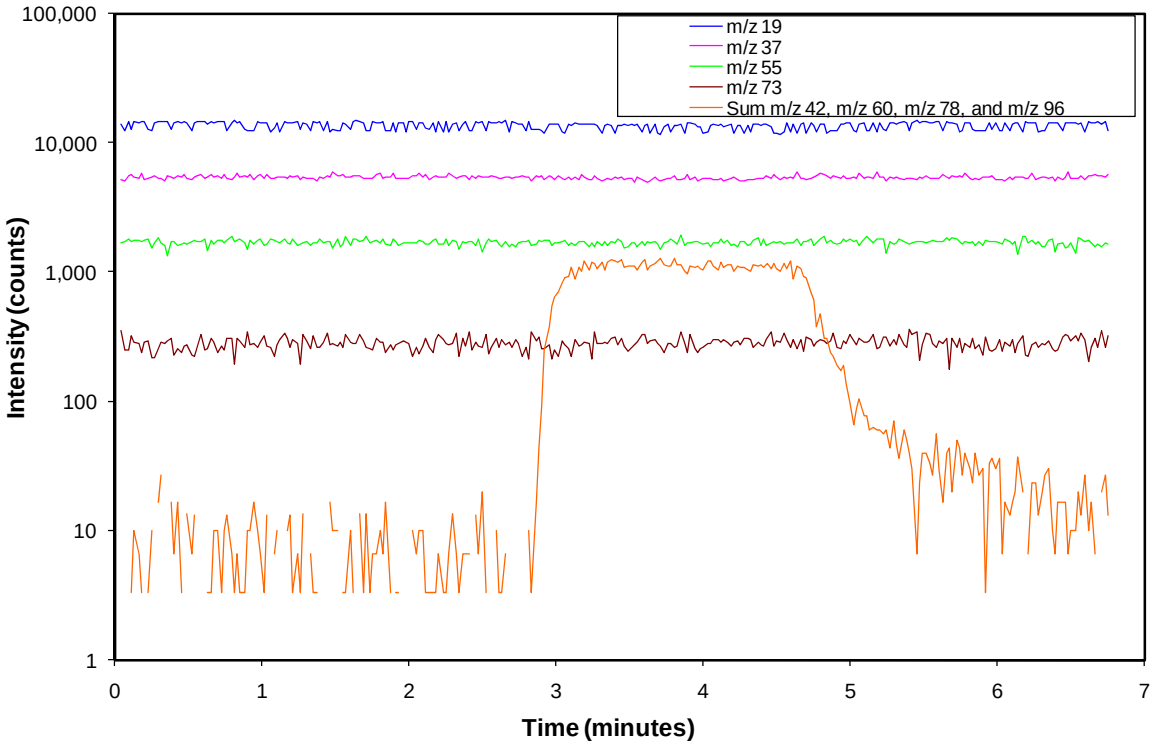

Figure 3.10: Chromatogram for the quantification of the headspace of a 500 ppm(v/v) acetonitrile solution.

5,000 ppm (v/v) acetone and acetonitrile solutions were compared to their extrapolated headspace concentrations from the Henry's Law plots that do not fit the 5,000 ppm (v/v) solutions, **Figure 3.11** and **Figure 3.12**. These results demonstrate that the calculated headspace concentrations do not fit the Henry's Law plots and validate the assumption that these points should not be fitted.

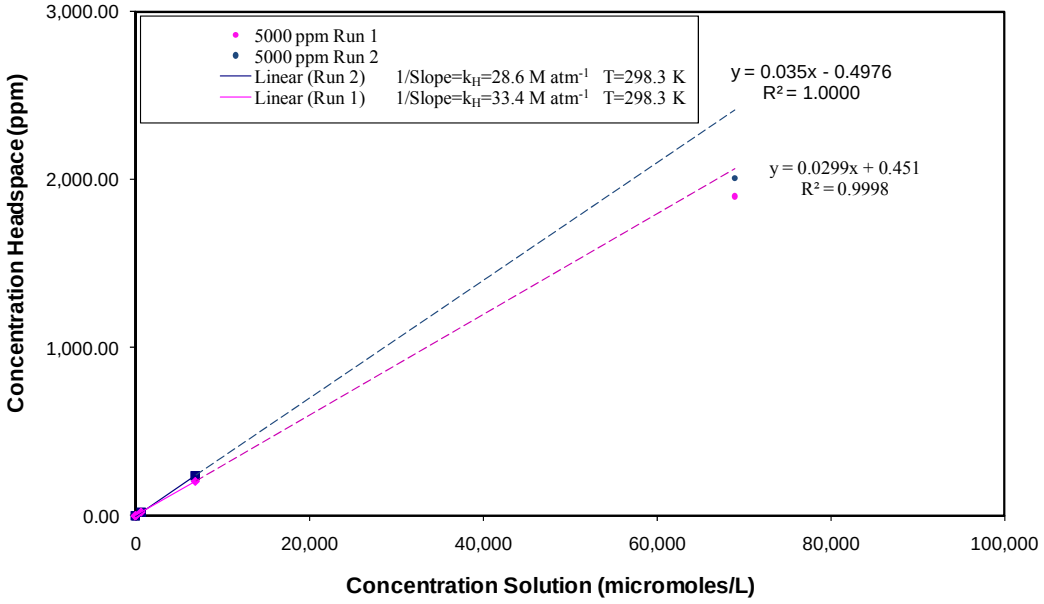

Figure 3.11: Comparison of 5,000 ppm (v/v) headspace concentration measurements to the extrapolated Henry's Law plots from the 500 ppm, 50 ppm, and two 5 ppm acetone solution headspace data points.

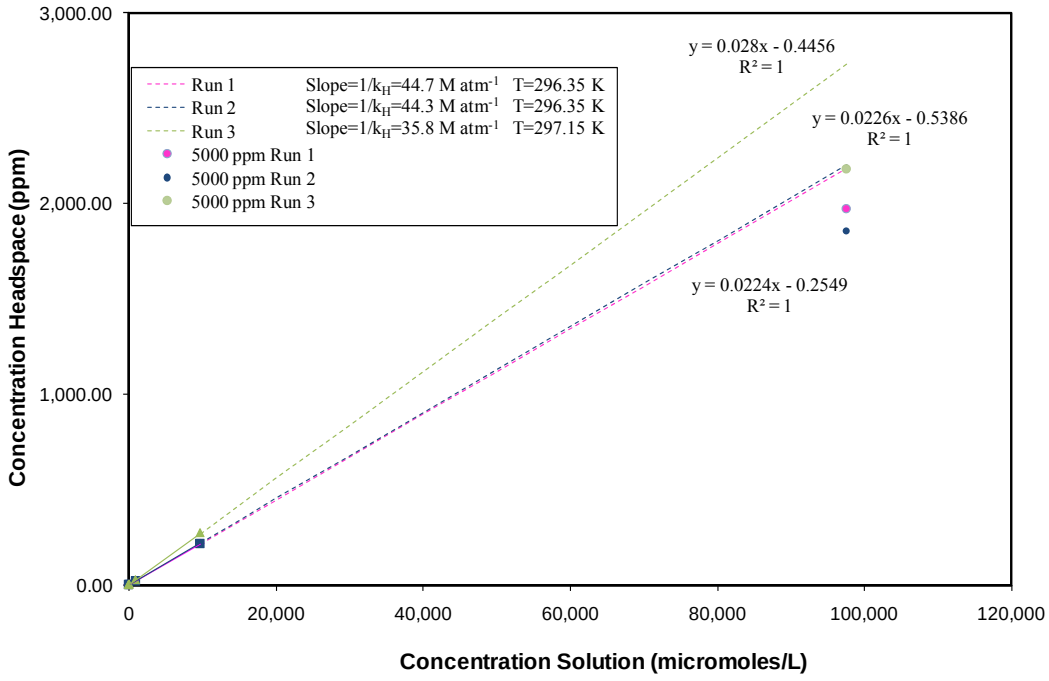

Figure 3.12: Comparison of 5,000 ppm (v/v) headspace concentration measurements to the extrapolated Henry's Law plots from the 500 ppm, 50 ppm, and two 5 ppm acetone solution headspace data points.

k_H^{θ} for each run was calculated by determining k_H, **Figure 3.13**, **Figure 3.14**, **Figure 3.15**, and **Figure 3.16** , from the inverse of the slope of each Henry's Law plot, and adjusting it

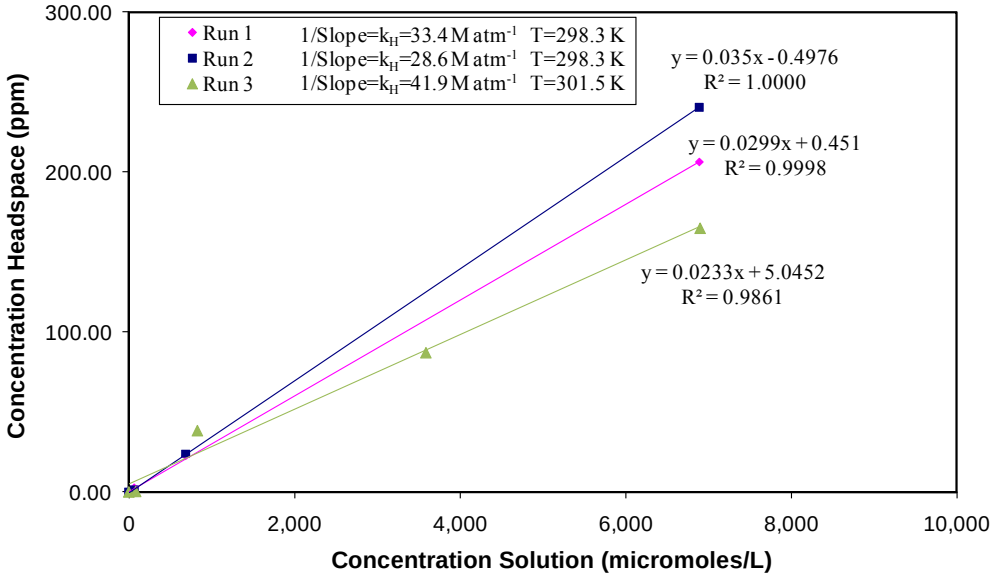

Figure 3.13: Henry's Law plots of headspace concentration (ppm) vs. solution concentration (µM) for acetone in water.

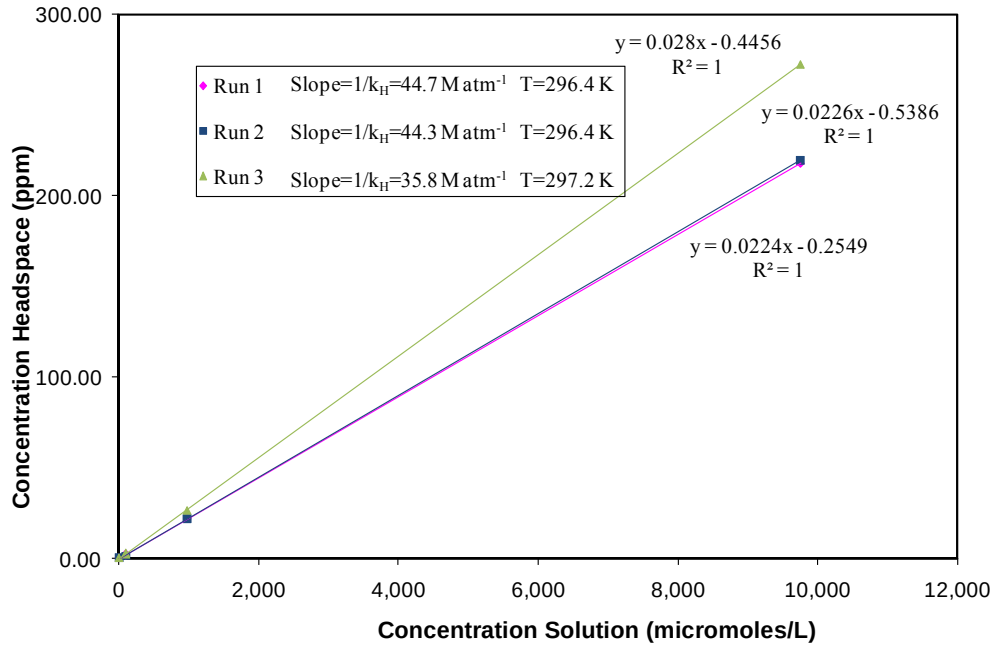

Figure 3.14: Henry's Law plots of headspace concentration (ppm) vs. solution concentration (µM) for acetonitrile in water.

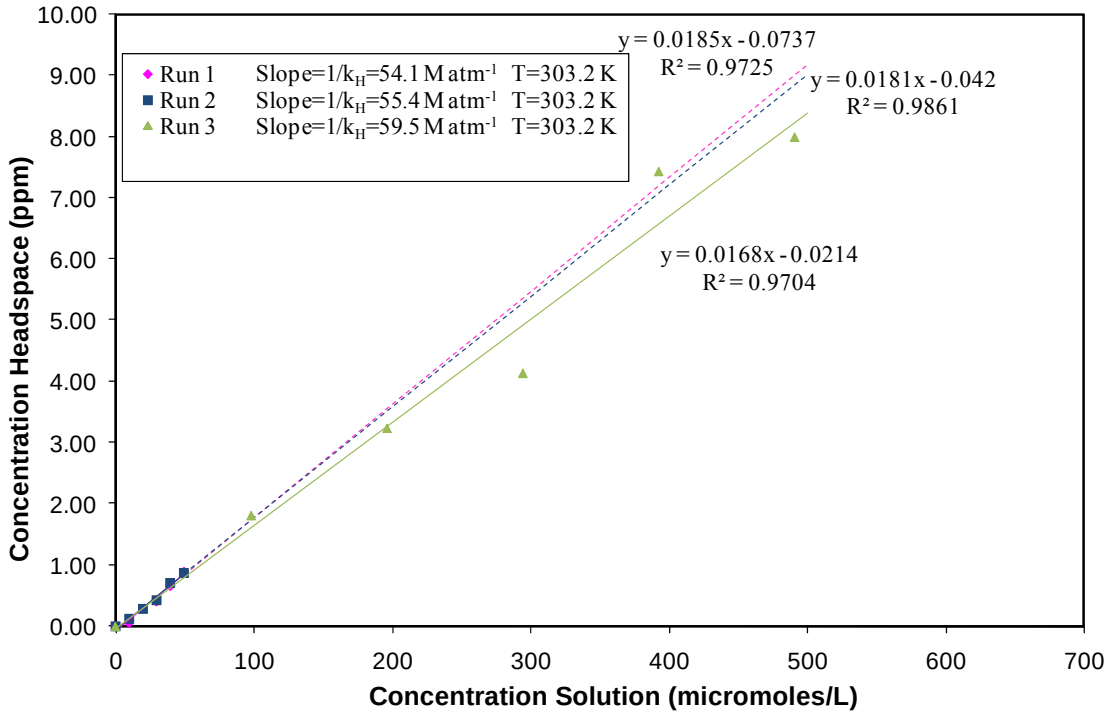

Figure 3.15: Henry's Law plots of headspace concentration (ppm) vs. solution concentration (µM) for benzaldehyde in water for the benzaldehyde/THF solutions.

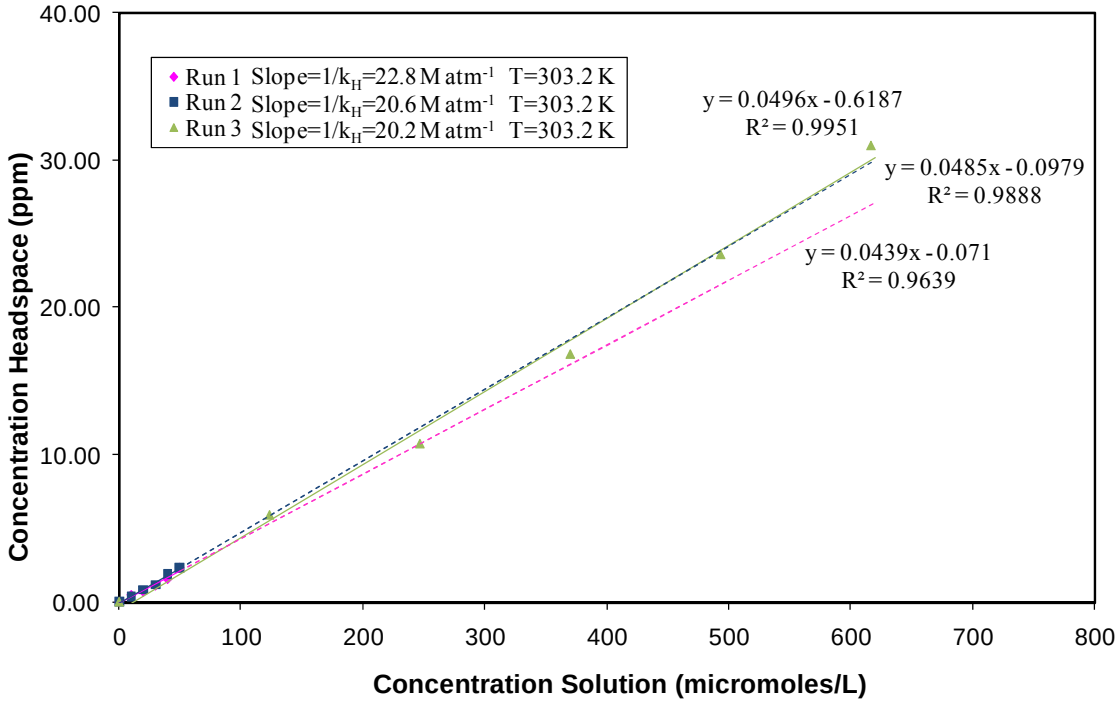

Figure 3.16: Henry's Law plots of headspace concentration (ppm) vs. solution concentration (µM) for THF in water for the benzaldehyde/THF solutions.

to 298.15 K via eq. 3.2 (**Sec. 3.2.4**), Table 3.3. The average k_H^θ values for acetone and acetonitrile in the single-component solutions are 32.1±3.3 and 45.2±6.5 M atm^{-1}, respectively. These k_H^θ values are both in perfect agreement within error of the literature values for acetone (28±3 M atm^{-1}) and acetonitrile (51±3 M atm^{-1}), respectively. The average k_H^θ for benzaldehyde and THF in the benzaldehyde/THF solutions are 41.6±2.1 and 14.8±1.0 M atm^{-1}, respectively. These values are also both in agreement with the literature averages of 39±3 and 17±5 M atm^{-1} for benzaldehyde and THF, respectively. It should be noted that only three values for the k_H^θ of THF in water have been found. Cabani et al.[62]and the Environmental Protection Agency[63] report k_H^θ values for THF of 14 and14.18 M atm^{-1}, respectively. This in great discrepancy with the value of 22 M atm^{-1} measured by Signer et al.[64] Our measured k_H^θ for THF of 14.8±1.0 M atm^{-1} suggest that the value of Cabani et al. and the California EPA to be much closer to the true value for the Henry's Law constant of THF at room temperature than that of Signer et al. The agreements of our k_H^θ within error to the literature values of acetone, acetonitrile, benzaldehyde, and THF imply that our flowing afterglow can accurately quantify multiple VOCs simultaneously via the CR-MS technique.

Table 3.3:
Comparison of temperature adjusted Henry's Law constants, k_H^{θ}, in the literature to those measured on our flowing afterglow using the CR-MS technique. All k_H^{θ} values are reported in M atm^{-1}.

	Single-Component Solutions				Multi-Component Solutions			
	Acetone		Acetonitrile		Benzaldehyde		THF	
	$k_{H\ (exp.)}^{\theta}$	$k_{H\ (lit.)}^{\theta}$	$k_{H\ (exp.)}^{\theta}$	$k_{H\ (lit.)}^{\theta}$	$k_{H\ (exp.)}^{\theta}$	$k_{H\ (lit.)}^{\theta}$	$k_{H\ (exp.)}^{\theta}$	$k_{H\ (lit.)}^{\theta}$
	33.2	28[m]	49.2	54[i]	39.9	36[e]	15.9	14[b]
	28.4	25[n]	48.7	49[j]	40.9	37[f]	14.4	22[d]
	34.6	26[j]	37.7	48[k]	43.9	42[g]	14.1	14.18[c]
		35[g]		53[l]		39[h]		
		32[o]						
		27[l]						
		25[p]						
		27[q]						
		30[h]						
Average	32.1	28	45.2	51	41.6	39	14.8	17
Standard Deviation	3.3	3	6.5	3	2.1	3	1.0	5
% Difference[a]		12		12		9		15

[a]% Difference from the average literature k_H^{θ}
[b]Cabani et al.[62]
[c]California Environmental Protection Agency[63]
[d]Signer et al.[64]
[e]Hine and Mookerjee[65]
[f]Betterton and Hoffman[66]
[g]Zhou and Mopper[67]
[h]Staudinger and Roberts[68]
[i]Hamm et al.[69]
[j]Snider and Dawson[70]
[k]Arijs and Brasseur[71]
[l]Benkelberg et al.[72]

[m]Burnett[73]
[n]Buttery et al.[74]
[o]Betterton[75]
[p]Vitenberg et al.[76]
[q]Hoff et al.[77]

3.4 Conclusions

The accuracy of using our flowing afterglow to quantify trace VOCs via the CR-MS technique has been determined. The CR-MS technique was utilized to quantify the headspaces of a series of acetone, acetonitrile, and benzaldehyde/THF aqueous solutions. These headspace concentrations were utilized to create Henry's Law plots and calculate k_H^{θ} values for acetone, acetonitrile, benzaldehyde, and THF of 32.1±3.3, 45.2±6.5, 41.6±2.1, and 14.8±1.0 M atm^{-1}, respectively. Our measured values for k_H^{θ} of acetone, acetonitrile, benzaldehyde, and THF are all within error from the literature, which suggests that our flowing afterglow can accurately quantify multiple trace VOCs simultaneously via the CR-MS technique.

4.0 DEVELOPMENT OF TRIMETHYLSILATED NITRITE REAGENT IONS; $R(TMS)ONO^+$

4.1 Background

The choice of an appropriate reagent ion is one of the keys to the successful utilization of the Chemical Reaction Mass Spectrometry (CR-MS) technique. The ideal reagent ion fulfills four requirements: it should be able to be generated cleanly, produce one product ion for each reaction, be unreactive towards the bulk components of air (nitrogen, oxygen, argon, carbon dioxide), and produce a reaction upon every ion-molecule collision with the trace gases being analyzed. The hydronium ion is the most commonly utilized reagent ion for CR-MS studies because it is produced easily via electron ionization or Penning ionization of water vapor, tends to produce one product ion for each reaction, is unreactive towards the bulk components of air, and reacts via exothermic proton transfer at the collisional rate with the majority of VOCs. Despite its advantages, H_3O^+ possesses two main disadvantages. The hydronium ion clusters with water to produce $H_3O^+(H_2O)_n$ (n=1-3) each of which can also react with the sample leading to complications of all aspects of VOC detection and quantification. Because H_3O^+ reacts predominantly via proton transfer, it also has difficulty distinguishing between isobaric molecules (i.e. molecules of the same mass). The development of reagent ions to circumvent

these problems is, therefore, a useful endeavor in order to improve the ability of the CR-MS technique to identify and quantify trace VOCs.

The trimethylsilyl group (TMS) has been previously described as a "large proton" due to its reaction tendencies.[78] $(CH_3)_3Si^+$ is protonated $(CH_3)_2Si{=}CH_2$, which has a high proton affinity of 226.5 kcal/mol.[25] Therefore, the trimethylsilyl cation is not easily deprotonated. So, like a proton, the trimethylsilyl cation has a tendency to form stable adducts with Lewis bases with an especially strong affinity towards oxygen bases such as acetone[79,80], eq. 4.1.[79]

$$(CH_3)_3Si^+ + (CH_3)_2CO \rightarrow (CH_3)_2CO^+{-}Si(CH_3)_3 + 45\ \text{kcal} \qquad (4.1)$$
$$k_{obs}=1.8 \times 10^{-9}\ \text{cm}^3\ \text{molecule}^{-1}\ \text{s}^{-1}$$
$$k_{obs}/k_{coll}=0.70$$

Trimethylsilyl analogs of the hydronium ion such as $TMSOH_2^+$ have been shown by Stone and coworkers to undergo trimethylsilyl transfer to many neutrals in the gas-phase.[81] One such example is the reaction of protonated trimethylsilanol with acetone, eq. 4.2.[8] Morris has utilized

$$(CH_3)_3SiOH_2^+ + (CH_3)_2CO \rightarrow (CH_3)_2CO^+{-}Si(CH_3)_3 + H_2O + 15\ \text{kcal} \qquad (4.2)$$
$$k_{II}=2.2 \times 10^{-9}\ \text{cm}^3\ \text{molecule}^{-1}\ \text{s}^{-1}$$
$$k_{II}/k_{coll}=0.88$$

a flowing afterglow to prepare TMS_2OH^+ from the proton transfer of $(CH_3)_3C^+$ to TMS_2O and demonstrated that increasing substitution of the trimethylsilyl group for protons in the hydronium ion minimizes the clustering problem associated with H_3O^+.[82]

NO^+ possesses the ability to decipher between isobaric compounds as it reacts with a neutral by one or more of the following means: hydride abstraction, hydroxide transfer, alkoxide transfer, adduct formation, and/or charge transfer. One such example is its ability to decipher between THF and butanone (**Sec. 1.2.2.2**). Smith et al.[83] have compared the reactions of NO^+ and those of H_2ONO^+, which is the result of substituting a nitrosyl group for a proton on the hydronium ion, with a series of neutrals. In many cases, the products of the neutral of interest

with NO^+ result in the same products as those with H_2ONO^+. In some cases, proton transfer occurs instead of or in addition to these reactions. In other instances, reactions that were observed with NO^+ are replaced with clustering reactions when allowed to react with H_2ONO^+. When the products from reactions of neutrals with NO^+ and H_2ONO^+ are different, it can be attributed to an additional activation energy, which is the NO^+-OH_2 bond energy. In addition, H_2ONO^+ has been determined experimentally and theoretically to be best described as NO^+ weakly solvated by a water molecule with a NO^+-OH_2 bond energy of 18.5 kcal mol^{-1}. [28,84] This information suggests that substituting a nitrosyl group for a proton in the hydronium ion results in an ion that is a good NO^+ donor as well as a good H^+ donor and useful in deciphering isobaric compounds.

Herein, the development of reagent ions for the CR-MS technique of the form $R(TMS)ONO^+$, where R is a proton, alkyl group, or trimethylsilyl group is attempted. Ions of this type were chosen to maintain the advantages of the H_3O^+ ion while minimizing clustering and problems deciphering isobaric molecules through substitution of the trimethylsilyl and nitrosyl group, respectively. The reactions of NO^+ + methoxytrimethylsilane, NO^+ + hexamethydisiloxane, $(TMS)_2OH^+$ + methyl nitrite, and $TMSOH_2^+$ + methyl nitrite were utilized in an attempt to develop the $R(TMS)ONO^+$ ions while the reactions of H_3O^+ + methyl nitrite and $(CH_3)_3C^+$ + methyl nitrite were utilized as control experiments.

4.2 Experimental

4.2.1 *Reagents and Chemicals*

The following chemicals were used without any further purification: nitric oxide (AGA Chemicals, 99.5%), sodium nitrite (J.T. Baker, 99.7%), methanol (Fisher Scientific, 99.9%), and sulfuric acid (EMD Chemicals, 17.8 M), hexamethydisiloxane (Sigma-Aldrich, 98+%), methoxytrimethylsilane (Acros, 98+%), tert-butyl chloride (Fisher Scientific, 99.9%), tetramethylsilane (Fluka, ≥99%), and distilled water.

4.2.2 *Preparation of Methyl Nitrite*

Via pressure equalizing addition funnel, a 150 mL aqueous solution containing 0.5 equiv. of CH_3OH and 0.5 equiv. of H_2SO_4 was added dropwise to a 135 mL aqueous solution, consistently stirred and held at 0˚C, containing 0.5 equiv. of CH_3OH and 1.0 equiv. of $NaNO_2$. The gaseous product was transferred via cannula to a 50 mL round-bottom flask that was held at -78˚C. The methyl nitrite flask was equipped with an on/off valve and kept at -78˚C after sample preparation. Identity of the turquoise product was confirmed via reaction with H_3O^+ in our flowing afterglow mass spectrometer. Methyl nitrite was prepared each day as needed.

4.2.3 *Data Collection*

The general procedure for data collection is explained in **Sec. 2.1**. Only details particular to these experiments are mentioned here. With the exception of the needle and syringe, all data

were obtained utilizing the neutral introduction system in **Figure 3.1** (**Sec. 3.2.3**) over the course of at least two different experimental days, where an experimental day is defined by the complete shut down and start-up of the instrument. With the exception of methyl nitrite, all samples were degassed via the freeze-pump-thaw method. All flasks, with the exception of methyl nitrite, were immersed in 500 mL of room temperature water during their introduction into the flow tube. The methyl nitrite flask was submerged in a dry ice/isopropanol bath during its introduction.

The following procedure was followed for the NO^+ + methoxytrimethylsilane, NO^+ + hexamethyldisiloxane, H_3O^+ + methyl nitrite, and $(CH_3)_3C^+$ + methyl nitrite experiments. NO^+, H_3O^+, and $(CH_3)_3C^+$ were produced via ionization of nitric oxide, water vapor, and tert-butyl chloride, respectively. At the beginning of data acquisition, the metering valves of both arms of the vacuum rack were closed as much as possible while the on/off valves to vacuum, on/off valves to the calibration bulbs, the valve to the methoxytrimethysilane, hexamethyldisiloxane, or methyl nitrite flask, and all the solenoid valves were closed. Background spectra were collected for 2-3 minutes. Port 3, corresponding to a reaction distance of 36.3 cm, was then opened and collected for 1-2 minutes. The valve to the lower arm of the vacuum rack was subsequently opened and data collected for 1-2 minutes. The valve on the methoxytrimethylsilane flask was then opened, the pressure in the vacuum rack recorded, and data collected for 1-2 minutes. Pressures in the vacuum rack were sequentially increased with data being collected for 1-2 minutes after each increase in flow. The valves were then closed in the reverse order in which they were opened with data being collected for 1-2 minute after each valve was closed with the exception of when port 3 was closed in which data was collected for 2-3 minutes.

$((CH_3)_3Si)_2OH^+$ and $(CH_3)_3SiOH_2^+$ were produced from reactions of $(CH_3)_3C^+$ with hexamethyldisiloxane and $(CH_3)_3Si^+$ with water, respectively, in the following manner. $(CH_3)_3C^+$ and $(CH_3)_3Si^+$ were produced from the ionization of tert-butyl chloride and tetramethylsilane, respectively. At the beginning of data acquisition, metering valves of both arms of the vacuum rack were closed as much as possible while the on/off valves to vacuum, on/off valves to the calibration bulbs, the valve to the hexamethyldisiloxane or water flask, and all the solenoid valves were closed. Background spectra were collected for 2-3 minutes. Port 3, corresponding to a reaction distance of 36.3 cm was then opened and data collected for 1-2 minutes. The valve to the lower arm of the vacuum rack was subsequently opened and data collected for 1-2 minute. The valve on the hexamethyldisiloxane or water flask was then opened and the flow increased via the metering valve until the *m/z* corresponding to the reagent ions appeared to be extinguished and replaced with *m/z* 163 or *m/z* 91 for $((CH_3)_3Si)_2OH^+$ and $(CH_3)_3SiOH_2^+$, respectively. The pressure in the vacuum rack at that point was recorded. The valves were closed in the reverse order in which they were opened and the lower arm was pumped on for 5 minutes. The hexamethyldisiloxane or water flask was then moved to the upper arm of the vacuum rack, which was connected to port 10 via Tygon tubing.

Data for the reactions of $((CH_3)_3Si)_2OH^+$ and $(CH_3)_3SiOH_2^+$ with methyl nitrite were collected as follows. Port 10 was opened and spectra collected for 1-2 minutes. The valve to the upper arm of the vacuum rack was subsequently opened and data collected for 1-2 minutes. The valve on the hexamethyldisiloxane or water flask was then opened and flow of hexamethyldisiloxane or water vapor increased to the previously recorded flow that was needed to extinguish the reagent ions when hexamethyldisiloxane or water was introduced through port 3. Background spectra were then collected for 2-3 minutes. Port 3, corresponding to a reaction

distance of 36.3 cm, was then opened and data collected for 1-2 minutes. The valve to the lower arm of the vacuum rack was subsequently opened and data collected for 1-2 minutes. The valve on the methyl nitrite flask was then opened, the pressure in the vacuum rack recorded, and data collected for 1-2 minutes. Pressures in the lower arm of the vacuum rack were sequentially increased with data being collected for 1-2 minutes after each increase in flow. The valves were then closed in the reverse order in which they were opened with data being collected for 1-2 minutes after each valve was closed with the exception of when port 3 and port 10 were closed in which data was collected for 2-3 minutes.

4.2.3.1 NO^+ + *Methoxytrimethylsilane*

Data was collected in Full Scan Mode (50 points/amu, 2 s/scan) in the range of 10-150 amu. Pressures in the vacuum rack were increased from 0.400 Torr to approximately 1.800 Torr in increments of 0.200-0.400 Torr.

4.2.3.2 NO^+ + *Hexamethyldisiloxane*

Data was collected in Full Scan Mode (50 points/amu, 1 s/scan) in the range of 10-210 amu. Pressures in the vacuum rack were increased from 0.400 Torr to approximately 1.800 Torr in increments of 0.200-0.400 Torr.

4.2.3.3 H_3O^+ + *Methyl Nitrite*

Data were collected in Full Scan Mode (10 points/amu, 1 s/scan) in the range of 10-350 amu. Pressures in the vacuum rack were increased from 0.400 Torr to approximately 2.000 Torr in increments of 0.100-0.200 Torr.

4.2.3.4 $(CH_3)_3C^+$ + *Methyl Nitrite*

Data were collected in Full Scan Mode (10 points/amu, 1 s/scan) in the range of 10-350 amu. Pressures in the vacuum rack were increased from 0.400 Torr to approximately 4.000 Torr in increments of 0.100-0.200 Torr until 1.000 Torr and then in increments of 1.000 Torr afterwards.

4.2.3.5 $((CH_3)_3Si)_2OH^+$ + *Methyl Nitrite*

Data were collected in Full Scan Mode (10 points/amu, 1 s/scan) in the range of 10-300 amu. Pressures in the lower arm of the vacuum rack were increased from 0.400 Torr to approximately 5.000 Torr in increments of 0.100- 0.200 Torr until 1.000 Torr was reached and then in increments of 1.000 Torr afterwards.

4.2.3.6 $((CH_3)_3Si)OH_2^+$ + *Methyl Nitrite*

Data were collected in Full Scan Mode (10 points/amu, 1 s/scan) in the range of 10-300 amu. Pressures in the lower arm of the vacuum rack were increased from 0.400 Torr to approximately 5.000 Torr in increments of 0.100-0.200 Torr until 1.000 Torr was reached and then in increments of 1.000 Torr afterwards.

4.3 Results and Discussion

4.3.1 *NO^+ + Methoxytrimethylsilane*

NO^+, produced from electron and Penning ionization of nitric oxide, **Figure 4.1**, was

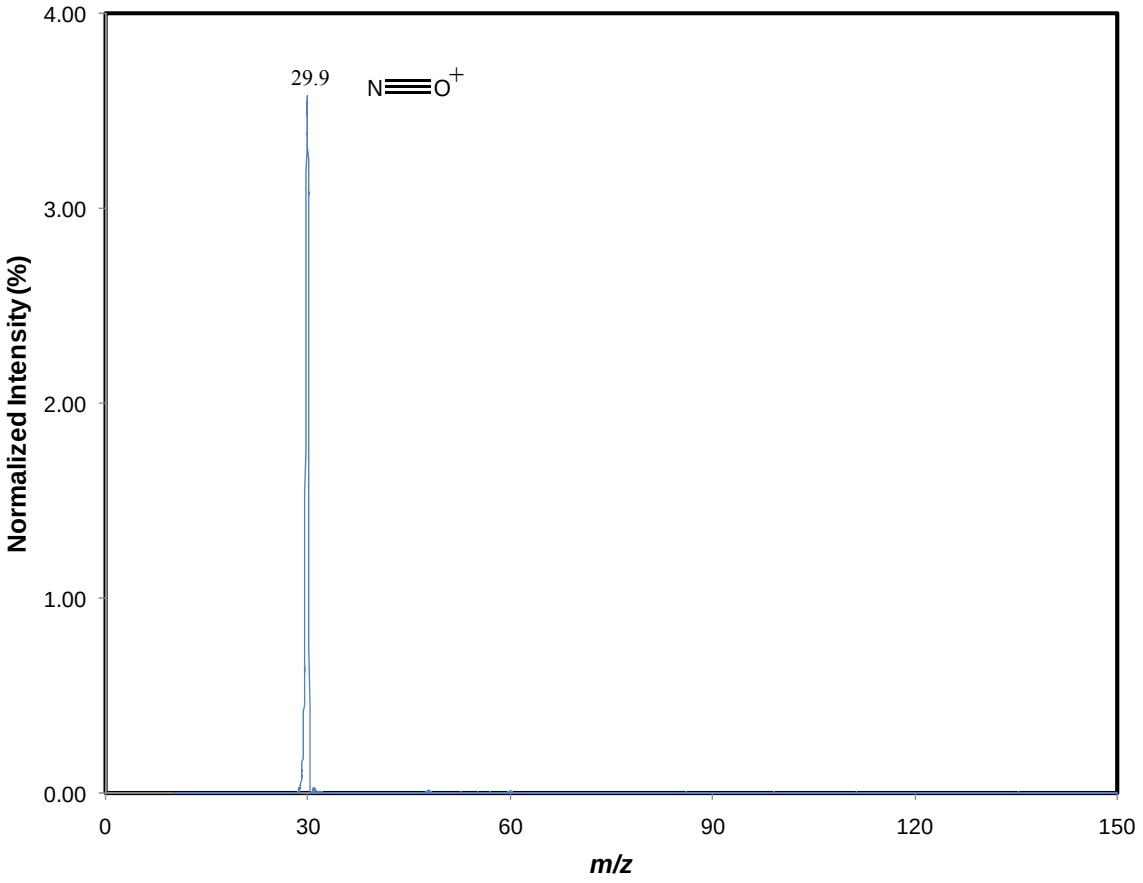

Figure 4.1: Precursor spectrum for the formation of NO^+ from the ionization of nitric oxide at a flow tube pressure of 0.3216 Torr.

allowed to reacted with methoxytrimethylsilane, introduced into the flow tube at port 3 at varying flow rates, in an attempt to make trimethylsilated methyl nitrite; $(TMS)(CH_3)ONO^+$. Product ions were observed at *m/z* 89, *m/z* 103, and *m/z* 134 at a vacuum rack pressure of 0.568 Torr and flow tube pressure of 0.3216 Torr, **Figure 4.2**. Even though the production of

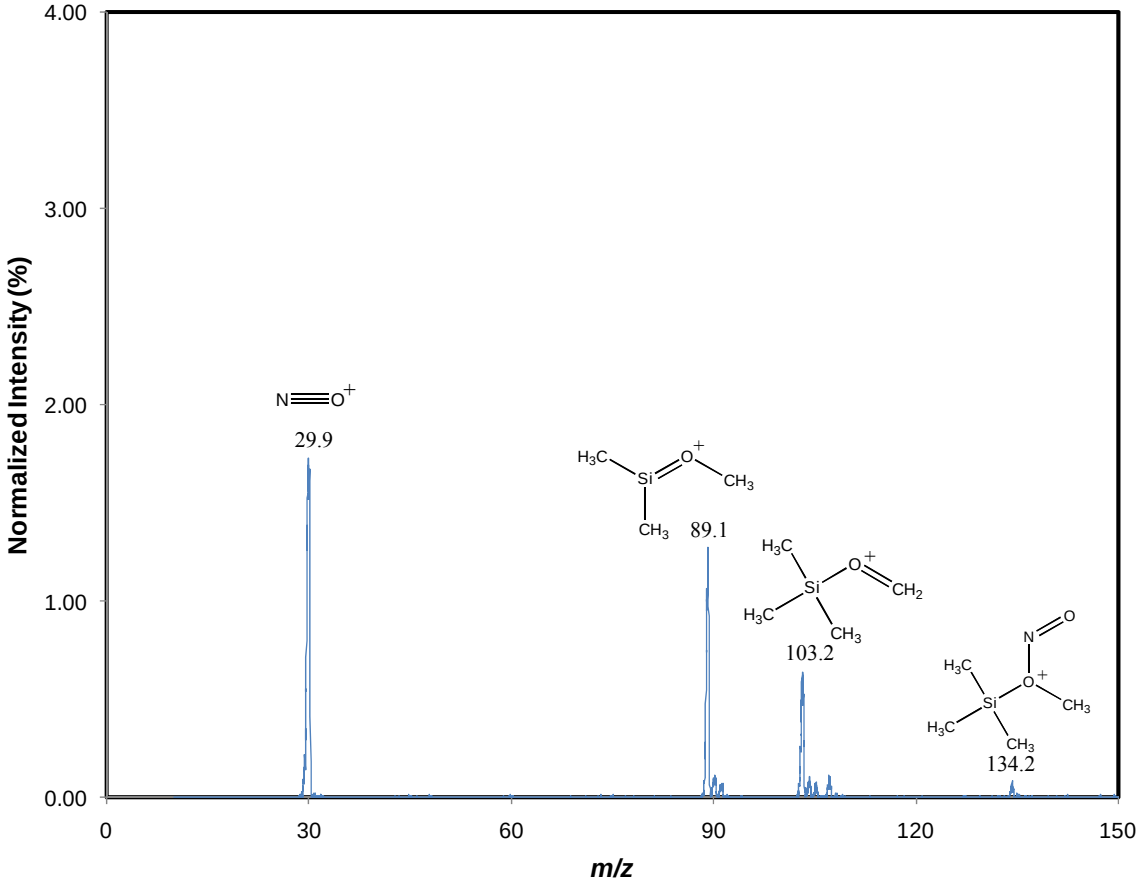

Figure 4.2: Mass spectrum of the reaction of NO^+ with methoxytrimethylsilane at a reaction distance of 36.3 cm, a vacuum rack pressure of 0.568 Torr, and flow tube pressure of 0.3216 Torr.

$(TMS)(CH_3)ONO^+$ from NO^+ and methoxytrimethylsilane is -33±3 kcal/mol exothermic, trimethysilated methyl nitrite (*m/z* 134) is the least abundant of the three products at only 2% of the total product ion intensity. The ΔH_f for $TMS(CH_3)ONO^+$ utilized to determine the exothermicity of this reaction is calculated from the ΔH_f of methoxytrimethylsilane, the ΔH_f of NO^+, the proton affinity of methoxytrimethylsilane, and the relationship established by Cacace et al.[85] via the ICR equilibrium method between the proton affinity of a compound containing binding sites other than π bonds and NO^+ binding energy to within ±2 kcal/mol, eq. 4.3. The fact

$$NO^+ \text{ Bonding Energy} = 0.367*(\text{Proton Affinity}) - 41.7 \qquad (4.3)$$

that this ion is trace is likely due to the fact that the formation of $TMS(CH_3)ONO^+$ proceeds via a three-body association mechanism, which is slower than the bimolecular mechanisms that produce *m/z* 89 and *m/z* 103 (Scheme 4.1). In the case of *m/z* 89 and *m/z* 103, NO^+ abstracts a

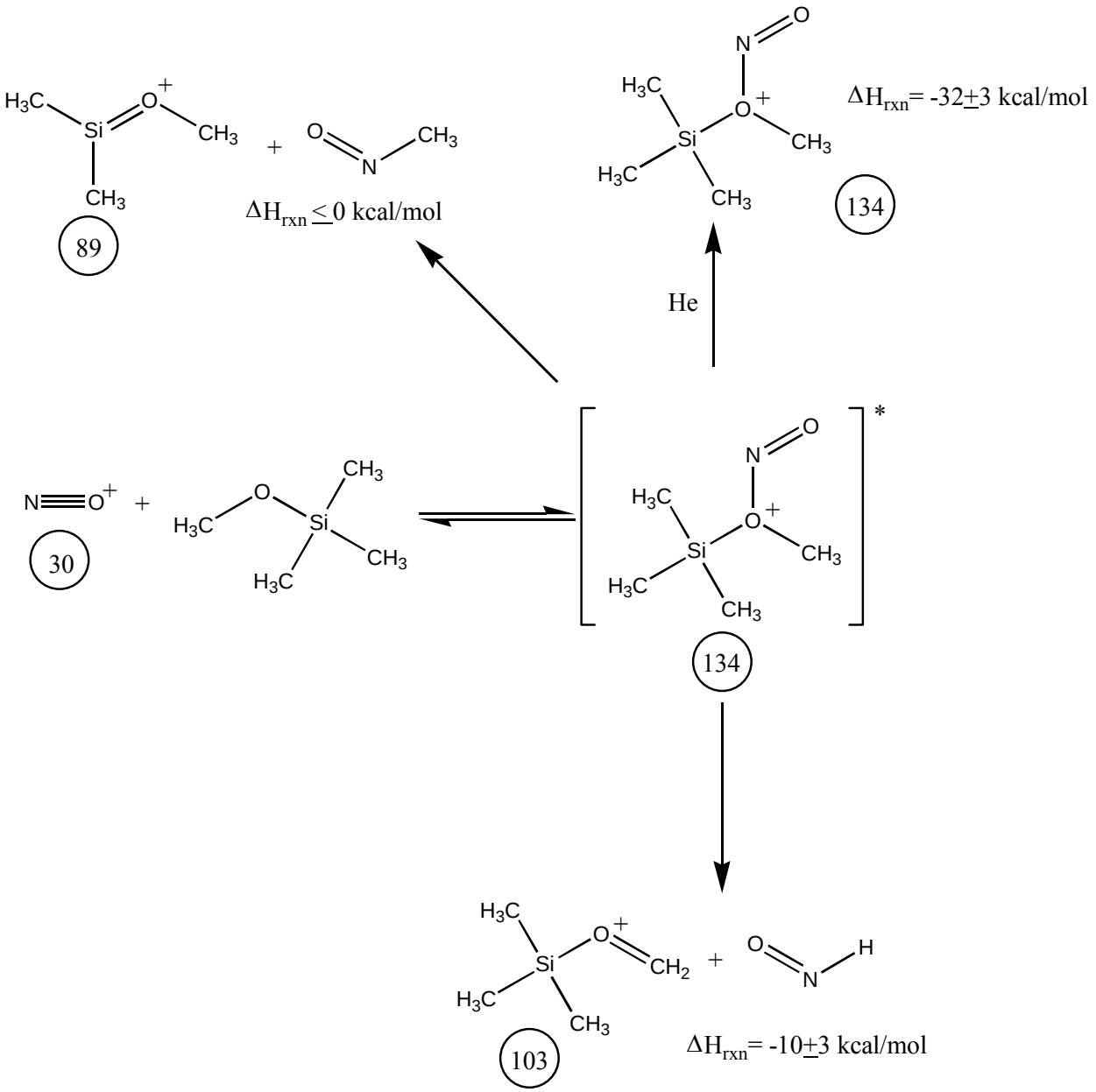

Scheme 4.1: Reactions of NO^+ with methoxytrimethylsilane.

methyl group from the trimethylsilyl moiety or a proton from the methyl moiety to form the resonance stabilized structures of $(CH_3)_2SiO^+–CH_3$ and $(CH_3)_3Si–^+OCH_2$, respectively. The ΔH_f

of *m/z* 103, trimethylsilated formaldehyde, is derived from the ΔH_f of formaldehyde, the ΔH_f of $(CH_3)_3Si^+$, the proton affinity of formaldehyde, and a relationship between the proton affinity of an oxygenated compound and its binding energy to $(CH_3)_3Si^+$ to within $\pm$2 kcal/mol, eq. 4.4.

$$\text{Proton Affinity} = 1.8354 * (\text{TMS}^+ \text{ Affinity}) + 109.74 \qquad (4.4)$$

The correlation between $(CH_3)_3Si^+$ binding energies and proton affinities has been previously demonstrated by Stone and coworkers.[86] The relationship utilized in eq. 4.4 is from Stone's TMS^+ binding energies and correlating them to the updated proton affinities reported in NIST webbook[25], **Figure 4.3**. A ΔH_{rxn} for the formation of methylated oxydimethylsilane (*m/z* 89)

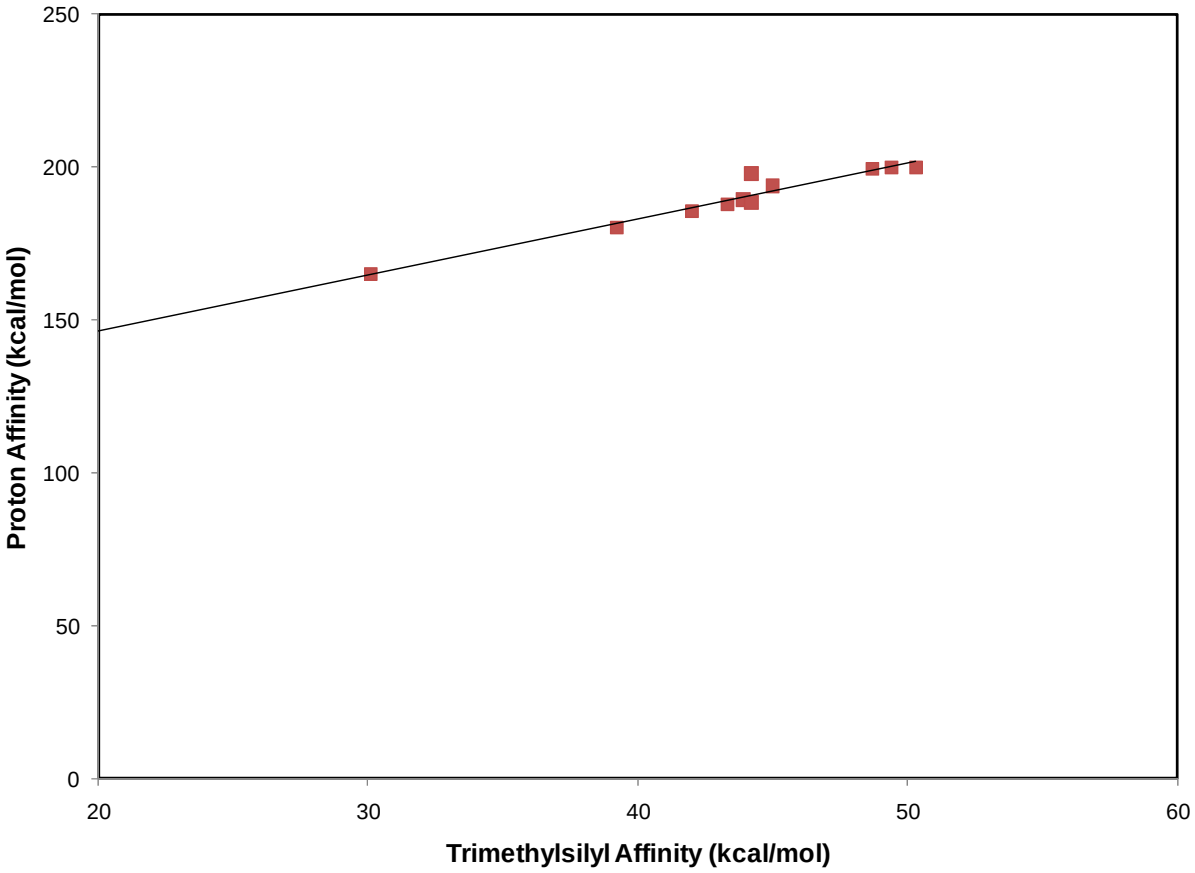

Figure 4.3: Correlation between the proton affinities obtained from NIST webbook[25] and the trimethylsilyl affinities of oxygenated compounds as calculated by Stone and coworkers[86].

could not be calculated because neither the ΔH_f of methylated dimethylsilanone nor the ΔH_f of dimethylsilanone is known. Considering *m/z* 89 is the major primary product ion, the reaction to produce methylated dimethylsilanone must exothermic. Recognizing that the ΔH_f of CH_3^+ is 262 kcal/mol[87], the proton affinity of oxydimethylsilane has been measured as 220.9±1.6 kcal/mol[88], the proton affinity of methanol is 180.3 kcal/mol[25], the methyl cation affinity of methanol has been measured by Kebarle and coworkers[89], and the 1:1 correlation of the proton affinity to methyl cation affinity to within ±2 kcal/mol for proton affinities ≥165 kcal/mol as noted by Kebarle and coworkers[89], the ΔH_f of oxydimethylsilane is ≤-32±3 kcal/mol from these results.

4.3.2 *NO^+ + Hexamethyldisiloxane*

NO^+, produced from electron and Penning ionization of nitric oxide, **Figure 4.1**, was allowed to reacte with hexamethyldisiloxane, introduced into the flow tube at port 3 at varying flow rates, in an attempt to make the nitrosyl adduct of hexamethyldisiloxane; TMS_2ONO^+. The only product ion observed is *m/z* 147, **Figure 4.4**. This ion is $(CH_3)_2SiO^+–Si(CH_3)_3$, formed from methide abstraction by NO^+ (Scheme 4.2). The heat of formation of this ion has not been previously determined. Assuming a ΔH_f of -32±3 kcal/mol for oxydimethylsilane (**Sec. 4.1.3**), a ΔH_f for TMS^+ of 150 kcal/mol,[90] a proton affinity of 220.9±1.6 kcal/mol for oxydimethylsilane[88], and utilizing eq. 4.4, a ΔH_f for $(CH_3)_2SiO^+–Si(CH_3)_3$ can be estimated as +57±4 kcal/mol. However, utilizing this as the heat of formation for $(CH_3)_2SiO^+–Si(CH_3)_3$ and -167 kcal/mol as the ΔH_f for hexamethyldisiloxane as determined by Morris[82], the ΔH_{rxn} for the production of *m/z* 147 ion is 6±4 kcal/mol. Due to its abundance as a product, the production of this ion must at least be thermoneutral. Therefore, the heats of formation of oxydimethylsilane and $(CH_3)_2SiO^+–Si(CH_3)_3$ are corrected to ≤-34±3 kcal/mol and ≤55±4 kcal/mol, respectively.

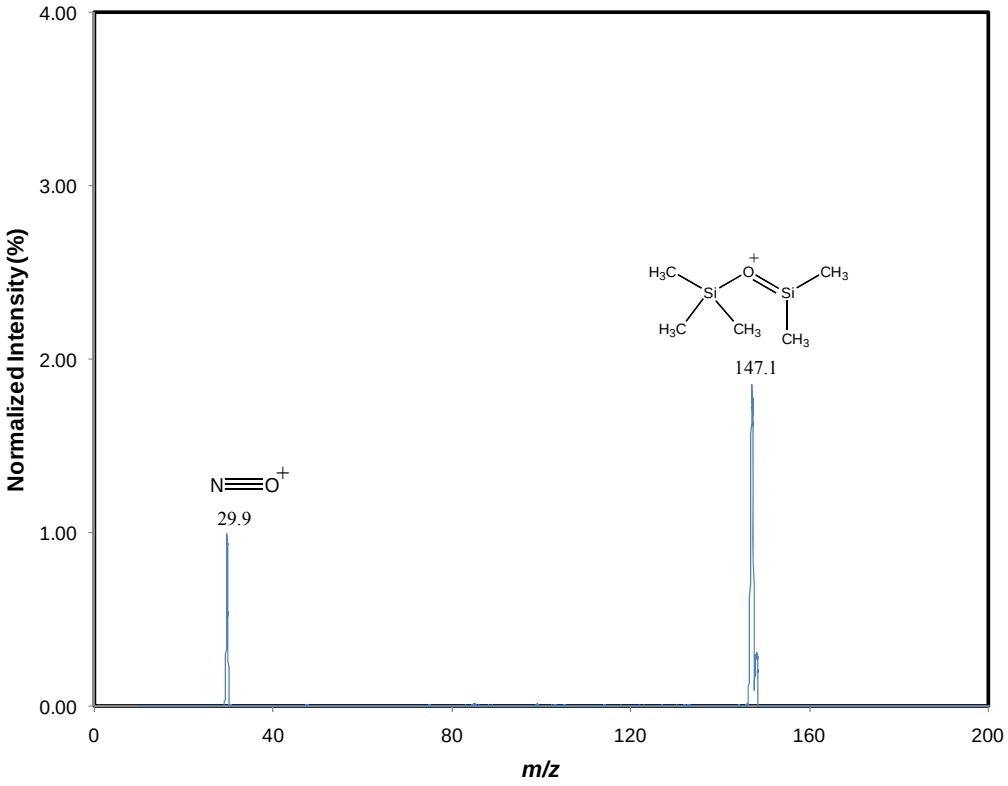

Figure 4.4: Mass spectrum of the reaction of NO^+ with hexamethyldisiloxane at a reaction distance of 36.3 cm, a vacuum rack pressure of 1.270 Torr, and flow tube pressure of 0.3377 Torr.

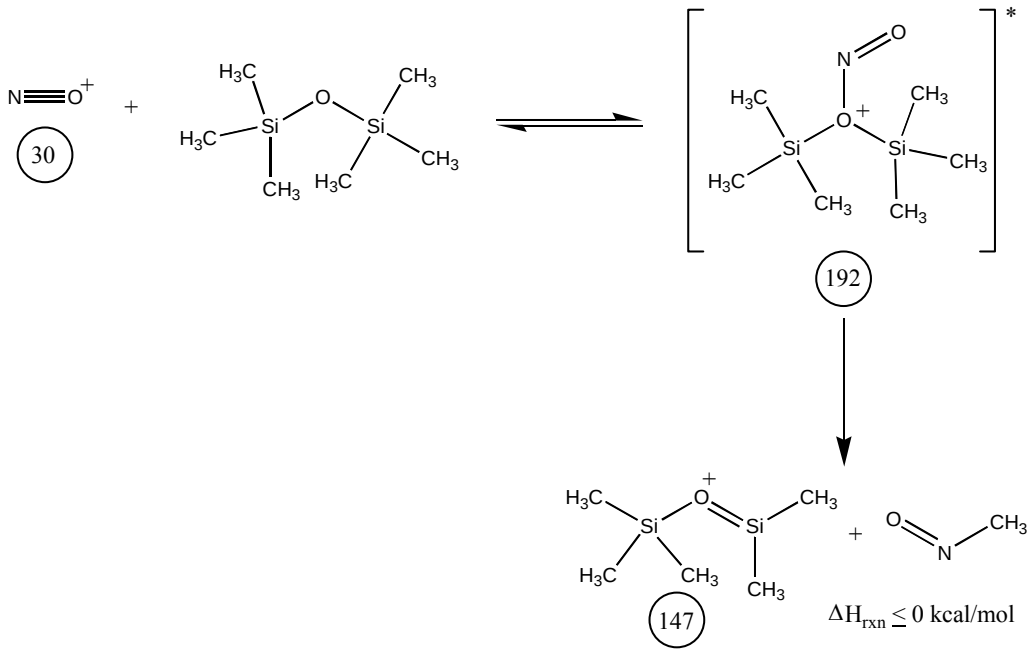

Scheme 4.2: Reaction of NO^+ with hexamethyldisiloxane.

While the formation of TMS_2ONO^+ (*m/z* 192) is estimated to be exothermic by 33±3 kcal/mol, it is not observed. This ΔH_{rxn} is derived from the proton affinity of TMS_2O, ΔH_f of TMS_2O, ΔH_f of NO^+, and utilization of eq. 4.3. The fact that *m/z* 192 is not observed could be attributed to the fact that this is a three-body association mechanism, which is often slower than a bimolecular reaction like the one that produced *m/z* 147.

4.3.3 *H_3O^+ + Methyl Nitrite*

The headspace of the turquoise product, prepared as described in **Sec. 4.2.2,** was introduced through the vacuum rack at varying pressures into the flow tube at port 3 and was allowed to react with H_3O^+ and its hydrates in order to validate that methyl nitrite had been prepared. Product ions are observed at *m/z* 30, *m/z* 48, *m/z* 62, *m/z* 80, and *m/z* 91, **Figure 4.5** and **Figure 4.6**. The formation of the primary products is displayed in Scheme 4.3. As can be observed in a graph of ion intensity vs. the pressure in the vacuum rack, **Figure 4.7**, which correlates to the flow of the neutral, *m/z* 30, *m/z* 48, *m/z* 62, and *m/z* 80 are primary product ions as evidenced by a sudden increase in intensity as soon as the flow of the neutral is increased followed by an intensity plateau at higher pressures. *m/z* 91 is a secondary product ion as its intensity increases without a plateau as the intensities of *m/z* 30, *m/z* 48, *m/z* 62, and *m/z* 80 begin to plateau, indicating a reaction of the neutral with the primary product ions to produce *m/z* 91. The major primary product ion is observed at *m/z* 62, which is the *m/z* of protonated methyl nitrite. This suggests that the neutral is methyl nitrite since the experimental proton affinity of methyl nitrite is 190.0±1.0 kcal/mol (**Appendix B)**, resulting in a ΔH_{rxn} for the reaction of the hydronium ion with methyl nitrite of 25.0±1.0 kcal/mol. This is the only manner in which *m/z* 62 is produced because proton transfer reactions from the hydrates of the

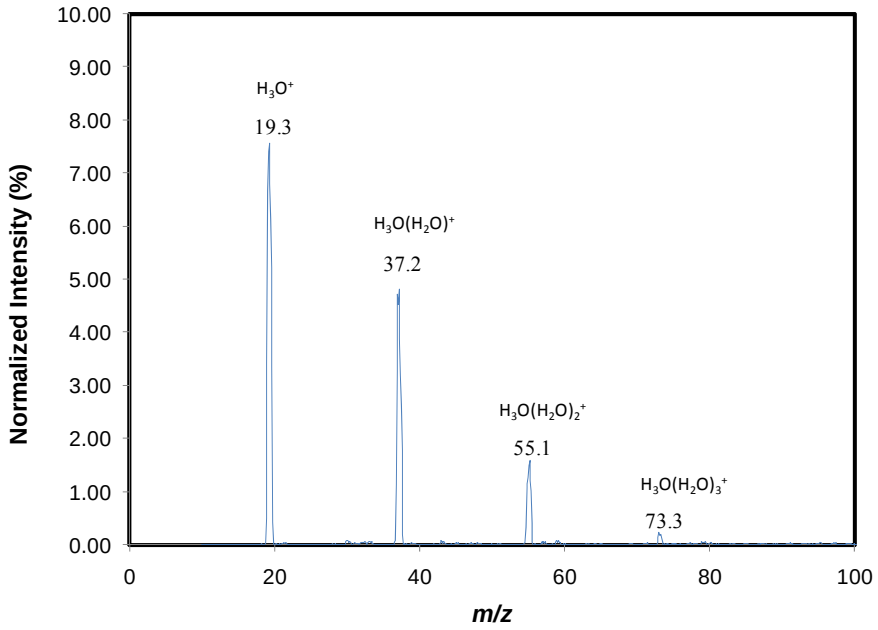

Figure 4.5: Precursor spectrum for the formation of $H_3O(H_2O)_n^+$ (n=0,1,2,3) from the ionization of water vapor at a flow tube pressure of 0.313 Torr.

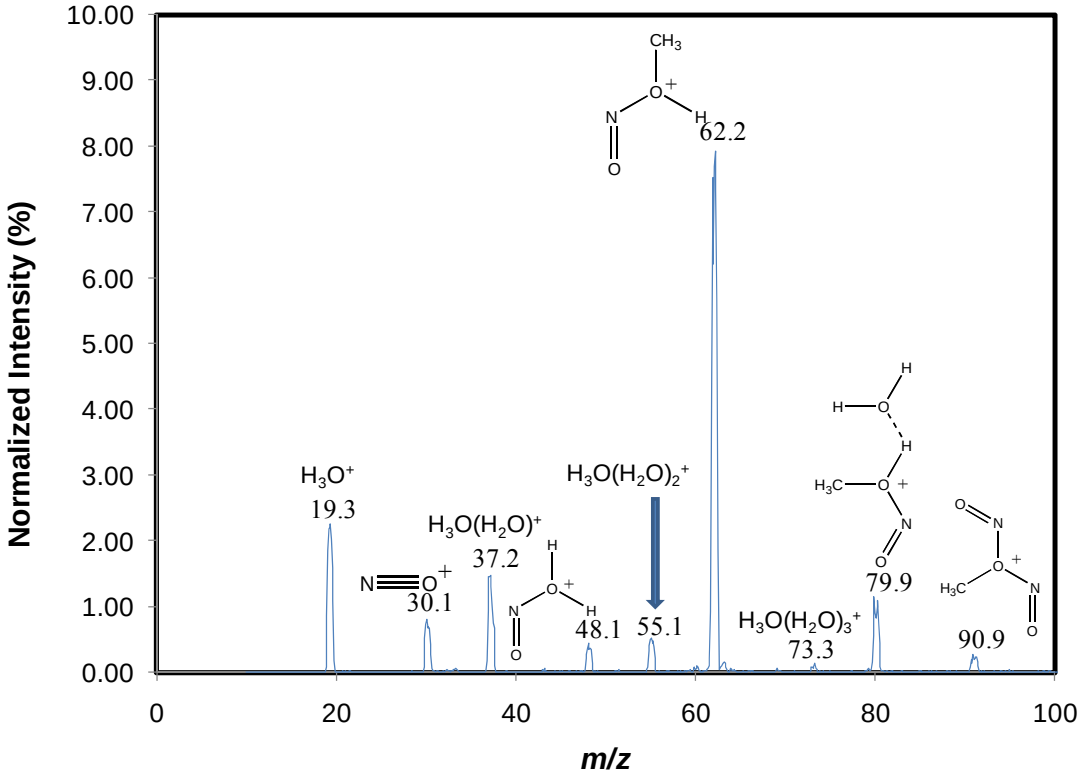

Figure 4.6: Mass spectrum of the reaction of H_3O^+, $H_3O(H_2O)^+$, $H_3O(H_2O)_2^+$, and $H_3O(H_2O)_3^+$ with methyl nitrite at a reaction distance of 36.3 cm, a vacuum rack pressure of 1.431 Torr, and flow tube pressure of 0.313 Torr in our flowing afterglow mass spectrometer.

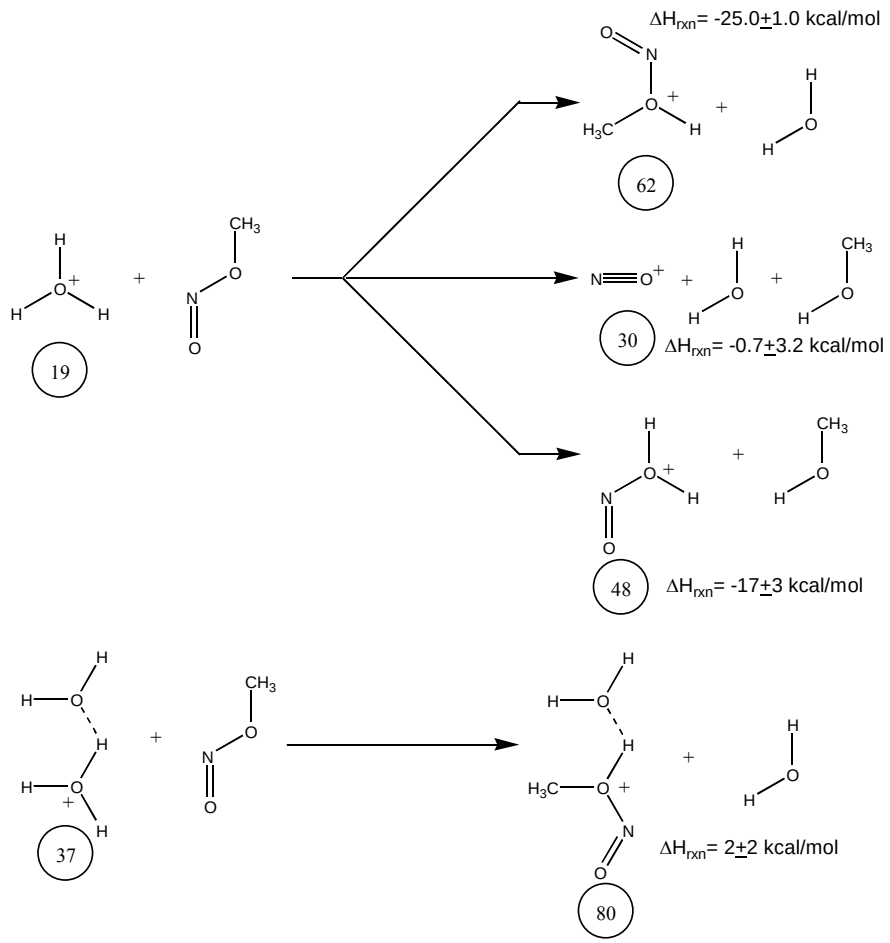

Scheme 4.3: Primary reactions of H_3O^+ and $H_3O(H_2O)^+$ with methyl nitrite.

hydronium ion to methyl nitrite are endothermic, eq. 4.5, eq. 4.6, and eq. 4.7. Due to the

$$H_3O(H_2O)^+ + H_3CONO \rightarrow H(H_3C)ONO^+ + 2H_2O \quad \Delta H_{rxn} = +9 \text{ kcal/mol} \tag{4.5}$$

$$H_3O(H_2O)_2^+ + H_3CONO \rightarrow H(H_3C)ONO^+ + 3H_2O \quad \Delta H_{rxn} = +29 \text{ kcal/mol} \tag{4.6}$$

$$H_3O(H_2O)_3^+ + H_3CONO \rightarrow H(H_3C)ONO^+ + 4H_2O \quad \Delta H_{rxn} = +46 \text{ kcal/mol} \tag{4.7}$$

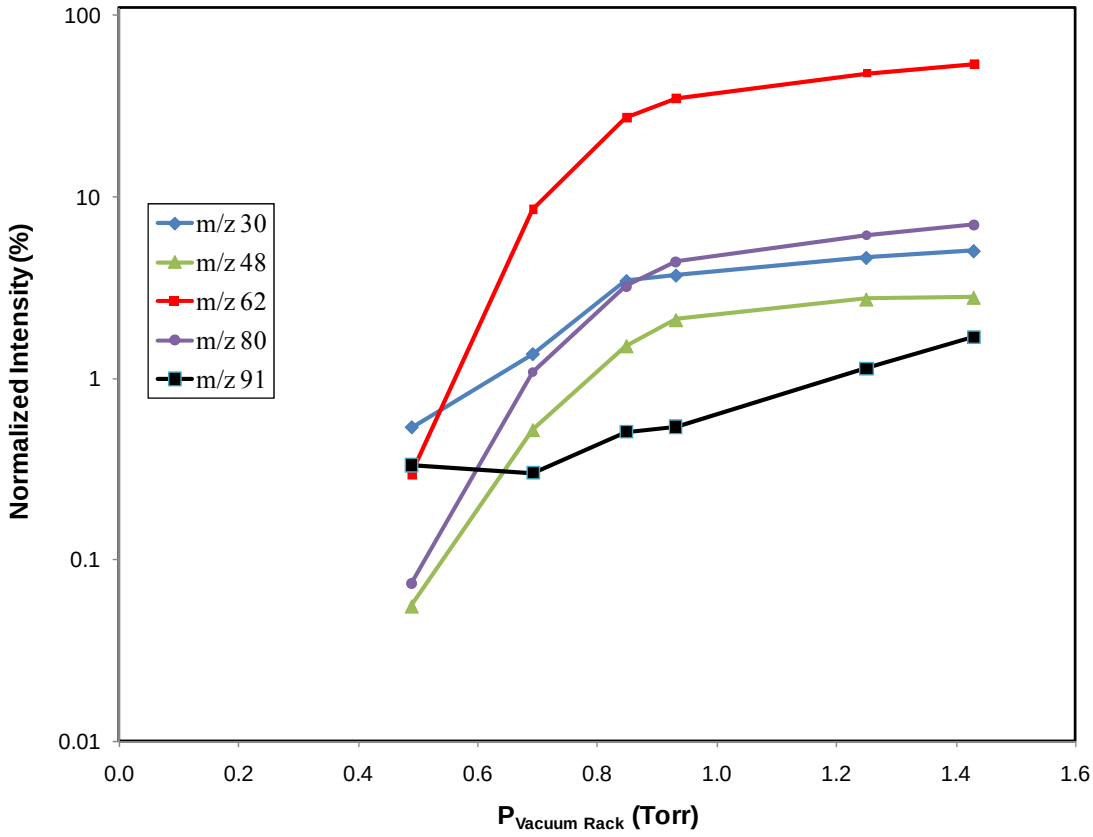

Figure 4.7: Graph of the intensity of the product ions from the reaction of the hydronium ion and its hydrates with methyl nitrite at a flow tube pressure of 0.313 Torr vs. pressure of the vacuum rack in Torr.

exothermicity of the protonation of methyl nitrite by H_3O^+ and the fact that the $H(CH_3)O\text{-}NO^+$ bond energy is 24.3±3.0 kcal/mol,[85,91] there is a finite probability that proton transfer from H_3O^+ to methyl nitrite is exothermic enough to cleave the $H(CH_3)O–NO^+$ bond to produce methanol and NO^+; *m/z* 30.

m/z 80 is a minor primary product and is the first hydrate of protonated methyl nitrite. It is likely produced via ligand-exchange reactions between one or more of the hydrates of the hydronium ion with methyl nitrite. The ΔH_f of the first hydrate of protonated methyl nitrite and ΔH_{solv} of protonated methyl nitrite with water are unknown, making the determination of ΔH_{rxn} for the production of *m/z* 80 impossible. In order for the ligand-exchange reactions between

$H_3O(H_2O)^+$, $H_3O(H_2O)_2^+$, and $H_3O(H_2O)_3^+$ with methyl nitrite that produce $H_2O{\cdot}H(CH_3)ONO^+$ to be at least thermoneutral, the ΔH_{solv} of protonated methyl nitrite with water needs to be $\leq$-9$\pm$2 kcal mol^{-1}, $\leq$-29$\pm$2 kcal mol^{-1}, and $\leq$-46$\pm$2 kcal mol^{-1}, respectively. Kebarle has reported that the first and second hydration enthalpies for protonated nitrous acid are -16.1 and -13.5 kcal mol^{-1}, respectively.[28] While it might be expected that the ΔH_{solv} for protonated methyl nitrite be similar to these values, the fact that *m/z* 80 reacts with methyl nitrite to produce *m/z* 91, **Figure 4.7**, indicates a value of -7$\pm$2 kcal/mol (**Appendix B)**. Such a value for the ΔH_{solv} with water for protonated methyl nitrite suggests $H_3O(H_2O)^+$ is the only hydrate that undergoes ligand switching with methyl nitrite to produce *m/z* 80.

m/z 48 is H_2ONO^+. While it is energetically feasible that some *m/z* 48 is formed via three-body association of NO^+ with adventitious water in the flow tube, eq. 4.8, this would

$$NO^+ + H_2O \rightarrow H_2ONO^+ \quad \Delta H_{rxn}=-18.5 \text{ kcal/mol} \tag{4.8}$$

result in *m/z* 48 being a secondary product. However, as **Figure 4.7** demonstrates, the majority of *m/z* 48 is formed as a primary product. This ion is likely formed from the clustering of the hydronium ion to methyl nitrite, followed by proton transfer to methyl nitrite, and then water/methanol ligand-switching in the resulting $H_2O{\cdot}H(CH_3)ONO^+$ intermediate. Reactions of $H_3O(H_2O)^+$, $H_3O(H_2O)_2^+$, and $H_3O(H_2O)_3^+$ with methyl nitrite that produce H_2ONO^+ are all endothermic, eq. 4.9, eq. 4.10, and eq. 4.11.

$$H_3O(H_2O)^+ + H_3CONO \rightarrow H_2ONO^+ + H_2O + CH_3OH \quad \Delta H_{rxn}=+15 \text{ kcal/mol} \tag{4.9}$$

$$H_3O(H_2O)_2^+ + H_3CONO \rightarrow H_2ONO^+ + 2H_2O + CH_3OH \quad \Delta H_{rxn}=+34 \text{ kcal/mol} \tag{4.10}$$

$$H_3O(H_2O)_3^+ + H_3CONO \rightarrow H_2ONO^+ + 3H_2O + CH_3OH \quad \Delta H_{rxn}=+52 \text{ kcal/mol} \tag{4.11}$$

As mentioned earlier, *m/z* 91 is a secondary product. The intensities of *m/z* 30, *m/z* 48, *m/z* 62, and *m/z* 80 all begin to plateau as *m/z* 91 is formed, indicating that reactions of these ions

are sources of *m/z* 91. The identity of *m/z* 91 can, therefore, be assigned to $(CH_3)(NO)ONO^+$. NO^+ (*m/z* 30) reacts to form this ion by adduct formation to methyl nitrite, eq. 4.12, while

$$NO^+ + CH_3ONO \rightarrow (CH_3)(NO)ONO^+ \quad \Delta H_{rxn} = -28 \text{ kcal/mol} \qquad (4.12)$$

H_2ONO^+ (*m/z* 48), $H(CH_3)ONO^+$ (*m/z* 62), and $H_2O{\cdot}(CH_3)HONO^+$ (*m/z* 80) undergo ligand-switching reactions with methyl nitrite, eq. 4.13, eq. 4.14, and eq. 4.15.

$$H_2ONO^+ + CH_3ONO \rightarrow (CH_3)(NO)ONO^+ + H_2O \quad \Delta H_{rxn} = -10 \text{ kcal/mol} \qquad (4.13)$$

$$H(CH_3)ONO^+ + CH_3ONO \rightarrow (CH_3)(NO)ONO^+ + CH_3OH \quad \Delta H_{rxn} = -4 \text{ kcal/mol} \qquad (4.14)$$

$$H_2O{\cdot}H(CH_3)ONO^+ + CH_3ONO \rightarrow (CH_3)(NO)ONO^+ + CH_3OH + H_2O \quad \Delta H_{rxn} = 0 \text{ kcal/mol} \qquad (4.15)$$

All these results suggest that the identity of the turquoise product synthesized is indeed methyl nitrite.

4.3.4 *$(CH_3)_3C^+$ + Methyl Nitrite*

Because protonated hexamethyldisiloxane was made via reaction of the tert-butyl cation with hexamethyldisiloxane, methyl nitrite was introduced through the vacuum rack at varying pressures into the flow tube at port 3 and was allowed to react with $(CH_3)_3C^+$ as a control experiment. The introduction of tert-butyl chloride into the ion source results in *m/z* 57, *m/z* 97, and *m/z* 113, **Figure 4.8**. The tert-butyl cation (*m/z* 57) is produced from electron ionization or Penning ionization of tert-butyl chloride while traces of *m/z* 113 and *m/z* 97 are formed from a secondary reaction of the tert-butyl cation with tert-butyl chloride and subsequent loss of methane from *m/z* 113, respectively (Scheme 4.4).

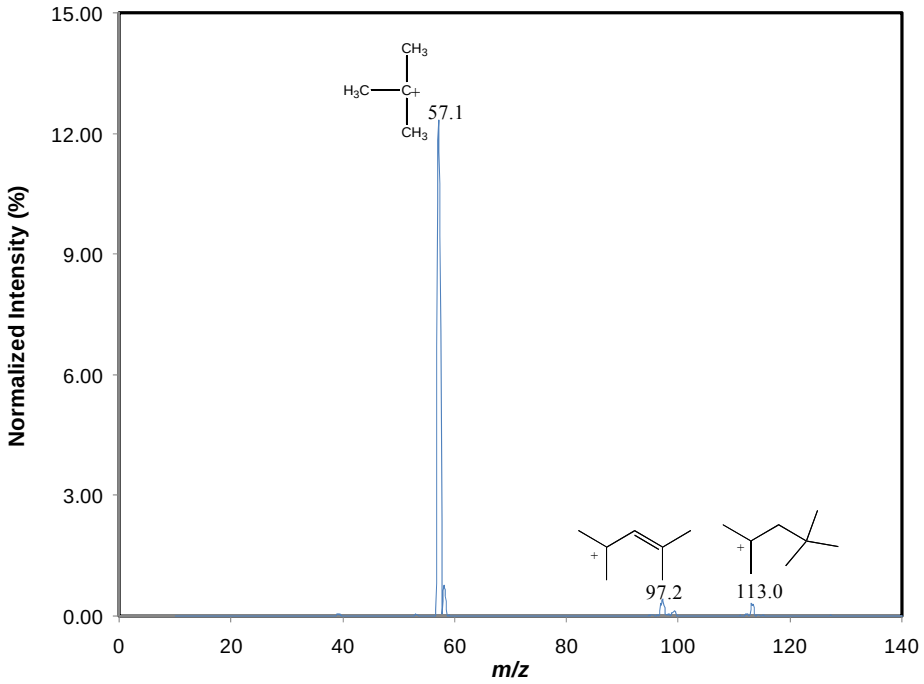

Figure 4.8: Precursor spectrum for the formation of the tert-butyl cation from the ionization of tert-butyl chloride at a flow tube pressure of 0.328 Torr.

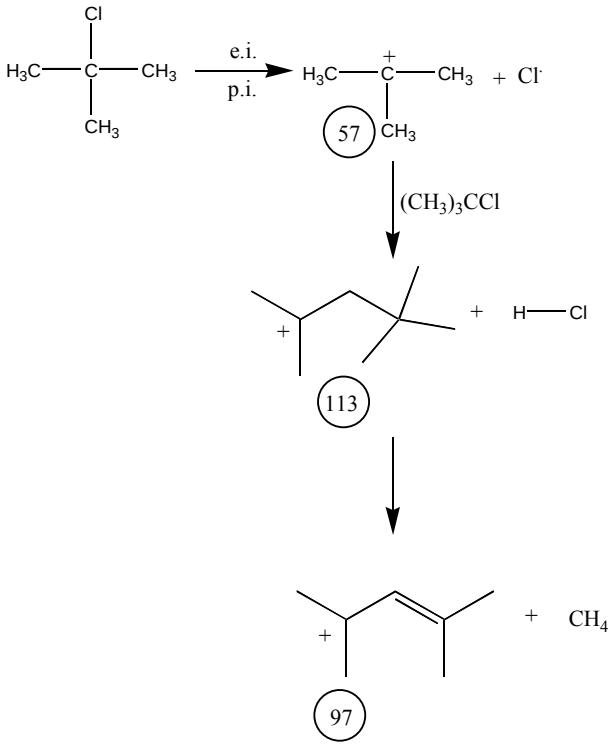

Scheme 4.4: Production of reagent ions from electron ionization (e.i.) and Penning ionization (p.i.) of tert-butyl chloride in the flow tube.

When methyl nitrite was introduced into the flow tube at port 3 with a pressure in the vacuum rack of 3.501 Torr, a major product ion at *m/z* 86 with minor product ions at *m/z* 87 and *m/z* 73 were observed, **Figure 4.9**. These reactions are displayed in Scheme 4.5. The fact that *m/z* 62, the proton transfer product, is not observed is further evidence that the proton affinity of methyl nitrite is 190.0±1.0 kcal/mol, since the proton affinity of isobutene is 191.6 kcal/mol[25].

Farid and McMahon have postulated that when *m/z* 86 is formed from the reaction of *t*-$C_4H_9^+$ with tert-butyl nitrite, a nitrosyl adduct to cyclopropanone is the product along with isobutane and methane.[92] However, recognizing that the proton affinity of cyclopropanone is 183 kcal/mol[93], that the ΔH_f of cyclopropanone is 3.8±1.0 kcal/mol[94], and utilizing eq. 4.3, a ΔH_f for the nitrosyl adduct of cyclopropanone of 213±2 kcal/mol is estimated. This suggests that the

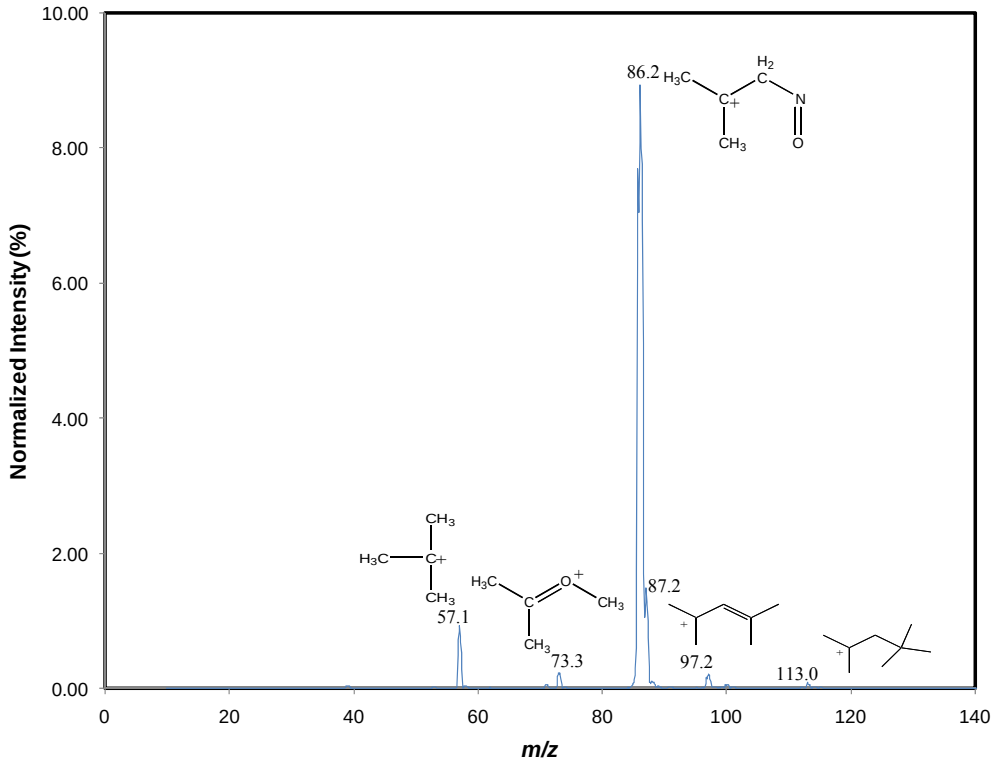

Figure 4.9: Product spectrum for the reaction of the tert-butyl cation with methyl nitrite at a flow tube pressure of 0.328 Torr and vacuum rack pressure of 3.501 Torr.

nitrosyl adduct of cyclopropanone from the reaction of the tert-butyl cation and tert-butyl nitrite, as proposed by Farid and McMahon, is not a viable source of *m/z* 86 as the reaction is endothermic by 34±2 kcal/mol, eq. 4.16. This is analogous to the formation of the nitrosyl

$$(CH_3)_3C^+ + (CH_3)_3CONO \rightarrow (CH_2)CONO^+ + CH_4 + (CH_3)_3CH \quad \Delta H_{rxn} = +34 \text{ kcal/mol} \qquad (4.16)$$

adduct of cyclopropanone from the tert-butyl cation and methyl nitrite, eq. 4.17, which is

$$(CH_3)_3C^+ + H_3CONO \rightarrow (CH_2)CONO^+ + 2CH_4 \quad \Delta H_{rxn} = +23 \text{ kcal/mol} \qquad (4.17)$$

endothermic by 23±2 kcal/mol and also not a viable reaction pathway. Instead, *m/z* 86 is likely the nitrosyl adduct of isobutene, formed by the reaction of the tert-butyl cation with methyl nitrite and exothermic by 8±4 kcal/mol (Scheme 4.5). The exothermicity of this reaction is determined using eq. 4.18, which has been shown by Cacace et al.[85] to correlate to the proton

$$NO^+ \text{ Bonding Energy} = 0.563*(\text{Proton Affinity}) - 72.7 \qquad (4.18)$$

affinity of compounds containing no binding sites except for π ponds to the NO^+ binding energy within ±2 kcal/mol.

The intensity of *m/z* 87 is 16% of *m/z* 86 and, therefore, not attributable to just an isotope of *m/z* 86 due to the fact that the isotopic abundance of *m/z* 87 would be expected to be approximately 5% of *m/z* 86 for the nitrosyl adduct of isobutene. *m/z* 87 is $(C_2H_5)(CH_3)CO^+ – CH_3$ and/or $(CH_3)_3C–^+OCH_2$ through adduct formation of the tert-butyl cation to methyl nitrite, followed by cleavage of the $((CH_3)_3C)(H_3C)O^+–NO$ bond, hydride transfer from either the tert-butyl or methyl moiety, respectively, to NO^+, and alkyl rearrangement in the case of $(C_2H_5)(CH_3)CO^+ – CH_3$. These reactions are exothermic by 27±2 and 10.9±2.1 kcal/mol, respectively. The ΔH_f of 104±2 kcal/mol for $(C_2H_5)(CH_3)CO^+ – CH_3$ utilized to estimate the ΔH_{rxn} for the first reaction is derived from the ΔH_f of the methyl cation, ΔH_f of butanone, proton affinity of butanone, the 1:1 correlation of proton affinity to methyl cation affinity within

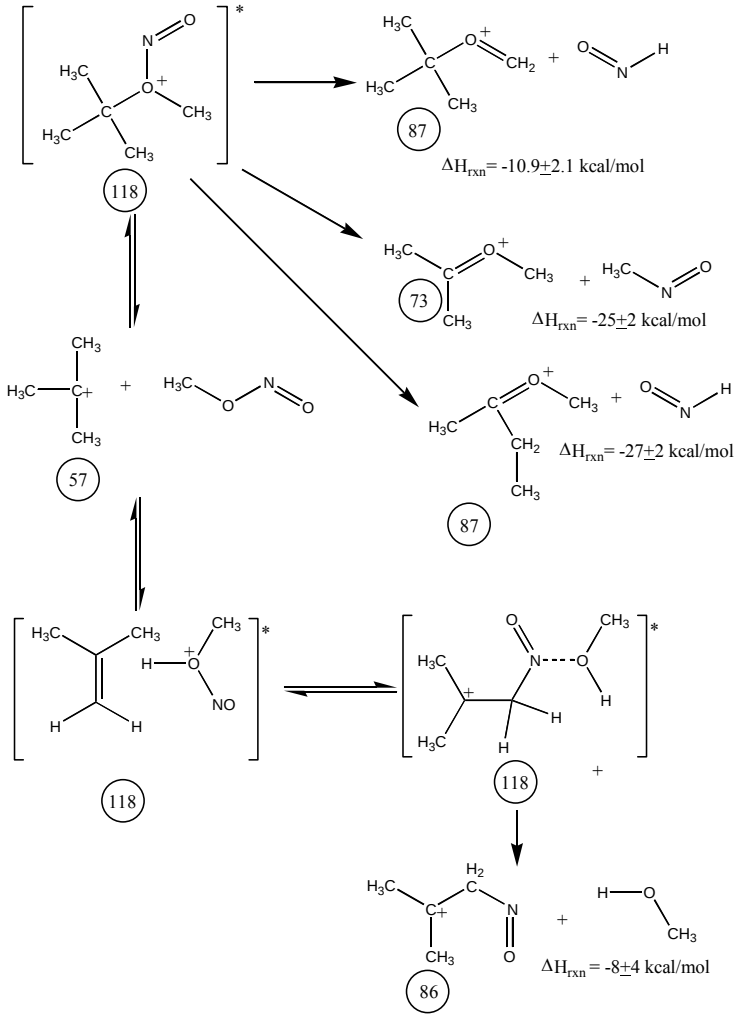

Scheme 4.5: Reactions of the tert-butyl cation with methyl nitrite in the flow tube.

± 2 kcal/mol at proton affinities ≥165 kcal/mol noted by Kebarle and coworkers[89], and both the proton affinity and methyl cation affinity of methanol as references. The ΔH_f of 120.0±2.0 kcal/mol for $(CH_3)_3C–^+OCH_2$ utilized to determine the ΔH_{rxn} for the second reaction is derived from the ΔH_f of formaldehyde, the proton affinity of formaldehyde, and the equation that correlates t-butyl cation affinity to proton affinity to within ±2 as calculated by Norrman and McMahon[95], eq. 4.19. In each reaction, the formation of the tert-butyl adduct to methyl nitrite

$$\text{Proton Affinity} = 1.43 * (\text{tert-butyl cation affinity}) + 138.53 \quad (4.19)$$

releases enough energy, 36.0±2.2 kcal/mol, determined from eq. 4.19, so that there is a finite probability that the $((CH_3)_3C)(H_3C)O^+$–NO bond of kcal/mol, 32.1±2.0 kcal/mol, estimated from eq. 4.3, is severed.

m/z 73 is $(CH_3)_2CO^+$–CH_3 and formed in a similar manner to *m/z* 87, except methide abstraction occurs instead of hydride abstraction. This reaction is calculated to be 25±2 kcal/mol exothermic based on the heat of formation of the methyl cation, heat of formation of acetone, proton affinity of acetone, and 1:1 correlation of the proton affinity to methyl cation affinity when the proton affinity is ≥165 kcal/mol[89].

4.3.5 *$((CH_3)_3Si)_2OH^+$ + Methyl Nitrite*

$((CH_3)_3Si)_2OH^+$ (*m/z* 163), produced from the reaction of the tert-butyl cation with hexamethyldisiloxane, introduced at port 10, was allowed to react with methyl nitrite, introduced into the flow tube at port 3 at varying flow rates, in an attempt to make trimethylsilated methyl nitrite; $TMS(CH_3)ONO^+$. No reaction is observed even at vacuum rack pressures as high as 5.021 Torr, **Figure 4.10.** The absence of the proton transfer product, $H(CH_3)ONO^+$ (*m/z* 62), is expected because the proton affinity of hexamethyldisiloxane is 202.3 kcal/mol[24] while the proton affinity of methyl nitrite is 190.0±1.0 kcal/mol, resulting in proton transfer being endothermic by 12.3±1.0 kcal/mol. The trimethylsilyl transfer reaction is calculated to be thermoneutral within error, ΔH_{rxn}=2.5±2.9 kcal/mol, by utilizing a proton affinity of methyl nitrite of 190.0±1.0 kcal/mol (**Appendix B**), 194.6 kcal/mol for the proton affinity of trimethysilanol[24], and eq. 4.4 to correlate proton affinity to the trimethylsilyl affinity. Even

though the reaction is thermoneutral within error, the absence of the trimethylsilyl transfer product indicates either that this reaction is endothermic or a kinetic barrier.

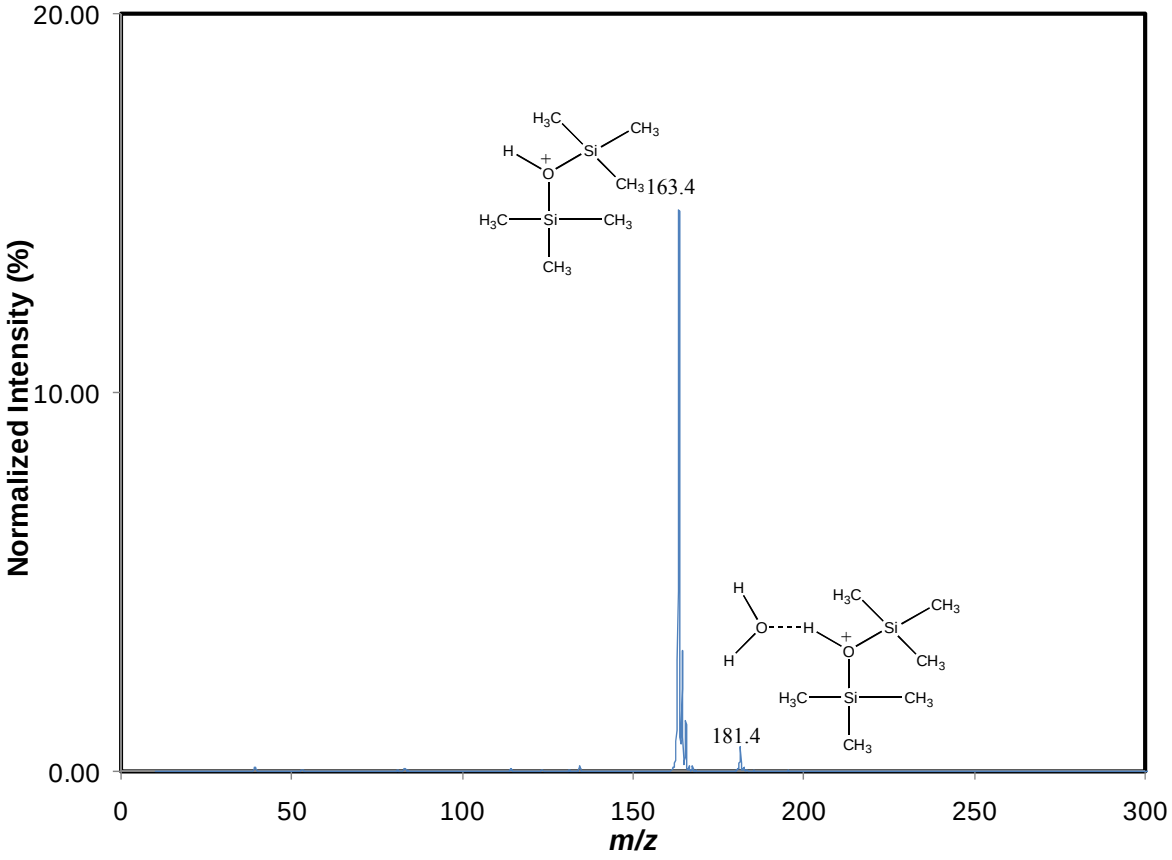

Figure 4.10: Product spectrum for the reaction of protonated hexamethyldisiloxane with methyl nitrite at a flow tube pressure of 0.324 Torr and vacuum rack pressure of 5.021 Torr.

4.3.6 *$(CH_3)_3SiOH_2^+$ + Methyl Nitrite*

$(CH_3)_3SiOH_2^+$ (*m/z* 91), produced from the reaction of the trimethylsilyl cation with water vapor, introduced at port 10, was reacted with methyl nitrite, introduced into the flow tube at port 3 at varying flow rates, in an attempt to make trimethylsilated methyl nitrite; $TMS(CH_3)ONO^+$. The trimethylsilyl affinity of water has been measured by Stone and coworkers via the ICR equilibrium method to be 30 kcal/mol.[86] This is significantly less than the

estimated trimethylsilyl affinity of trimethylsilanol of 46.2±2.0 kcal/mol, which suggests that protonated trimethylsilanol is a better trimethylsilyl transfer reagent than protonated hexamethyldisiloxane. This trimethylsilyl affinity of water is also significantly less than the 43.7±2.1 kcal/mol trimethylsilyl affinity determined for methyl nitrite. Trimethylsilyl transfer between $(CH_3)_3SiOH_2^+$ and methyl nitrite is highly feasible as evidenced by the fact that the ΔH_{rxn}=-14±3 kcal/mol. The *m/z* corresponding to $TMS(CH_3)ONO^+$ (*m/z* 134) is indeed observed as a primary product ion, **Figure 4.11** and **Figure 4.12** from the reaction of *m/z* 91 with methyl

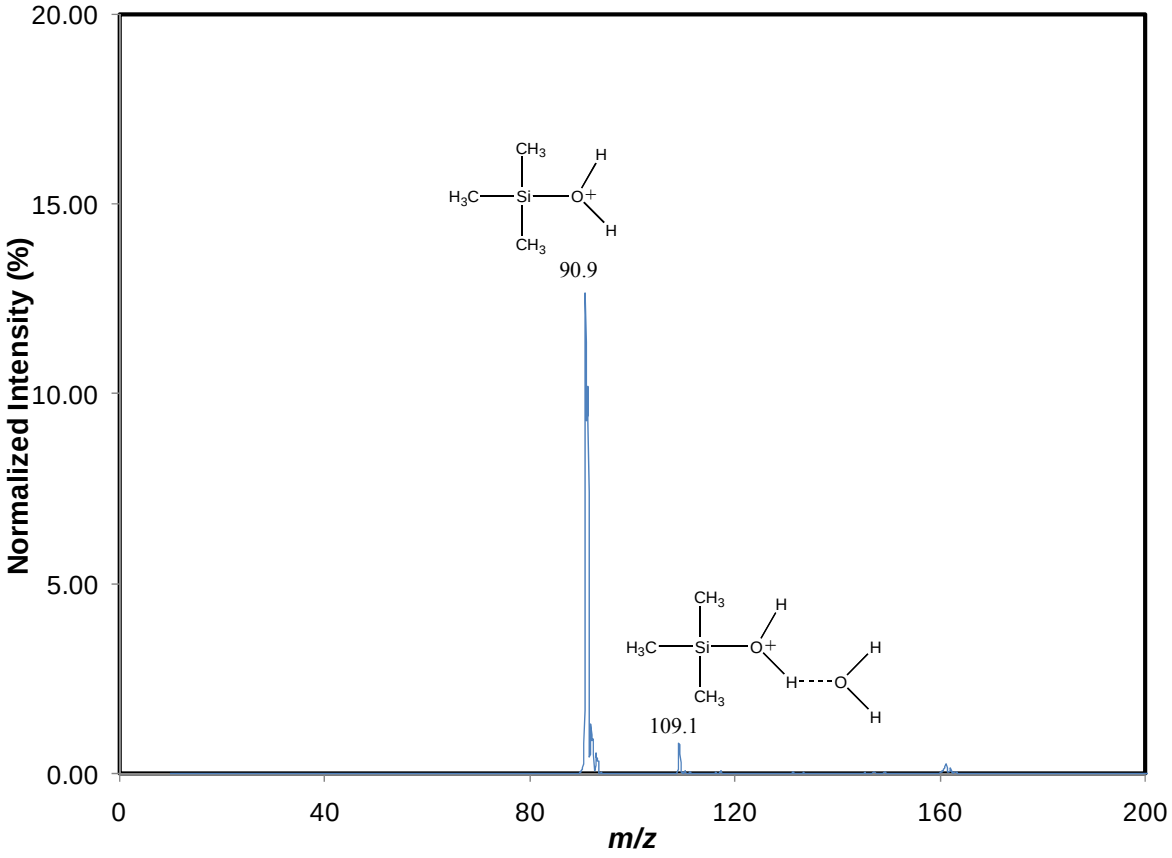

Figure 4.11: Precursor spectrum for the formation of protonated trimethylsilanol from the addition of water to the trimethylsilyl cation at a flow tube pressure of 0.332 Torr.

nitrite. *m/z* 120 is observed as another primary product ion. *m/z* 120 is likely protonated trimethylsilyl nitrite, $H(TMS)ONO^+$, formed from initial clustering of protonated

trimethylsilanol to methyl nitrite, followed proton transfer to methyl nitrite within the intermediate, and then NO^+ transfer to trimethylsilanol (Scheme 4.6). Even though the formation of a proton transfer product does not occur due to the proton affinity of trimethylsilanol being 194.6 kcal/mol[25] and that of methyl nitrite being 190.0±1.0 kcal/mol (**Appendix B**), it is possible that these proton affinities are close enough such that the intermediate is long enough lived to explain the occurrence of this reaction.

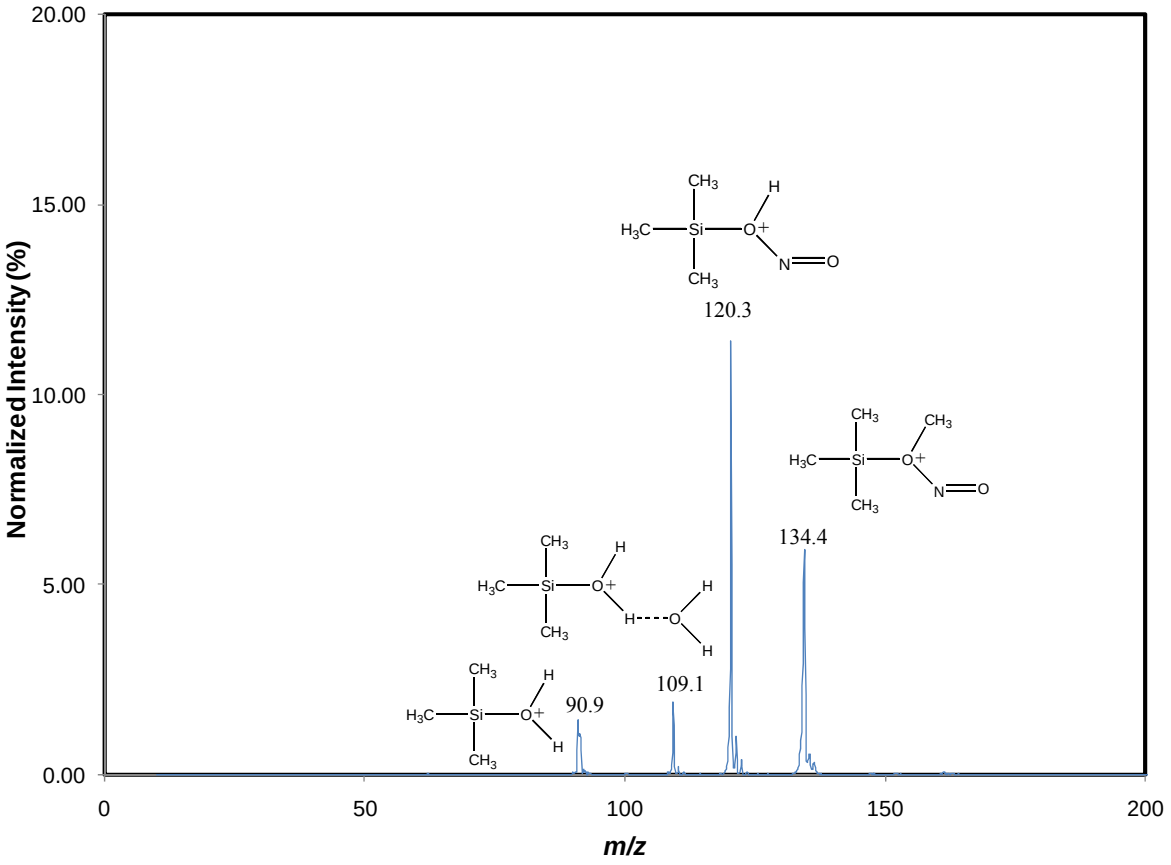

Figure 4.12: Product spectrum for the reaction of protonated trimethylsilanol with methyl nitrite at a flow tube pressure of 0.324 Torr and methyl nitrite vacuum rack pressure of 4.012 Torr.

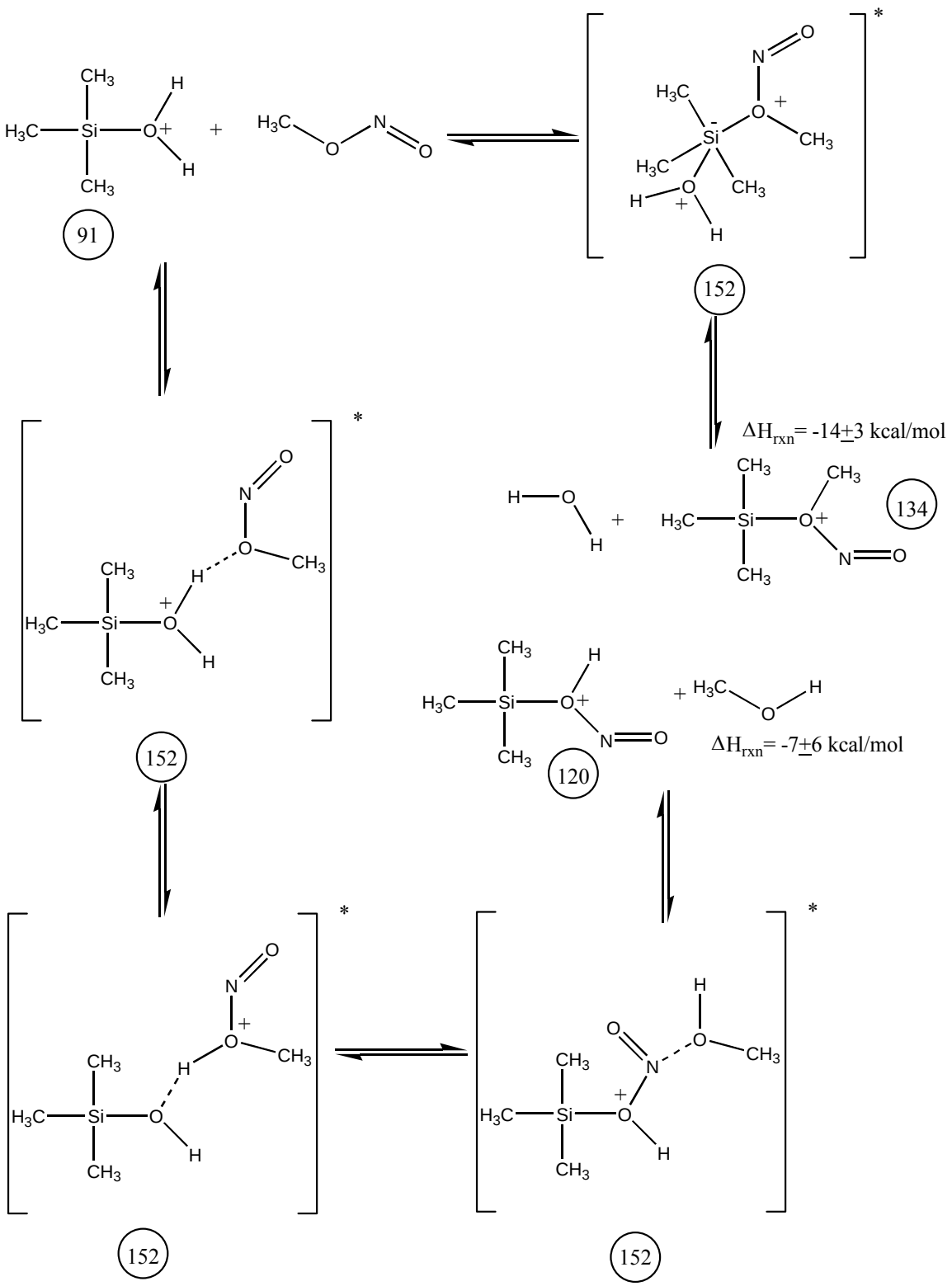

Scheme 4.6: Reactions of protonated trimethylsilanol with methyl nitrite.

4.4 Conclusions

The clean generation of an ion of the form $R(TMS)ONO^+$, where R is a proton, alkyl, trimethylsilyl group, remains elusive. Attempts at the association of NO^+ to neutrals of the form $ROSi(CH_3)_3$ resulted in only trace formation of $R(TMS)ONO^+$ with the alkyl and/or hydride abstraction reaction pathways dominating. These results indicate that NO^+ association is not an efficient reaction pathway when alternate reaction pathways are available. Protonated hexamethyldisiloxane does not react with methyl nitrite at thermal conditions. Protonated trimethylsilanol was found to react with methyl nitrite to produce ions of the form $R(TMS)ONO^+$. However, there was no clean generation of a single primary product as both $H(TMS)ONO^+$ (*m/z* 120) and $TMS(CH_3)ONO^+$ (*m/z* 134) were both observed to be produced in abundance.

APPENDIX A

NEUTRAL DATA USED TO CALCULATE k_{coll}

	μ (Debye)[a]	α (10^{-24} cm^3)[a]	Molar Mass (g)[a]
Acetone	2.88	6.40	58.08
Acetonitrile	3.92	4.50	41.05
Benzaldehyde	3.18[b,c]	13.08[d]	106.12
Ethanol	1.69	5.11	46.07
Methanol	1.70	3.32	32.04
Methyl Acetate	1.72	6.94	74.08
THF	1.63	7.87[e]	72.11

[a]Unless noted otherwise, data taken from CRC Handbook of Chemistry and Physics, 73rd Edition
[b]Kawashima and Kozima[96]
[c]Desyatnyk et al.[97]
[d]Lias et al.[98]
[e] Fromon and Treiner[99]

APPENDIX B

LITERATURE AND CALCULATED THERMODYNAMIC DATA OF NEUTRALS

	Proton Affinity (kcal/mol)	Gas Phase Basicity (kcal/mol)
Benzaldehyde	199.3	191.7
Tetrahydrofuran	196.5	189.9

[a]All values obtained from NIST webbook[25]

	Proton Affinity (kcal/mol)	ΔH_f (kcal/mol)	$(CH_3)_3Si^+$ Affinity (kcal/mol)	NO^+ Affinity (kcal/mol)	$(CH_3)_3C^+$ Affinity (kcal/mol)	H_3C^+ Affinity (kcal/mol)
Acetone	194 [b]	-52.23±0.14 [b]				96.9±2.0
Butanone	197.7 [b]	-57.02±0.20 [b]				100.6±2.0
Cyclopropanone	183 [h]	3.8±1.0 [i]		25±2		
Formaldehyde	170.4 [b]	-27.701 [b]	33.1±2.0		22.3±2.0	
Hexamethyldisiloxane	202.3 [b]	-167.0 [f]		32.5±2.0		
Isobutane		-32.07±0.15 [b]				
Isobutene	191.6±0.3 [g]	-4.29±0.26 [b]		35.2±2.0		
Methane		-17.89 [b]				
Methanol		-49.0±3.0 [b]		24.3±3.0 [m]		83.2 [l]
2-methoxy-2-methyl propane	201.1 [b]	-68.12 [b]				
Methoxytrimethylsilane	202.4 [b]	-112.0±2.0 [d]		32.6±2.0		
Methyl Nitrite	190.0±1.0 [e]	-15.29±0.33 [b]	43.7±2.1	28.0±2.0		
Nitrosyl Hydride		23.80 [b]				
Nitrosomethane		17.0±0.7 [d]				
Nitrous Acid	188±2 [k]	-18.34 [b]	42.6±2.3			
Oxydimethylsilane	220.9±1.6 [c]	≤ -34±3	60.6±2.6			123.8±2.6
tert-butyl nitrite		-41.0±1.0 [b]				
Trimethylsilanol	194.6 [b]	-109.0 [f]	46.2±2.0			
Water	165 [b]	-57.799 [b]	30 [j]			

[a]Items highlighted in yellow are calculated values
[b]NIST webbook[25]
[c]Audier et al.[88]
[d]Lias et al.[100]
[e]Calculated from the bracketing data of McAllister and Pittman[101] and Farid and McMahon[92]
[f]Morris[82]
[g]Traeger[103]
[h]Corkran et al.[93]
[i]Rodriguez et al.[94]
[j]Stone and coworkers[86]
[k]Massimiliano and Grandinetti[91]
[l]Kebarle and coworkers[89]
[m]Calculated from data of Cacace et al.[85] and Massimiliano and Grandinetti[91]

APPENDIX C

LITERATURE AND CALCULATED THERMODYNAMIC DATA OF IONS

	ΔH_f (kcal/mol)	ΔH_{solv} with water (kcal/mol)
H^+	365.2 [b]	
H_3O^+	142	-32 [e]
$H_3O(H_2O)^+$	53	-20 [e]
$H_3O(H_2O)_2^+$	-25	-17 [e]
$H_3O(H_2O)_3^+$	-100	
NO^+	235 [b]	
$(CH_3)_3Si^+$	150 [c]	
$(CH_3)_3SiOCH_2^+$	89±2	
H_3C^+	262 [b]	
$((CH_3)_3Si)(CH_3)ONO^+$	90±3	
$(CH_3)_2SiOCH_3^+$	≤ 104±4	
$((CH_3)_3Si)_2ONO^+$	35±2	
$(CH_3)_2SiOSi(CH_3)_3^+$	≤ 55±4	
H_2ONO^+	159 [d]	
$H(CH_3)ONO^+$	162±2 [b]	
$H_2O{\cdot}H(CH_3)ONO^+$	97±2	
$H_3CO(NO)_2^+$	191.7±2.0	
$(CH_3)_3C^+$	170.0±0.3 [f]	
$(CH_3)CCH_2NO^+$	196±2	
$C_3H_4ONO^+$	213±2	
$(CH_3)_3COCH_2^+$	120.0±2.0	
$(CH_3)_2COCH_3^+$	113±2	
$(CH_3)_3SiOH_2^+$	62.5±5.0 [g]	
$((CH_3)_3Si)HONO^+$	89±2	

[a]Items highlighted in yellow are calculated values
[b]Rosenstock et al.[87]
[c]Szepes and Baer[90]
[d]Kebarle and coworkers[102]
[e]Kebarle[28]
[f]Traeger[103]
[g]Morris[82]

BIBLIOGRAPHY

[1]Perez, A.G.; Rios, J.J.; Sanz, C.; Olias, J.M. *J. Agric. Food Chem.* **1992,** *40,* 2232-2235.

[2]Honkanen, E.; Pyysalo, T.; Hirvi, T. *Z. Lebensm. Unters. Forsch.* **1980,** *171,* 180-182.

[3]Edwards, R.A.; Dainty, R.H.; Hibbard, C.M. *J. Applied Bacteriol.* **1987,** *63,* 427-434.

[4]Dainty, R.H.; Edwards, R.A.; Hibbard, C.M. *J. Applied Bacteriol.* **1984,** *57,* 75-81.

[5]Paredi, P.; Kharitonov, S.A.; Barnes, P.J. *Am. J. Respir. Crit. Care. Med.* **2000,** *162,* 1450-1454.

[6]Olopade, C.O.; Christon, J.A.; Zakkar, M.A.; Hua, C.; Swedler, W.I.; Scheff, P.A. *Chest.* **1997,** *111,* 1500-1504.

[7]Olopade, C.O.; Zakkar, M.; Swedler, W.I.; Rubinstein, I. *Chest.* **1997,** *111,* 862-865.

[8]Phillips, M.; Cataneo, R.N.; Cummin, A.; Gagliardi, A.J.; Gleeson, K.; Greenberg, J.; Maxfield, R.A.; Rom, W.N. *Chest.* **2003,** *123,* 2115-2123.

[9]Phillips, M.; Cataneo, R.N.; Greenberg, J.; Grodman, R.; Salazar, M. *Heart Disease.* **2003,** *5,* 95-99.

[10]Greenberg, M.M. *Environmental Research.* **1997,** *1,* 1-7.

[11]http://www.epa.gov/iaq/voc.html

[12]Finlayson-Pitts, B.J. and Pitts Jr., J.N. *Science.* **1997,** *276,* 1045-1051.

[13]Wolfrum, E.J.; Meglen, R.M.; Peterson, D.; Sluiter, J. *Sensors and Actuators B* **2006,** *115*, 322-329.

[14]Bohme, D.K. *Interactions between Ions and Molecules;* Ausloos, P., editor; Plenum: New York, NY; p. 489

[15]Bouchoux, G.; Salpin, J.Y.; Leblanc, D. *Int. J. Mass. Spectrom. Ion. Proc.* **1996,** *153,* 37-48.

[16]Hunter, E.P. and Lias, E.G. *J. Phys. Chem. Ref. Data.* **1998,** *27,* 413-656.

[17]Smith, D.; Wang, T.; Spanel, P. *Rapid Comm. Mass Spectrom.* **2003,** *17,* 2655-2660.

[18]Diskin, A.M.; Wang, T.; Smith, D.; Spanel, P. *Int. J. Mass. Spectrom.* **2002,** *218,* 87-101.

[19]Spanel, P. and Smith, D. *Int. J. Mass. Spectrom.* **1998,** *181,* 1-10.

[20]Spanel, P. and Smith, D. *Int. J. Mass. Spectrom. Ion. Proc.* **1997,** 167/168, 375-388.

[21]Spanel, P.; Van Doren, J.M.; Smith, D. *Int. J. Mass. Spectrom.* **2002,** *213,* 163-176.

[22]Spanel, P. and Smith, D. *Int. J. Mass. Spectrom. Ion. Proc.* **1998,** *172,* 137-147.

[23]Spanel, P. and Smith, D. *Int. J. Mass. Spectrom. Ion. Proc.* **1998,** *172,* 239-247.

[24]Brimblecombe, P. *Air Composition and Chemistry,* 2nd Edition; Cambridge Environmental Chemistry Series, No. 6; Cambridge University Press: Cambridge, U.K, 1996; p. 2.

[25]NIST Chemistry Webbook. http://webbook.nist.gov/chemistry/

[26]Arnold, S.T.; Viggiano, A.A.; Morris, R.A. *J. Phys. Chem. A.* **1998,** *102,* 8881-8887.

[27]Lau, Y.K.; Ikuta, S.; Kebarle, P. *J. Am. Chem. Soc.* **1982,** *104,* 1462-1469.

[28]Kebarle, P. *Annu. Rev. Chem. Phys.* **1977,** *28,* 445-476.

[29]Wilson, P.F.; Freeman, C.G.; McEwan, M.J. *Int. J. Mass. Spectrom.* **2003,** *229,* 143-149.

[30]Spanel, P. and Smith, D. *Int. J. Mass. Spectrom.* **1998,** *176,* 167-176.

[31]Lindinger, W.; Hansel, A.; Jordan, A. *Int. J. Mass. Spectrom. Ion. Proc.* **1998,** *173,* 191-241.

[32]Wehinger, A.; Schmidt, A.; Mechtcheriakov, S.; Ledochowski, M.; Grabmer, C.; Gastl, G.; Amann, A. *Int. J. Mass. Spectrom.* **2007,** *265,* 45-59.

[33]Jobson, B.T.; Alexander, M.L.; Maupin, G.D.; Muntean, G.G. *Int. J. Mass. Spectrom.* **2005,** *245, 78-89.*

[34]Filella, I. and Penuelas, J. *Atmospheric Environment* **2006,** *40,* 7752-7769.

[35]Guenther, A.; Geron, C.; Pierce, T.; Lamb, B.; Harley, P.; Fall, R. *Atmospheric Environment* **2000,** *34,* 2205-2230.

[36]Fehsenfeld, F.C.; Schmeltekopf, A.L.; Goldan, P.D.; Schiff, H.I.; Ferguson, E.E. *J. Chem. Phys.* **1966,** *44,* 4087-4094.

[37]Dushman, S. and Lafferty, J.M. *Scientific Foundations of Vacuum Technique;* John Wiley and Sons; New York, 1962.

[38]Ferguson, E.E.; Fehsenfeld, F.C.; Schmeltekopf, A.L. *Advan. At. Mol. Phys.* **1969,** *5,* 1-56.

[39]Gioumousis, G. and Stevenson, D.P. *J. Chem. Phys.* **1958,** *29*, 294-299.

[40]Su, T. and Bowers, M.T. *J. Chem. Phys.* **1978,** *69*, 2243-2250.

[41]Moran, T.F. and Hamill, W.H. *J. Chem. Phys.* **1963,** *39,* 1413-1422.

[42]Dugan, J.V. and Magee, J.L. *J. Chem. Phys.* **1967,** *47,* 3103-3112.

[43]Su, T. and Bowers, M.T. *J. Chem. Phys.* **1972,** *58*, 3027-3037.

[44]Su, T. and Bowers, M.T. *Int. J. Mass. Spectrom. Ion Phys.* **1975,** *17,* 211-212.

[45]Su, T. and Bowers, M.T. *Int. J. Mass. Spectrom. Ion Phys.* **1973,** *12,* 347-356.

[46]Su, T. and Bowers, M.T. *J. Chem. Phys.* **1977,** *69*, 2243-2250.

[47]Su, T. and Chesnavich, W.J. *J. Chem. Phys.* **1982**, *76,* 5183.

[48]Spanel, P. and Smith, D. *Rapid Comm. Mass. Spectrom.* **2000**, *14,* 1898-1906.

[49]Spanel, P. and Smith, D. *J. Am. Soc. Mass. Spectrom.* **2001,** *12,* 863-872.

[50]Spanel, P.; Dryahina, K.; Smith, D. *Int. J. Mass. Spectrom.* **2006,** *249/250,* 230-239.

[51]Sander, R. http://www.mpch-mainz.mpg.de/~sander/res/henry.html

[52]Li, J.; Shen, C.; Wang, H.; Han, H.; Zheng, P.; Xu, G.; Jiang, H.; Chu, Y. *Wuli Huaxue Xuebao*. **2008,** *24*, 705-708.

[53]von Hartungen, E.; Wisthaler, A.; Mikoviny, T.; Jaksch, D.; Boscaini, E.; Dunphy, P.; Maerk, T. *Int. J. Mass. Spectrom.* **2004,** *239,* 243-248.

[54]Abbott, S.; Elder, J.; Spanel, P.; Smith, D. *Int. J. Mass. Spectrom.* **2003,** *228,* 655-665.

[55]Lee, H.S.; Drucker, M.; Adams, N.G. *Int. J. Mass. Spectrom. Ion Proc.* **1992,** *117,* 101-114.

[56]Mackay, G.I.; Betowski, L.D.; Payzant, J.D.; Schiff, H.I.; Bohme, D.K. *J. Phys. Chem.* **1976**, *80*, 2919-2922.

[57]Yang, X.; Zhang, X.; Castleman, A.W. *Int. J. Mass. Spectrom. Ion Proc.* **1991,** *109,* 339-354.

[58]Spanel, P. and Smith, D. *J. Phys. Chem.* **1995,** *99,* 1551-1556.

[59]Bohme, D.K.; Mackay, G.I.; Tanner, S.D. *J. Amer. Chem. Soc.* **1979,** *101,* 3724-3730.

[60]Spanel, P. and Smith D. *J. Phys. Chem.* **1998,** *176,* 203-211.

[61]Smith, D.; Adams, N.G.; Alge, E. *Planet Space Sci.* **1981,** *29,* 449-454.

[62]Cabani, S.; Conti, G.; Lepori, L. *Trans. Faraday Soc.* **1971,** *67,* 1943–1950.

[63]California Environmental Protection Agency. http://www.calepa.ca.gov/

[64]Signer, R.; Arm, H.; Daenicker, H. *Helv. Chim. Acta*. **1969,** *52,* 2347–2351.

[65]Hine, J. and Mookerjee, P.K. *J. Org. Chem.* **1975,** *40,* 292–298.

[66]Betterton, E. A. and Hoffmann, M.R. *Environ. Sci. Technol.* **1988,** *22,* 1415–1418.

[67]Zhou, X. and Mopper, K. *Environ. Sci. Technol.* **1990,** *24,* 1864–1869.

[68]Staudinger, J. and Roberts, P.V. *Crit. Rev. Environ. Sci. Technol.* **1996,** *26,* 205–297.

[69]Hamm, S.; Hahn, J.; Helas, G.; Warneck, P. *Geophys. Res. Lett.* **1984,** *11,* 1207–1210.

[70]Snider, J. R. and Dawson, G.A. *J. Geophys. Res.* **1985,** *90D,* 3797–3805.

[71]Arijs, E. and Brasseur, G. *J. Geophys. Res*. **1986,** *91D,* 4003–4016.

[72]Benkelberg, H.J.; Hamm, S; Warneck, P. *J. Atmos. Chem.* **1995,** *20,* 17–34.

[73]Burnett, M. G. *Anal. Chem.* **1963,** *35,* 1567–1570.

[74]Buttery, R. G.; Bomben, J.L.; Guadagni, D.G.; Ling, L.C. *J. Agric. Food Chem*. **1971,** *19,* 1045–1048.

[75]Betterton, E. A. *Atmos. Environ.* **1991,** *25A,* 1473–1477.

[76]Vitenberg, A. G.; Ioffe, B.V.; Dimitrova, Z.S.; Butaeva, I.L. *J. Chromatogr*. **1975,** *112,* 319–327.

[77]Hoff, J. T.; Mackay, D.; Gillham, R.; Shiu, W.Y. *Environ. Sci. Technol.* **1993,** *27,* 2174–2180.

[78]Fleming, I. *Chem. Soc. Rev.* **1981**, *10*, 83-111.

[79]Stone, J. A. *Mass Spec. Rev.* **1997**, *16*, 25-49.

[80]Orlando, R.; Ridge, D.P.; Munson, B. *J. Am. Soc. Mass. Spectrom.* **1990,** *1,* 144-148.

[81]Chen, Q.-F.; Stone, J. A. *Int. J. Mass Spectrom. Ion Proc.* **1997**, *165/166*, 195-207.

[82]Morris, M. Using the Flowing Afterglow as a Chemical Reaction Mass Spectrometer. Ph.D. Dissertation, University of Pittsburgh, Pittsburgh, PA, 2007.

[83]Smith, D.; Wang, T.; Spanel, P. *Int. J. Mass. Spectrom.* **2003,** *230,* 1-9.

[84]Francisco, J.S. *J. Chem. Phys.* **2001,** *115,* 2117-2122.

[85]Cacace, F.; DePetris, G.; Pepi, F. *Proc. Natl. Acad. Sci.* **1997,** *94,* 3507-3512.

[86]Wojtyniak, A.C.M. and Stone, J.A. *Int. J. Mass. Spec. Ion. Proc.* **1986,** *74,* 59-79.

[87]Rosenstock, H.M.; Draxl, K.; Steiner, B.W.; Herron, J.T. *J. Phys. Chem. Ref. Data.* **1977,** *6,* 1-779.

[88]Audier, H.E.; Fossey, J.; Denhez, J.P.; Jacquet, J.P.; Mourgues, P. *Int. J. Mass. Spectrom.* **2003,** *227,* 381-389.

[89]McMahon, T.B.; Heinis, T.; Nicol, G.; Hovey, J.K.; Kebarle, P. *J. Am. Chem. Soc.* **1988,** *110,* 7591-7598.

[90]Szepes, L. and Baer, T. *Magyar Kemiai Folyoirat*. **1986,** *92*, 297-301.

[91]Massimiliano, A. and Grandinetti *Chem. Phys. Lett.* **1996,** *258,* 123-128.

[92]Farid, R. and McMahon, T.B. *Int. J. Mass. Spectrom. Ion. Phys.* **1978,** *27,* 163-183.

[93]Corkran, G. and Ball, D.W. *J. Molec. Struct.* **2004,** *668,* 171-178.

[94]Rodriguez, H.J.; Chang, J.C.; Thomas, T.F. *J. Am. Chem. Soc.* **1976,** *98,* 2027-2034.

[95]Norrman, K. and McMahon, T.B. *J. Am. Chem. Soc.* **1996,** *118,* 2449-2457.

[96]Kawashima, Y. and Kozima, K. *Bull. Chem. Soc. Jpn.* **1974,** *47,* 2879-2880.

[97]Desyatnyk, O.; Pszcolkowski, L.; Thorwirth, S.; Krygowski, T.M.; Kisiel, Z. *Phys. Chem. Chem. Phys.* **2005,** *7,* 1708-1715.

[98]Lias, S.G.; Liebman, J.F.; Levin, R.D. *J. Phys. Chem. Ref. Data.* **1984,** *13*, 695-808.

[99]Fromon, M. and Treiner, C. *J. Chem. Soc.* **1979,** *75,* 1837-1848.

[100]Lias, S.G.; Bartmess, J.E.; Liebmann, J.F.; Holmes, J.L.; Levin, R.D.; Mallard, W.G. *J. Phys. Chem. Ref. Data.* **1988**, 17.

[101]McAllister, T. and Pitman,P. *Int. J. Mass. Spectrom. Ion Phys.* **1976,** *19,* 241-248.

[102]French, M.A.; Hills, L.P.; Kebarle, P. *Can. J. Chem.* **1973,** *51,* 456-461.

[103]Traeger, J.C. *Rapid. Comm. Mass. Spectrom.* **1996,** *10,* 19-22.